ESTIMATION OF ACOUSTIC VELOCITIES AND ROCK MECHANICAL PARAMETERS USING ARTIFICIAL INTELLIGENCE TOOLS

BY

Zeeshan Tariq

A Thesis Presented to the
DEANSHIP OF GRADUATE STUDIES

KING FAHD UNIVERSITY OF PETROLEUM & MINERALS

DHAHRAN, SAUDI ARABIA

In Partial Fulfillment of the
Requirements for the Degree of

MASTER OF SCIENCE

In

PETROLEUM ENGINEERING

November, 2016

KING FAHD UNIVERSITY OF PETROLEUM & MINERALS

DHAHRAN- 31261, SAUDI ARABIA

DEANSHIP OF GRADUATE STUDIES

This thesis, written by **Zeeshan Tariq** under the direction of his thesis advisor and approved by his thesis committee, has been presented and accepted by the Dean of Graduate Studies, in partial fulfillment of the requirements for the degree of **MASTERS OF SCIENCE** in **Petroleum Engineering**.

Dr. Abdulazeez Abdulraheem
(Advisor)

Dr. Abdullah S. Sultan
Department Chairman

Dr. Salaheldin Ahmed Elkatatny
(Co-Advisor)

Dr. Salam A. Zummo
Dean of Graduate Studies

Dr. Mohamed Mahmoud
(Member)

20/12/16
Date

Dr. Dhafer Abdullah Al-Shehri
(Member)

Dr. Rafi ul Hassan
(Member)

Dedication

To my beloved parents (Abu and Ammi), Sister

&

Teachers.

ACKNOWLEDGMENTS

First of all, thanks to almighty Allah, all praises are due to Allah the most merciful and graceful, who had given me the strength and courage to successfully complete this thesis.

Acknowledgements are due to King Fahd University of Petroleum & Minerals for providing me the research opportunities to produce this thesis work and to my thesis advisor Dr. Abdulazeez Abdulraheem for his assistance and incessant support. His patience and support helped me overcome many challenging situations. I acknowledge my co-advisor Dr. Salaheldin Elkatatny for his excellent guidance, caring, patience, and providing me with an excellent atmosphere for doing research. I would like to express my sincere gratitude to other advisors, Dr. Mohamed Mahmoud, Dr. Dhaffer Al-Shehri and Dr. Rafi-ul Hasan for their ceaseless guidance and support throughout the thesis work. Without their insightful comments and suggestions, the completion of this work would not have been possible. I also want to thanks Dr. Abdullah Sultan the chairman of the department for his continuous motivation and kind support.

I would also like to thank all my colleagues, friends and seniors at KFUPM for providing the moral support and a pleasant atmosphere. Special thanks to my friends Ahmed Sadeed, Mirza Talha Baig, Saad Waseem, Aneeq Nasir, Owais Ahmed, Ahmed Mehboob, Shams Kalam, Najm-us-Sakib, Adil Ahmed, Mutsaid Shirazi and Hasan Sheikh for making my time at KFUPM memorable.

Table of Contents

LIST OF TABLES

LIST OF FIGURES

LIST OF ABBREVIATIONS

AAPE	Average absolute percentage error.
ANFIS	Adaptive neuro fuzzy inference system
ANN	Artificial neural network.
b_1	Bias between input and hidden layer of neural network.
b_2	Bias between hidden and output layer of neural network.
C	Regularization parameter
CC	Correlation coefficient.
E_{max}	Maximum error between actual and predicted.
E_{min}	Minimum error between actual and predicted.
E_{static}	Static Young's Modulus
FANG	Friction Angle
FFNN	Feed Forward Neural Network
GR	Gamma Ray, API
J	Total number of input parameters.
MAE	Maximum absolute error
N	Total number of neurons.
NPHI	Neutron Porosity, vol/vol
PR	Poisson's Ratio
P-wave	Compressional wave
PHIT	True Porosity
R	Correlation coefficient
R^2	Coefficient of determination
RBF	Radial basis function

RMSE	Root mean square error
RHOB	Bulk Density, g/cc
SVM	Support Vector Machine
S-wave	Shear wave
UCS	Unconfined Compressive Strength, ksi
V_P	Compressional wave velocity, km/s
V_S	Shear wave velocity, km/s
x	Input parameters
y	Output variable
W_1	Weights vector between input and hidden layer of neural network.
W_2	Weights vector between hidden and output layer of neural network.

ABSTRACT

Full Name : ZEESHAN TARIQ

Thesis Title : ESTIMATION OF ACOUSTIC VELOCITIES AND ROCK MECHANICAL PARAMETERS USING ARTIFICIAL INTELLIGENCE TOOLS

Major Field : Petroleum Engineering

Date of Degree : November 2016

Rock Mechanical parameters are critical in alleviating the risks associated with the drilling and maximizing the reservoir productivity. These parameters are used in the optimization of the well placement, well bore instability, completion design, draw-down limits to avoid sanding, hydraulic fracturing, and many more. The appropriate estimation of these parameters is very essential for the development and production phases of hydrocarbon recovery. Incorrect estimation of rock mechanical parameters may wrongly lead to heavy investment decisions and inappropriate field development plans.

To carry out any operation, a continuous profile of rock mechanical parameters is needed. Retrieving reservoir rock samples throughout the depth of the reservoir and performing laboratory tests are extremely expensive and time consuming. Therefore, these parameters are estimated from the sonic and compressional wave velocities obtained from Well-logs. Parameters obtained from laboratory tests are termed as static parameters while those obtained from Well-logs are dynamic parameters. The former case represents closely the condition in the reservoir. Since the Well-logs

provide a continuous profile of parameters, they have to be calibrated with respect to the static parameters.

Since rock properties change with the depth, a realistic estimation of static values remains a big challenge. In carbonate rocks because of heterogeneity the problem is more critical compared to sandstone. In addition to that shear and compressional wave velocity data is not always available from Well logs that makes the problem more challenging.

This research deals with the development of new artificial intelligence models to predict both the acoustic waves and the rock mechanical parameters. The proposed models will use different wire-line logs as an input. Three different AI techniques will be implemented and the one with the optimal performance on the basis of maximum coefficient of determination and minimum average absolute percentage error will be selected.

ملخص الرسالة

الاسم الكامل: زيشان طارق

عنوان الرسالة: تقدير السرعات الصوتية و عوامل الصخور الميكانيكية بإستخدام أدوات الذكاء الاصطناعي

التخصص: هندسة البترول

تاريخ الدرجة العلمية: نوفمبر 2016

تلعب العوامل الميكانيكية للصخور دور مهم في تقليل المخاطر الناتجة أثناء عمليات الحفر و عمليات زيادة إنتاجية المكامن. هذه العوامل يمكن إستخدمها في الامور التالية : تحديد أفضل موقع لبئر الإنتاج, تحديد إستقرارية قاع البئر, تصميم عملية إكمال البئر, تجنب انتاج الرمل من البئر وتصميم عمليات التكسير الهيدروليكي. يعتبر التقدير المناسب لهذه العوامل أمر أساسي في تطوير و انتاج الهيدروكربون (النفط والغاز), كما أن التقدير الخاطئ للعوامل الميكانيكية قد يؤدي الى إتخاذ قرارت هامة بصورة خاطئه ومن ثم تطوير حقل الإنتاج بصورة غير ملائمة.

قبل تنفيذ اي عملية على المكمن; يجب أن تتم دراسة عوامل الصخور الميكانيكية بصورة دقيقة و عمل مخطط مستمر لتغير هذه العوامل. تعتبر عمليات أخذ عينات صخرية من جميع أعماق المكمن و إجراء إختبارات معملية عليها تعتبر عمليات مكلفة للغاية و تأخذ وقت طويلا. و بالتالي; يتم تقدير هذه العوامل عند طريقة دراسة الموجات الصوتية و الموجات الانضغاطية التي يتم التحصل عليها من عمليات قياس البئر. تسمى العوامل التي يتم قياسها في المعمل بالعوامل الساكنة, كما تسمى تلك التي يتحصل عليها في عمليات قياس البئر بالعوامل المتحركة او الديناميكية, كل هذه العوامل يجب قياسها في ظروف مماثل للظروف المكمنية من حيث درجة الحرارة و الضغط.

لذلك يتم فحص و معايرة كل القياسات الناتجة من عمليات قياس البئر مع تلك المتحصل عليها في المعمل للتأكد من صحة و دقة هذه القياسات.

تتغير العوامل الصخرية مع العمق, لذلك يعتبر التقدير الحقيقي و الدقيق لقيم هذه العوامل يعتبر تحدي في غاية الصعوبة. يزداد هذه التحدي صعوبة في حالة الصخور الكربونة بسبب عدم تجانس هذه الصخور مقارنة بالصخور الرملية. بإلاضافة الى ذلك, فإن موجات القص والضغط تكون غير متوفرة في الغالب و لا يمكن التحصل عليها من عمليات قياس البئر, الامر الذي يجعل التحدي أكثر صعوبة.

في هذا البحث يتم تطوير نماذج جديدة للذكاء الاصطناعي من أجل تقدير الموجات الصوتية و عوامل الصخور الميكانيكية. هذه النماذج المقترحة سوف تستخدام قياسات مختلفة من عمليات قياس البئر كمدخلات لهذه النماذج. سوف يتم تطبيق ثلاثة من تقنيات الذكاء الاصطناعي, و بعد ذلك سوف يتم إختيار أفضل نموذج بناءا على اقل قيمة لمتوسط الخطاء النسبي و اقصى قيمة لمعامل الإرتباط.

Chapter 1

INTRODUCTION

1.1 Background

Good understanding of the mechanical behavior of reservoir rock is very important in reducing the problems related to Wellbore stability, sand production and reservoir subsidence. Mechanical properties of the rock refer to the elastic and failure parameters. There are two ways to measure rock elastic parameters in the lab: (i) the dynamic method which measures the ultrasonic wave velocities, i.e., compressional (P-wave) and shear (S-wave); and (ii) the static method, which implies the measurement of deformation by the application of known force, usually done by uniaxial and triaxial compressional tests (Barree et al. 2009). Static parameters are determined in the laboratory on rock samples extracted from the depth of interest in a reservoir section. In petroleum industry, the direct method to measure dynamic elastic moduli is from the wireline logging tool that uses the shear and compressional wave velocities (Colin et al. 1997). However, the failure parameters cannot be estimated directly from these logs.

Acoustic and density logs of the reservoir rock are used to obtain dynamic elastic parameters. These dynamic parameters have to be calibrated with respect to the static parameters. Because static parameters more truly represent the reservoir in situ stress strain conditions, oil and gas industry relies on the basic regression method to calibrate dynamic elastic parameters with static parameters. In these regression methods a transfer function is obtained between the static and dynamic mechanical parameters by using cross-plotting and curve-fitting procedures. Another method, called AUTOSCAN, was developed by KFUPM researchers for the calibration of dynamic data. So far no universal calibration procedure is devised and therefore Artificial Intelligence techniques are expected to play a vital role in estimation of static properties from the Well log data.

1.2 Statement of the Problem

In the field, rock mechanical parameters are obtained from the sonic and compressional wave velocities while in the lab they can be obtained from laboratory tests (Triaxial or uniaxial compression tests). Mechanical parameters estimated from the sonic log (termed as dynamic parameters) are usually calibrated with the core derived static parameters because the static measurement more truly reflects the reservoir in-situ mechanical conditions. Retrieving reservoir rock samples throughout the depth of the reservoir and performing laboratory tests are extremely expensive and time consuming. Ultimately, mechanical parameters obtained from the selected intervals are used to calibrate the dynamic parameters. Though rock properties change with the depth, a realistic determination of static values remains a big challenge. In limestone the problem is more severe compared to sandstone. Further, shear wave velocity data is not always available, making the problem more difficult.

1.3 Thesis Objective

The objective of this research study is to explore recent advanced and robust Artificial Intelligence techniques and use them to estimate acoustic velocities and rock mechanical parameters using real field wire line log and laboratory measured core data in the carbonate reservoir formation. More specifically, the objectives of this work are listed below

(1) Develop a new model based on artificial intelligence technique to predict sonic logs for missing intervals, and rock elastic and failure parameters from the basic Well log data.
(2) Assess the best artificial intelligence technique.
(3) Derive Empirical correlation from the artificial intelligence model.
(4) Validate the new correlation with actual measured lab data.
(5) Compared the results with other published correlations.

1.4 Approach

In this thesis, three efficient and latest artificial intelligence techniques are implemented for the prediction of each parameter using MATLAB software. The three techniques were then compared to come up with the best optimized model to predict acoustic values and rock mechanical parameters. Many Artificial Intelligence techniques are available but those that perform better in the oil and gas industry were investigated here. In each AI technique different scenarios were investigated to developed the best architecture for the optimum model. Different wireline logs data were used as the input while the laboratory

data from core tests were used as the target data. Wireline log and core data was obtained from a middle eastern carbonate reservoir.

In order to evaluate the model performance various statistical quality checks were adopted for the purpose of comparison between different AI models. The model with the highest correlation coefficient and minimum error was recommended for future use.

1.5 Thesis Organization

This thesis is prepared according to the guidelines stated by the Deanship of Graduate Studies of King Fahd University of Petroleum & Mineral. It is divided into six chapters as follows:

In chapter one, we presented the introduction, the research objective and the approach of the study.

In chapter two, literature review on the estimation of sonic wave velocities, rock elastic and failure parameters is described with main focus on the application of artificial intelligence techniques for the prediction of these wave velocities and parameters.

Chapter three contains a brief overview of the artificial intelligence techniques used in this study.

In chapter four we described in detail the step by step methodology of the research work.

Chapter five deals with the implementation and comparison of results using ANN, ANFIS and SVM for the prediction of acoustic velocities, elastic parameters and failure parameters.

Chapter six presents the conclusions of this research work along with some recommendations.

CHAPTER 2

LITERATURE REVIEW

This chapter highlights the most commonly used empirical correlations and models to predict acoustic velocities and rock mechanical parameters. The drawbacks and knowledge gap still left after these models or correlations is also presented in brief.

2.1 Estimation of Acoustic Velocities

Compressional and shear wave travel times are very important parameters used in production and exploration geophysics characterization. They are also used to determine rock elastic parameters such as Poisson's ratio and Young's modulus (Abdulraheem et al. 2009 and Edlmann et al. 1999). Rock elastic parameters are critical in alleviating the risks associated with the drilling and Wellbore stability. Therefore, the availability of sonic logs is very important for the development and production phases of hydrocarbon recovery. In some cases, sonic logs are not recorded by oil companies because of cost or time saving purposes. In such cases, these logs are estimated from empirical correlations. Selecting a suitable set of correlations for a given field or specific rock type is of a great

challenge. Poor prediction of sonic logs can result in wrong estimation of rock elastic parameters and therefore can affect severely the heavy investment decisions relied on them.

(Caroll et al. 1969) studied the rocks having Poisson's ratio ranges between 0.22 to 0.28 and developed a correlation to estimate shear wave velocity using compressional wave velocity as an input. Their correlation is valid only for compressional velocity ranges 4000 – 6000 m/sec. Their empirical correlation is given by Eq. 1:

$$V_s = 0.756090x\, V_P^{0.81846} \quad (1)$$

(Castagna et al. 1985 and 1993) stated that the shear velocity can be determined from the compressional velocity using different correlations based on the rock types. Eqs. 2 - 5 are used to determine the shear velocity as a function of compressional velocity for limestone formation, calcareous sandstones, dolomite, and calcareous shale respectively.

$$V_s = -0.05509V_P^2 + 1.0168V_P - 1.0305 \quad (2)$$

$$V_s = 0.8042V_P - 0.8559 \quad (3)$$

$$V_s = 0.583V_P - 0.07776 \quad (4)$$

$$V_s = 0.77V_P - 0.8674 \quad (5)$$

(Eskandari et al. 2004) predicted shear wave velocity from wire line log data using regression and artificial intelligence techniques. They developed the correlation using 35 data points from four different wells in a carbonate formation. They used compressional velocity (Vp), bulk density (RHOB), and Neutron porosity (NPHI) as input parameters (Eq. 6).

$$V_s = 17.0885 + 0.4068 * V_P - 2.1907 * NPHI^2 - 1.1794 * NPHI - 3.2747 * RHOB^2 + 15.3587 * RHOB \quad (6)$$

(Brocher 2005 and 2008) predicted shear wave velocity using compressional wave velocity as given by Eq. 7. His correlation is valid only for compressional velocity ranges 1.5 km/s to 8.5 km/s.

$$V_s = 0.7858 - 1.2344\, V_P + 0.7949\, {V_P}^2 - 0.1238\, {V_P}^3 + 0.006\, {V_P}^4 \quad (7)$$

(Augusto and Martins 2009) predicted compressional wave velocity using non-linear regression technique. The input parameters of their model were gamma ray, effective porosity, shaliness and electrical resistivity. They made 28 empirical correlations similar to Eqs. 8 - 9 where, V_{PO} V_{P1} V_{P2} and V_{P3} depend upon various parameters like clay volume, effective porosity, and resistivity.

$$V_P = V_{P0} + V_{P1} + V_{P2} + V_{P3} \quad (8)$$

$$V_P = V_{P0}\, e^{V_{P1}+V_{P2}+V_{P3}} \quad (9)$$

(Wadhwa et al. 2010) predicted shear wave velocity using compressional wave velocity. They used 185 data points from sandstone formation. Their correlation is valid for the range of 4000 – 6000 m/s of compressional wave velocity and the rocks having Poisson's ratio between 0.22 – 0.28. Their correlation is given by Eq. 10.

$$V_s = 0.9238195^{V_P} \quad (10)$$

(Soltanzadeh 2013) developed a relationship between compressional and shear wave velocities using 207 data points from clastic rocks. Their relationship is given below:

$$V_s = 0.8374 V_P - 1105.2 \quad (11)$$

Using support vector regression (SVR) Maleki et al. (2014) predicted shear wave velocity for carbonate reservoirs. Their model input parameters were Gamma Ray (Gr),

Bulk Density (RHOB), effective porosity, true formation resistivity log (RT), caliper log (Cal), and compressional wave travel time (DT).

2.2 Estimation of Rock Elastic Parameters

Linear elastic behavior of a rock is represented by two parameters, i.e., Young's modulus and Poisson's ratio. These two are the key parameters for making the 1D and 3D geo-mechanical earth model (Chang et al. 2006). Young's modulus is defined as the measure of resistance by an object against being deformed and Poisson's ratio is the ratio of lateral expansion to longitudinal contraction (Howard and Fast 1970).

The static Young's modulus is used to estimate the in-situ stresses and to make geo-mechanical earth model which in turn is needed for fracture mapping and fracture design (Gatens et al.1990). The value of Young's modulus varies with the lithology and rock properties such as bulk density, porosity, pore structure, temperature, pore pressure, fluid saturation, and the rock consolidation (Ameen et al. 2009 and Al-Anazi et al. 2011). Soft formations like shale have a low young's modulus value (0.1-1 MPsi) compared to medium formations like sandstone (2 – 10 MPsi) and hard formation limestone (8 – 12 MPsi) (Howard and Fast 1970). The ranges presented show that there is no typical value of Young's modulus for a given rock and that measuring the Young's modulus is a must in order to conduct the geo-mechanical analysis for the formation of interest. Value of Poisson's ratio for any rock lies in between 0 – 0.5 (Cregger et al. 1984).

Rock elastic parameters calculated from Sonic and density logs give dynamic elastic parameters. There are two ways to measure rock elastic parameters in the lab: (i) the dynamic method in which we measure the ultrasonic compressional (p-wave) and shear

(s-wave) velocities; and (ii) the static method, which is based on the measurement of deformation as a result of the application of a known force. The dynamic elastic moduli and dynamic Poisson's ratio of the rock can be calculated by Eqs. 12 and 13.

$$E_{dyn} = \frac{\rho V_S^{\,2}\left(3V_P^{\,2} - 4V_S^{\,2}\right)}{V_P^{\,2} - V_S^{\,2}} \tag{12}$$

$$\vartheta_{dyn} = \frac{V_P^{\,2} - V_S^{\,2}}{2\left(V_P^{\,2} - V_S^{\,2}\right)} \tag{13}$$

Whereas ρ is the bulk density in g/cc, V_P is the compressional wave velocity in km/s and V_S is the shear wave velocity in km/s. Eq. 12 gives dynamic elastic moduli in Giga pascals (GPa).

For a given rock the static and dynamic moduli always different from each other. Usually dynamic Young's modulus is 1.5 to 3 times greater than static Young's modulus (Larsen et al. 2000 and Abdulraheem et al. 2009). The reason behind this difference is due to the deformation (strain) amplitude between the two types of tests. For the static tests the strain rate is about 10^{-2} s^{-1} or even lower while for the dynamic tests the rate of strain varies from 1 s^{-1} to 10^{-4} s^{-1}. Further, the strain amplitude in dynamic tests is around 10^{-6}-10^{-7} whereas for static tests the amplitude is around 10^{-2}-10^{-3} (Fjaer et al. 1992). The difference between static and dynamic moduli also depends upon the rock minerals and physical origin of the rock. The difference is greater in weak rocks and this difference gets reduced with increasing rock strength (Kings 1983). For example, for a pure homogenous material like steel, the dynamic and static elastic moduli are same (Ledbetter 1993).

Static elastic parameters more truly represent the reservoir rock behavior in the field (Canady et al. 2011); however, retrieving cores throughout the reservoir section and conducting compressional test on rock samples is very expensive and time consuming (Khaksar et al. 2009 and Abdulraheem et al. 2009). Because of high capital investment on retrieving core sample and conducting laboratory tests, quite often few core samples are taken from the depth of interest and then a correlation is developed between log and the core samples that have been retrieved. These log derived correlations are used to calibrate dynamic elastic moduli values to give static moduli values throughout the depth of reservoir section (Gatens et al. 1990 and Abdulraheem et al. 2009). However, the applicability of each of these model and correlations is limited to specific rock type under certain conditions.

(Belikov et al. 1970) developed a correlation for microcline and granite rock to estimate the static Young's modulus from the dynamic one. (Gorjainov et al. 1979) introduced two relationships valid for clays and wet soils. The equation proposed by (McCann and Entwisle 1992) is valid for Jurassic granites. The correlation given by (Morals and Marcinew 1993) can be used to estimate static Young's modulus for high permeable rocks. (Bradford et al. 1998) formulated the Young's modulus correlation dependent on dynamic Young's modulus as given by Eq. 14.

$$E_{st} = 0.4145\, E_{dyn} - 1.0593 \tag{14}$$

(Kings 1983) established a correlation for E_{static} using $E_{dynamic}$ for igneous and metamorphic rocks which is given by Eq. 15.

$$E_{st} = 1.26\, E_{dyn} - 29.5 \tag{15}$$

(Eissa and Kazi 1988) used 714 data points from the literature and developed a correlation for static Young's modulus with dynamic Young's modulus and density as input (Eq. 16).

$$\log_{10} E_{st} = 0.02 + 0.77 \log_{10}(\gamma E_{dyn}) \quad (16)$$

(Wang 2000) developed correlations for static Young's modulus valid for hard and soft rocks (Eq. 17).

$$E_{st} = 1.26\, E_{dyn} - 15.2 \quad (17)$$

(Canady 2011) used non-linear regression technique on several data points and developed a correlation for E_{static} using $E_{dynamic}$ (Eq. 18).

$$E_{st} = \frac{\ln\left[\left(E_{dyn} + 1\right) * \left(E_{dyn} - 2\right)\right]}{4.5} \quad (18)$$

Based on 45 core data points from limestone formation Najebi et al. (2015) introduced a new correlation between static Young's modulus and compressional wave velocity as given by Eq. 19.

$$E_{st} = 0.169 * V_P{}^{3.24} \quad (19)$$

Whereas ρ is the bulk density in g/cc, V_P is the compressional wave velocity in km/s. Eq. 19 gives static Young's modulus in Giga pascals (GPa).

(Abdulraheem et al. 2009) used artificial neural network to predict static Young's Modulus using bulk density and compressional time. They used only 77 data points to build the model.

(Bandar et al. 2011) estimated static Young's modulus using artificial neural network technique. The input parameters of their model were porosity, bulk density, compressional time, shear time, pore pressure, minimum horizontal stress and over

burden stress. They built the model on 600 data points. The main disadvantage of their model was that it depends upon pore pressure, minimum horizontal stress and over burden stresses as one of the purpose of finding static Young's modulus is to find these parameters.

(Al-Anazi et al. 2010) used support vector machine to predict static Young's modulus and Poisson's ratio. The input data for their models were porosity, bulk density, minimum horizontal stress, pore pressure, over burden stress, compressional wave velocity and shear wave velocity. They used 600 data points to build their model and used fuzzy ranking system to rank influential input parameters to predict static Young's modulus and Poisson's ratio. The main disadvantage of their model is that it is depend upon minimum horizontal stress, pore pressure and over burden stress whereas minimum horizontal stress, pore pressure and over burden stress usually predict from the elastic parameters.

(Asoodeh et al. 2013) used committee machine intelligence system to predict Poisson's ratio using 600 data points from carbonate reservoir. He implemented multistage technique, in first stage he predicted shear wave travel time from Well logs and in next stage he used predicted shear wave travel time log with other Well logs as an input parameter to predict Poisson's ratio.

2.3 Estimation of Failure Parameters

Failure parameters define the physical strength of the rock. There are three failure criteria for rock namely; Mohr's Coulumb criterion, the modified Lade criterion (Ewy 1998) and

(Drucker Prager 1952) criterion. The commonly used Mohr's Coulumb failure criteria is given by Eq. 20

$$\sigma_1 = \mathrm{UCS} + \sigma_3 * \tan^2(45 + \varphi/2) \quad (20)$$

Where φ is the material property termed as angle of internal friction and UCS is unconfined compressive strength.

Phi (φ) is defined as the angle measured from horizontal of the plane along which shear failure occurs in a triaxial testing on a core sample. φ also measures the effect of rock strength on confining pressure. Higher the value of angle of internal friction the more the rock is sensitive towards confining pressure.

UCS defines the strength of the rock when subjected to uniaxial loading. It is the maximum axial compressive stress that a right-cylindrical sample of material can withstand under unconfined conditions when the confining stress is zero.

Cohesion is the strength or force that hold sand grains together.

In laboratory the failure parameters can be determined directly only by static methods whereas elastic parameters can be determined by static and dynamic methods both (Jaeger et al. 2007).

The failure parameters can be obtained from the laboratory based triaxial or uniaxial compressional tests on a perfectly right cylindrical cores retrieved from the depth of interest. However, most of the time the core samples are not available. In such a case empirical correlations are used that relates geophysical logs with failure parameters. Uniaxial compressive strength, friction angle and cohesion are the most important failure

parameters for any geo-mechanical modeling. Therefore, finding the appropriate correlations for these parameters is very essential for any realistic analysis.

Several researchers have developed the correlations for failure parameters. (Freyberg et al. 1972) developed empirical correlation to relate the UCS with compressional wave velocity. His correlation is given by Eq. 21

$$\mathrm{UCS} = 0.035\ \mathrm{V_P} - 31.5 \tag{21}$$

where UCS is in MPa and V_p in km/s

(Militizer et al. 1973) developed the correlation for UCS using compressional wave travel time. His correlation has limited range of application and is valid for carbonate rocks only, Eq. 22

$$\mathrm{UCS} = \left(\frac{7682}{\Delta t}\right)^{1.82} \tag{22}$$

where UCS is in MPa and Δt in μs/ft.

(Golubev et al. 1976) developed a correlation for UCS valid for limestone only using compressional wave travel time (Eq. 23)

$$\mathrm{UCS} = 10^{\left(2.44+{}^{109.14}/_{\Delta t}\right)} \tag{23}$$

where UCS is in MPa and Δt in μs/ft.

Inoue and (Ohomi et al. 1981) studied many weak rocks to develop relation between UCS and basic well logs including; P-wave velocity and density. Their empirical relation for UCS is given by Eq. 24

$$\mathrm{UCS} = \mathrm{k}\ \rho\ \mathrm{V_P}^2 + \mathrm{A} \tag{24}$$

where ρ is bulk density in g/cc, V_p is compressional wave velocity in km/s and UCS in kg/cm^2.

(McNally et al. 1987) studied fined grained, both consolidated and unconsolidated rocks with wide range of porosity values, to develop the correlation between UCS and compressional wave travel time given by Eq. 25

$$\mathrm{UCS} = 1200\exp^{(-0.036\Delta t)} \tag{25}$$

where UCS is in MPa and Δt in μs/ft.

For weak and unconsolidated sands (McNally et al. 1987) developed the correlation for UCS given by Eq. 26

$$\mathrm{UCS} = 1.413\mathrm{x}10^{7}\Delta t^{-3} \tag{26}$$

(Fjaer 1992) studied sandstones and developed the correlation for UCS using bulk density and compressional wave velocity. His correlation is given by Eq. 27

$$\mathrm{UCS} = 3.3\ \mathrm{x}10^{-20}\rho^{2}{V_P}^{4}[(1+v)/(1-v)^{2}] * (1-2v)\left[1+0.78 * v_{clay}\right] \tag{27}$$

(Venik et. al 1993) used rock porosity to determine UCS given by Eq. 28

$$\mathrm{UCS} = 254\ (1-2.7\emptyset)^{2} \tag{28}$$

(Moos et al. 1999) developed the correlation between bulk density and compressional wave velocity given by Eq. 29. Their correlation is valid for sandstones only.

$$\mathrm{UCS} = 1.745\ \mathrm{x}\ 10^{-9}\ \rho\ V_P - 21 \tag{29}$$

where UCS is in MPa, Density g/cc and Vp in km/s

(Bradford et al. 1998) developed the relation between UCS and Young's modulus given by Eq. 30 valid for all type of rocks

$$\mathrm{UCS} = 2.28 + 4.1089\ \mathrm{E} \tag{30}$$

where UCS is in MPa, static Young's modulus E in GPa.

(Kharaman et al. 2001) proposed empirical correlation for UCS which depend upon compressional wave velocity. He made his correlation on 27 data points only and got R^2 of 0.5 between actual and predicted UCS. This low value of R^2 shows that his correlation is not reliable. Kharaman correlation is given by Eq. 31

$$\mathrm{UCS} = 9.95\ \mathrm{V_P}^{1.21} \tag{31}$$

Chang et al. (2006) developed the UCS correlation for sandstone and limestone given by Eqs. (32 and 33).

$$\mathrm{UCS} = 277\exp^{(-10\emptyset)} \tag{32}$$

$$\mathrm{UCS} = 13.8\ \mathrm{E}^{0.51} \tag{33}$$

where UCS is in MPa, static Young's modulus E in GPa.

(Chang et al. 2006) also studied several empirical correlations for sandstone, limestone and shale to predict unconfined compressive strength and angle of internal friction. They applied some of the studied correlations using the published data and found that some of these correlations work reasonably good and rest of them made poor prediction. They concluded that calibration with respect to lead rocks is always required before using any of the published correlations.

(Lal 1999) proposed the new empirical correlation for angle of internal friction using compressional wave velocity. His correlation is valid for shale formation only, given by Eq. 34

$$\emptyset = \mathrm{Sin}^{-1}[(\mathrm{V_P} - 1000)/(\mathrm{V_P} + 1000)] \tag{34}$$

(Weingartens and Parkin 1995) developed a linear correlation between angle of internal friction and porosity. Their correlation is valid for sandstone formation, given by Eq. 35

$$\emptyset = 57.8 - 105 * \text{Porosity} \tag{35}$$

(Chang et al. 2006) proposed a correlation between angle of internal friction and gamma ray log for shaly sedimentary rocks, given by Eq. 36

$$\emptyset = \tan^{-1}\left(\frac{(\text{GR} - \text{GR}_{\text{sand}})\mu_{\text{shale}} + (\text{GR}_{\text{shale}} - \text{GR})\mu_{\text{sand}}}{\text{GR}_{\text{shale}} - \text{GR}_{\text{sand}}}\right) \tag{36}$$

2.4 Knowledge Gap

2.4.1 Acoustic Wave Travel Time Prediction Knowledge Gap

It is clear from the literature survey of the acoustic velocity estimation that most of the empirical correlations were developed to predict shear wave velocity using compressional wave velocity. There is no correlation developed to estimate shear wave velocity independent of compressional wave velocity. To bridge the knowledge gap, different AI techniques (ANN, ANFIS, and SVM) were used to predict compressional and shear wave travel times, and their performance was compared on the basis of correlation coefficient and absolute percentage error (between actual real field and predicted data). The one which performed better is recommended for future use.

2.4.2 Elastic Parameters Prediction Knowledge Gap

In the light of vast literature survey of elastic parameters, till now there is no general empirical correlation to calculate the Poisson's ratio directly from the basic well logs. Most of the presented correlations in the literature for static Young's modulus depends upon the dynamic Young's modulus except Najebi et al. (2015). To bridge the knowledge gap, different AI techniques were used to achieve following objectives:

(1) Develop a new models based on artificial intelligence techniques to estimate the static Young's modulus and Poisson's ratio directly from the well log.

(2) Assess the best artificial intelligence technique.

(3) Derive empirical correlation from the artificial intelligence model to make a prediction in new well without using AI software.

(4) Validate the new model on measured lab or published data.

2.4.3 Failure Parameters Prediction Knowledge Gap

From the literature survey of failure parameters prediction, it is clearly observed that the empirical correlations developed to predict UCS are mainly depend on static Young's modulus or compressional wave travel time. The behavior of UCS function is very complex, one variable as an input is not enough to capture the highly complex and non-linear nature of UCS.

There is no correlation for cohesion with wireline log is reported in the literature. For friction angle the correlations reported in the literature are valid only for shale and sandstones.

2.5 Quality Measurement using Statistics

To compare the accuracy and performance of the proposed model with other models from the literature, various statistical checks were performed, which are as follows:

2.5.1 Goodness of fit tests

There are several ways to measure the goodness of fit tests such as normal probability distribution curves, coefficient of kurtosis and skewness, plots of estimated versus residual variables, frequency histograms, and correlation coefficient cross plots. Correlation coefficient is represented by (CC or R). The equation to find CC is given by Eq. 37.

$$CC = \frac{k\sum xy - (\sum x)(\sum y)}{\sqrt{k(\sum x^2) - (\sum y)^2}\sqrt{k(\sum b^2) - (\sum b)^2}} \tag{37}$$

CC measures the strength of linear dependency between two variables. The value of CC always lies in between -1 and 1, value of zero shows poor dependency while the value of -1 and 1 values shows strong correlation. Value of -1 shows strong inverse relation while +1 show strong direct relation between two variables. Square of CC is coefficient of determination R^2. In this work cross plots with R^2 are used to evaluate goodness of fit tests.

2.5.2 Error measurement

Several methods for error measurement are available such as root mean squared error (RMSE), mean squared error (MSE), average absolute percentage error (AAPE), mean absolute error (MAE). In this work, two type of errors (RMSE and AAPE) are used to evaluate the performance of model. These error types are defined by Eq. 37 and 38.

$$RMSE = \sqrt{\frac{\sum(a_i - b_i)^2}{n}} \tag{37}$$

$$AAPE = \frac{\sum | (x_i - y_i) | \, x \, \frac{100}{x_i}}{k} \tag{38}$$

2.5.3 Standard Deviation

Standard deviation shows the deviation of the data from its mean value, given by Eq. 39

$$SD = \sqrt{\frac{1}{n}\sum_{n=1}^{N}(X - \overline{X})^2} \tag{39}$$

CHAPTER 3

ARTIFICIAL INTELLIGENCE TECHNIQUES

3.1 What is Artificial Intelligence?

Artificial Intelligence is the science or art to perform the tasks that normally require human intelligence, such as image processing, speech recognition, visual perception, translation between languages, and decision-making. It is usually recognized as the study and design of intelligent agents. By artificial intelligence any non-linear function can be captured when there is no relation exists between input and output space.

Currently, many artificial intelligence tools are available. The following artificial intelligence techniques were used to achieve the objective of this research study:

1- Artificial Neural network (ANN).
   - Feed Forward Neural Network (FFNN)
   - Radial Basis Back Propagation Neural Network (RBNN)
2- Adaptive Neuro Fuzzy Inference System (ANFIS).
3- Support vector machine (SVM).

3.1.1 Artificial Neural Network

Artificial Neural network (ANN) is a powerful statistical tool. Its uses are found in many small and industrial scale applications, in order to recognize and classify complex patterns or systems (Huang Z 1996 and Castillo 2012). ANN is inspired from biological neurons that are found in human brain (Graves et.al 2009). The beauty of this technique is that it does not need any physical phenomenon that describes the system under study (Lippmann 1987). It has the capability to approximate any non-linear complex function between input and output parameters.

Many researchers have applied ANN in petroleum engineering especially in the field of rock mechanics (Abdulraheem et al. 2009, Cranganu et al. 2015, Huang et al 1996, Kumoluyi and Daltaban 1994 and Rammay M. H. et al. 2016).

ANN models are structured on many components such as hidden layers, number of neurons, learning algorithm, transfer function (between hidden layers and output layer) and epoch size (Abdulraheem et al 2009). The ANN network model comprises of at-least three layers, input layer, hidden layer and output layer as shown in Fig 3.1. Each layer connects with other layers by the help of weights.

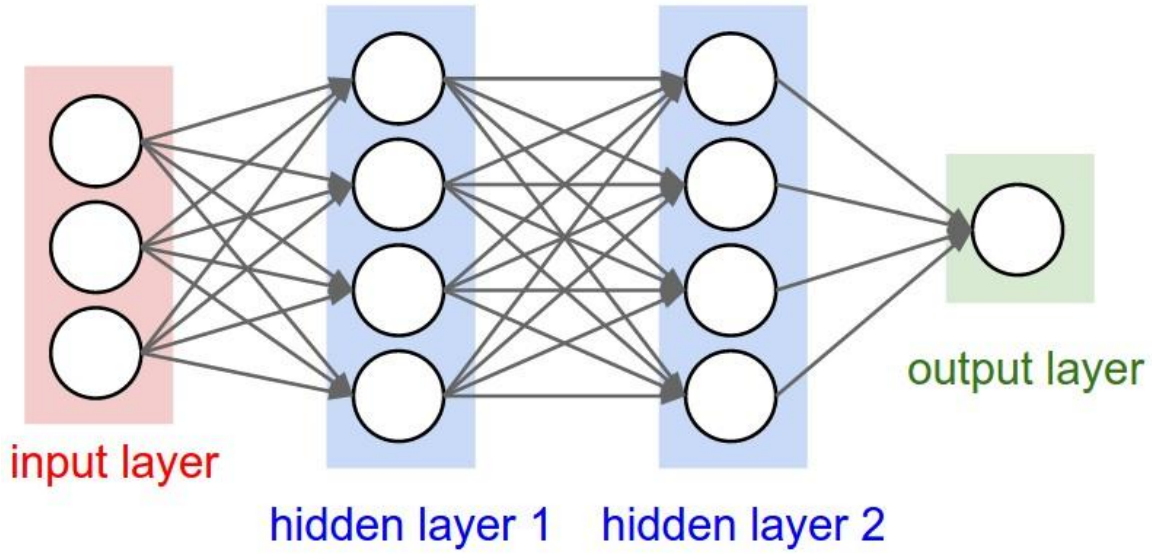

Figure 3. 1 Typical structure of two layers Neural Network model.

The network performance is based on the adjustment of weights and biases between the hidden layers. The number of hidden layers, number of neurons in each layer and training functions associated with each layer also plays a vital role in model prediction performance (Hinton et al 2006 and Mohaghegh 2000). Hidden layers assigned with 'log-sigmoidal' or 'tan-sigmoidal' type transfer function. Output layer is assigned with 'pure linear' activation function. All the data goes in to the model is by default normalized between the value of -1 and 1 (Niculescu SP 2003).

The first step is the training of the network; data are process through the input layer to hidden layer(s) then all the way to the output layer. In the output layer the data is compared with the actual data. The difference between actual and predicted data is transferred back to the model to update the individual weights and biases between each connection. This process is called epoch. In this way training continues for all the data set until the average error reduce to certain defined limit (S.S. Liew, et al. 2015).

Fewer number of neuron causes under-fitting and excessive number of neurons cause over-fitting, so optimization is required for the selecting the appropriate number of neurons (Hinton et al 2006). Increasing the size of the model by increasing the number of hidden layer neuron not only increases the computational time but can also cause data memorization which resulted in poor prediction during testing of unseen data (Wang 2015). Too much training also causes over fitting (Sadra et al 2015). In over-training the model performance is absolutely accurate when it reproduces the data on which it is trained but it loses all its generalization capabilities when it is tested on unseen data. In order to alleviate over fitting "early stopping" criteria are recommended by dedicating certain portion of the data for validation purposes (Constantin et al 2015). It is very necessary to evaluate when to stop the training and move towards testing and validation phases. During training of the AI model, initially both training and validation errors shows decreasing trend and it keeps on decreasing until over fitting starts, when overfitting starts the validation error goes high while training error continuously goes down with the passage of time, the time when the validation and training errors start separating each other is the optimum time to stop the training as shown in Fig 3.2. At this optimum time the weights and biases obtained are accurate for certain set of neural network conditions.

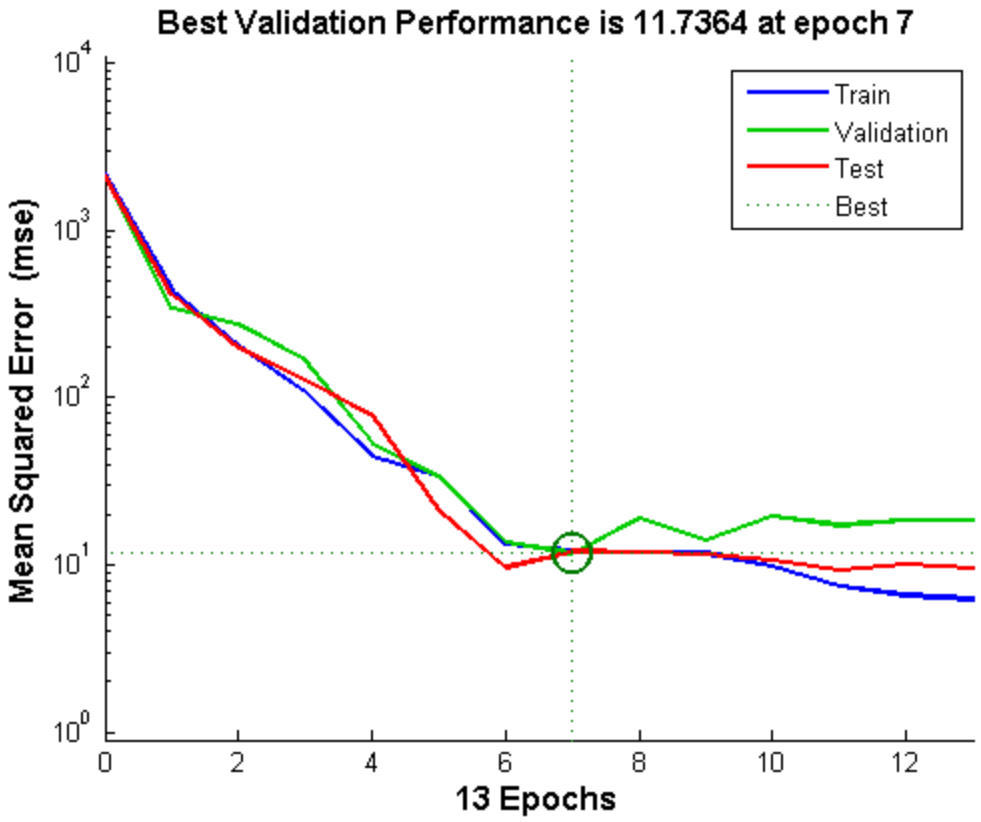

Figure 3. 2 Optimum Condition of Neural Network.

3.1.1.1 Feed Forward Neural Network (FFNN)

In feed forward neural network the information moves only in one direction i.e. in the forward direction for example from input layer to hidden layer(s) then all the way to the output layer.

3.1.1.2 Radial Basis Function Neural Network (RBF).

For interpolation in multidimensional space, radial basis back propagation neural networks served as a powerful technique. In RBF the information moves in the cycles and the hidden layers assigned with the Gaussian type activation function. RBF works better when the number of neurons in the hidden layers are equal to the number of number of data points (Hinton et al. 2006).

3.1.2 Adaptive Neuro Fuzzy Inference System (ANFIS)

ANFIS is the combination of neural network and fuzzy logic and it is very robust supervised learning technique. It is the kind of neural network that uses Sugeno fuzzy inference system (Jang et al. 1993). ANFIS has the capability to extract the benefits of both mentioned AI techniques in a single platform (Tahmasebi et al. 2012). In order to get best out of this technique one should use any evolutionary algorithm to optimize the parameters of ANFIS (Tahmasebi et al. 2012).

ANFIS maps input parameters to input membership functions, converting input membership functions to set of fuzzy rules, converting set of fuzzy rules to an output characteristic, then convert output characteristics to output membership functions and finally this membership function to one valued output or any classification based on output. In ANFIS instead of just fixing the shape of membership function, by analyzing the data it automatically assigned the type and shape of membership function. Fig 3.3 shows the typical structure of five layered ANFIS model.

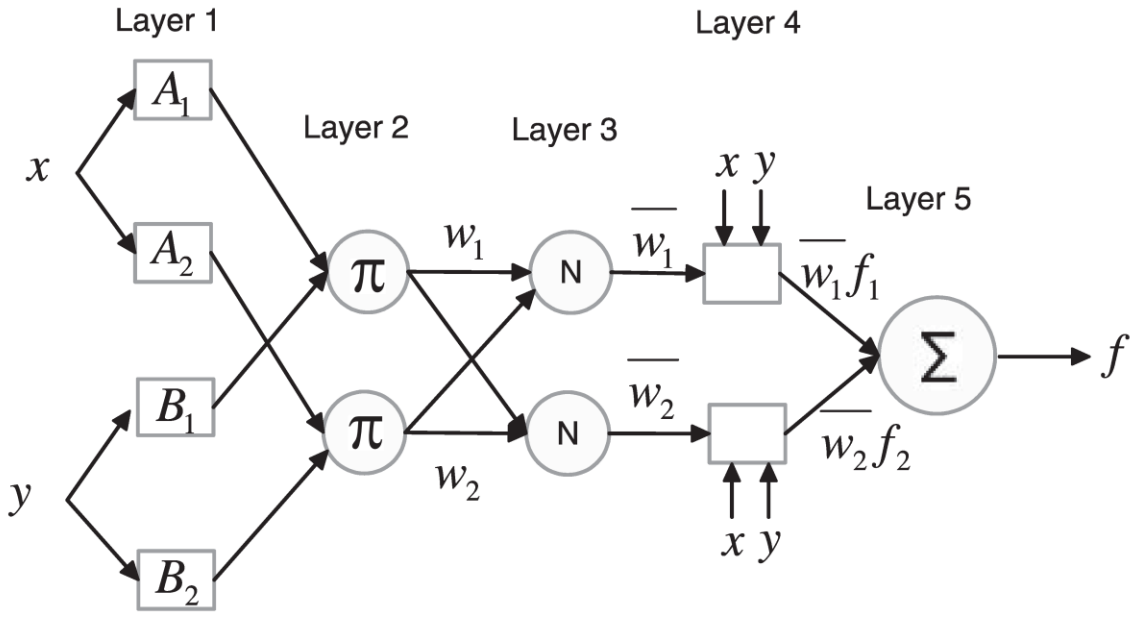

Figure 3. 3 ANFIS Structure (Al-Hmouz).

3.1.3 Support Vector Machine (SVM)

Support Vector machine is the type of supervised learning that is mostly used for regression and pattern recognition purposes. Based on soft margin hyper-plane and structure risk minimization, support vector machine have been introduced as new artificial intelligence tool framework for both classification and function approximation. Instead of sigmoidal type transfer function like in artificial neural network, support vector machine stands on the kernel neuron function which definitely allows projection to higher planes and able to solve more complicated and complex highly nonlinear problems. SVM applications can be found in many fields like medical, business, civil and electrical engineering.

A good characteristic of SVM worth mentioning at this point is its “stability”. This is a characteristic that ensures that once the data set is fixed, running it several times will always produce the same results unlike the Neural Networks that will be generating

different results for difference runs even when the data set is fixed. Even when SVM is run on different data set arrangement from same set, it will still arrive at results with very small ranges of values. Moreover, SVM can be able to handle large features space, it can effectively avoid over fitting by limiting the margin, identify automatically a small subsets of useful information that are called as support vectors (Sunday 2010).

The use of SVM proposed here is interesting and challenging as it is related to oil and gas, which is characterized by scarcity of data thereby making it difficult to find sufficient amount of data set for training and testing a model. However, several research outcomes have demonstrated SVM as a potential extreme machine learning technique to produce relatively accurate predictions based on training with very small data sets.

3.2 Summary of AI Techniques

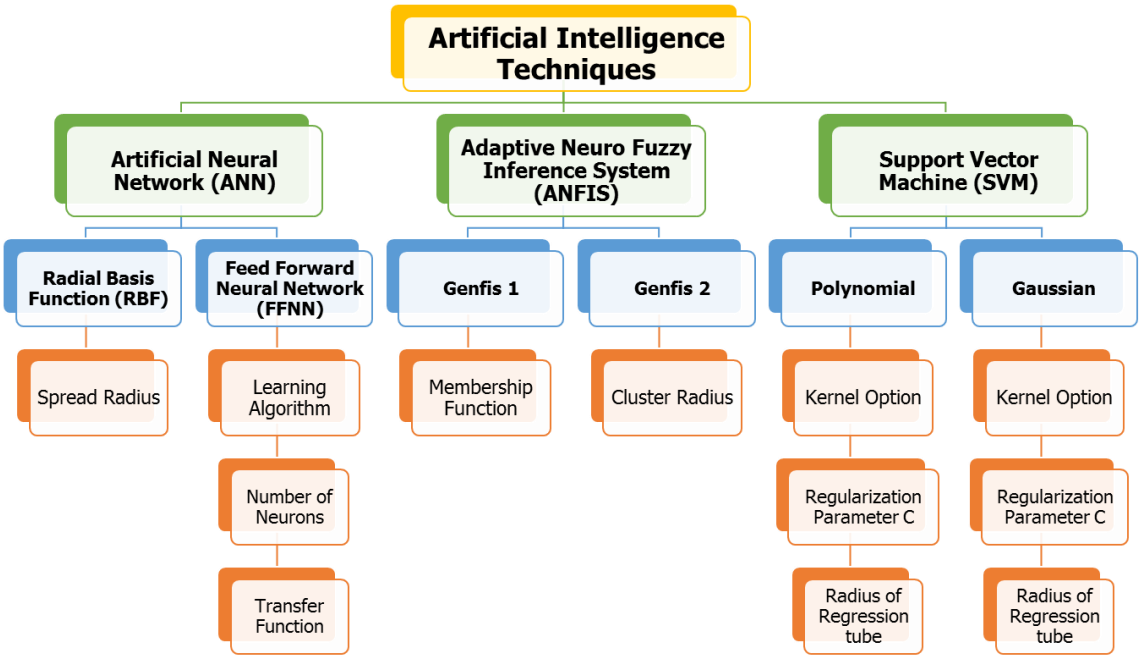

Figure 3. 4 Summary of AI techniques implemented.

CHAPTER 4

METHODOLOGY

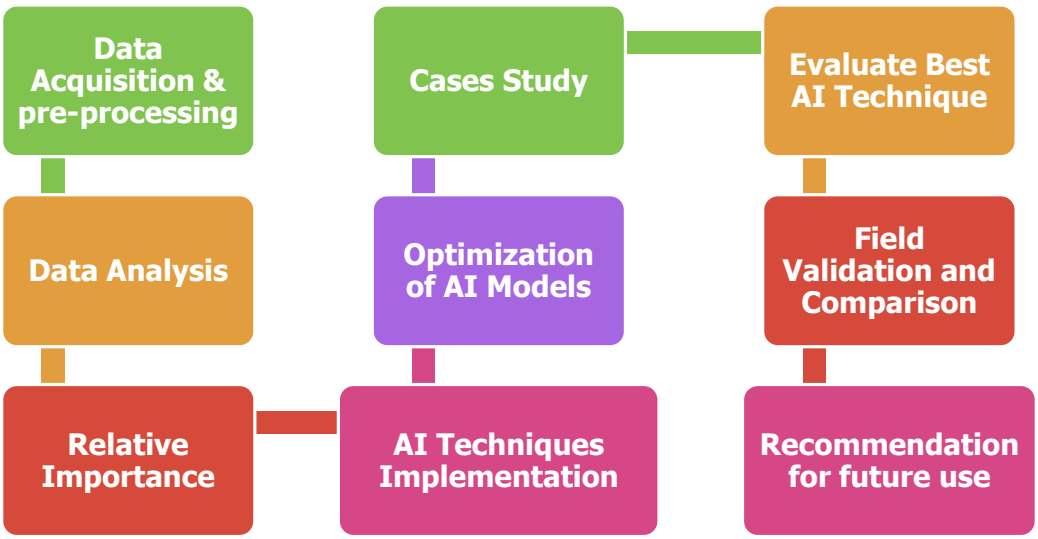

Figure 4. 1 Streamline of the proposed models.

4.1 Data Acquisition & Processing

Data pre-processing is the vital step before feeding any data to the AI models. This can improve the prediction performance of the AI models. Their predictive performance also

depends on the quality of the data (Al-Anazi et al. 2011). Core and well log data sets are highly confidential in petroleum industry in addition to that obtaining mechanical parameters from laboratory using triaxial tests are very rare due to high sophistication and high cost. For elastic and failure parameter study, core and well log data set served as an input parameter while for acoustic wave model well log data served as the input parameter.

The first step taken was to match the log data depth with the exact core retrieval depth. Log data were taken at 0.5 feet intervals which may not match the depth of the core plugs. To measure the depth shift, plot of log and lab values of GR and porosity were analyzed to visualize difference in depths. This is necessary because depth measured for log values using cables is not the same as that measured from the number of drill strings and core lengths for core data. The depth shift correction was added to core data as follows:

$$\mathrm{Depth}_{\mathrm{Log}} = \mathrm{Depth}_{\mathrm{Core}} + \mathrm{Depth}_{\mathrm{Shift}} \tag{38}$$

The wireline log data consist of: gamma ray, bulk density, neutron porosity, true porosity, compressional and shear wave velocities. Core data consists of static Young's modulus, Poisson's ratio, unconfined compressive strength, angle of internal friction and cohesion.

4.2 Data Analysis

This steps involves defining the complete statistical description of the data sets that were used to make the models. Statistical description includes maximum, minimum, range, skewness, kurtosis, variance and standard deviation. This research work involves the development of three main parameters (acoustic velocities, rock elastic parameter and rock failure parameter) with sub-category of each parameter i.e. acoustic velocities

(compressional and shear wave velocities), elastic parameter (static Young's modulus and Poisson's ratio) and failure parameters (unconfined compressive strength, angle of internal friction and cohesion). Three different separate sets of data were used to make these models.

4.3 Relative Importance

This step involves defining the relative importance of each input parameter with the target variable by the help of linear regression correlation coefficient analysis given by Eq. 40.

$$CC = \frac{k\sum xy - (\sum x)(\sum y)}{\sqrt{k(\sum x^2) - (\sum y)^2}\sqrt{k(\sum b^2) - (\sum b)^2}} \tag{40}$$

Inserting all the available parameter in AI model to serve as an input parameter does not always guaranteed good results rather this strategy some time makes the model performance worse, so it is always the best practice to find which input parameter is more influential by means of correlation coefficient between input variable and target variable. This analysis gives preliminary idea about the input variable selection.

4.4 Applying Artificial Intelligence Techniques

After determining the initial best input parameters for the corresponding output variable. Next step is to apply the artificial intelligence techniques. Three AI techniques implemented namely; ANN, ANFIS and SVM. MATLAB software were used to execute these techniques.

4.5 Optimization of AI Models

An individual parametric study was performed on each AI technique to enhance the model prediction capabilities. A small script inside MATLAB was developed to search for the combination of the optimum model parameters by doing the sensitivity of each technique parameters. The sensitivity of each technique parameter is then presented in tabular form with correlation coefficient and average absolute percentage errors for both training and testing phases. The purpose is to find each technique optimum parameters. Several cases were performed to arrive at the optimum parameter values of each technique which led to the optimum model.

4.6 Cases Study

After performing the parametric analysis, several cases were run with different combinations of input parameters and with different functional links in different domains (logarithmic or exponential). The purpose was to find the optimal input parameters.

4.7 Evaluate Best Technique

After several cases were studied, the next step was to compared each technique models on the basis of correlation coefficient and average absolute percentage error.

4.8 Field Validation and Comparison with Commercial Correlations

This step was designed to evaluate the generalization capabilities of the optimum models by testing them on real field data, which was totally unseen by the model. To test the accuracy and performance of the proposed models with the commonly used empirical

correlations in the oil industry, the proposed model predictions were compared with the empirical correlations predictions on unseen data set.

CHAPTER 5

RESULTS AND DISCUSSIONS

This chapter describes the results of the study which is based on the application of various AI techniques on the prediction of acoustic velocities and rock mechanical parameters. The results of each technique are discussed here to develop an optimum model.

5.1 Acoustic Waves Travel Time Prediction

Acoustic waves are compressional and shear waves. To predict the travel time of these waves, three different artificial intelligence techniques were used, namely, Artificial Neural Networks (ANNs), Adaptive Neuro Fuzzy Inference System (ANFIS), and Support Vector Machines (SVM).

5.1.1 Data Analysis for Acoustic Wave Travel Time Model

Geophysical well log data were used for the prediction. The data set consists of gamma ray, bulk density, neutron porosity, and true porosity logs. 6000 data points were obtained from 10 different wells. Most of the data was from a limestone formation with a low

percentage of sandstone and had some gas effects as shown in Fig 5.1. 70% of the total data was randomly selected using MATLAB command for training of the model. The remaining 30% of the data was used for testing. Table 5.1 shows the complete description of the training/testing datasets. Data were stratified randomly in such a way that the testing data lied within the boundaries of the training data set.

Table 5.1 Statistical analysis of the data used for acoustic velocities prediction.

Parameters	Max	Min	Mean	Range	St. Deviation	Skewness	Kurtosis
Gamma Ray (API)	166.08	5.02	36.05	166.08	17.059	1.652	6.475
Bulk Density (g/cc)	3.02	1.81	2.613	1.21	0.181	-.699	.296
Neutron Porosity (V/V)	0.43	-0.01	0.0785	0.44	0.181	1.424	1.653
True Porosity (V/V)	0.287	-0.019	0.068	0.306	0.095	3.0291	13.0641
Compressional Time (µs/ft.)	109.392	25.467	55.798	83.924	9.278	1.4383	2.1519
Shear Time (µs/ft.)	176.335	71.407	105.020	104.927	16.679	1.3403	1.8521

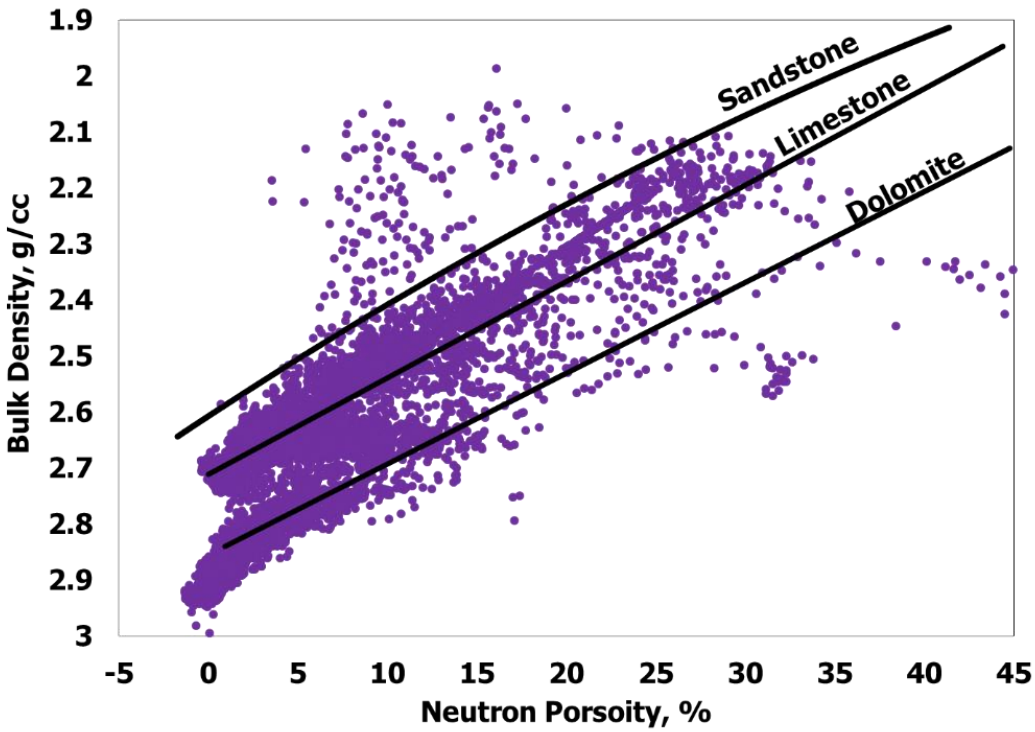

Figure 5. 1 Acoustic wave model cross plot (density & neutron porosity) for the lithology identification.

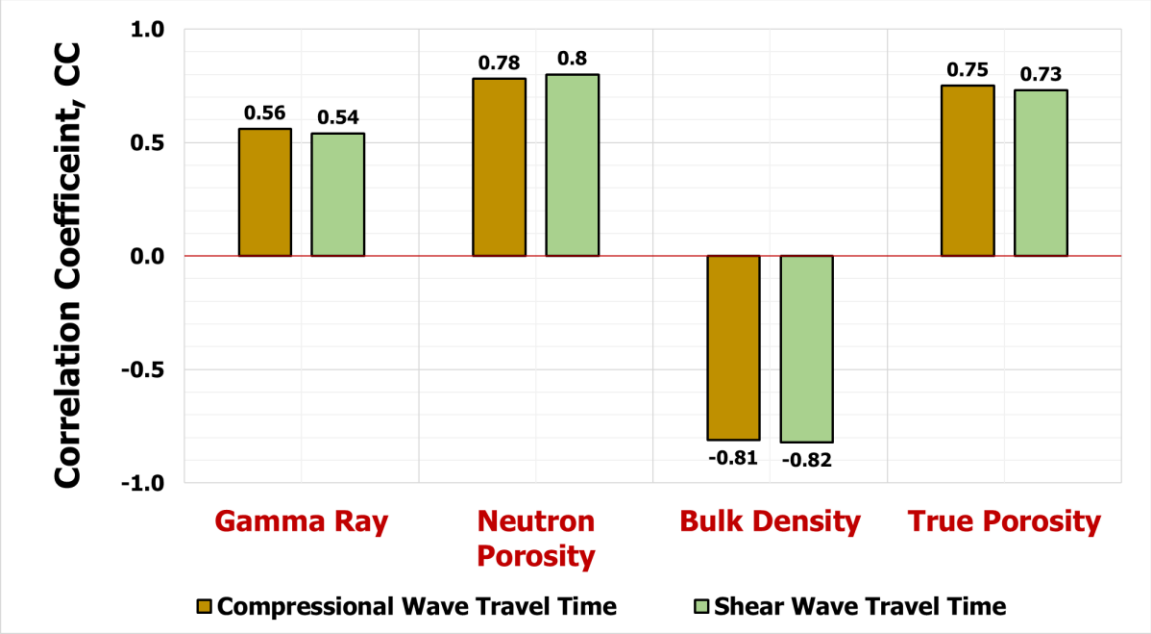

Figure 5.2 Relative importance of basic well logs with the compressional and shear wave travel time.

5.2 Modeling for Compressional Wave Travel Time Prediction

5.2.1 Results from ANN to Predict Compressional Wave Travel Time

Two types of ANN techniques were implemented to predict compressional wave travel time, namely, Feed Forward Neural Network (FFNN) and Radial Basis Function (RBF).

Table 5.2 shows the performance of FFNN and RBF. During training, FFNN model gave an AAPE of 2.584 and a RMSE of 1.918 while RBF gave an AAPE of 4.415 and a RMSE of 3.63. During testing, FFNN model gave AAPE of 2.478 and RMSE of 1.811 while RBF model gave AAPE of 4.66 and RMSE of 3.46. On comparing the coefficient of determination, FFNN produced a value of 0.959 during training and 0.967 during testing while RBF produced 0.853 during training and 0.879 during testing. From this comparison it is clear that FFNN performed better than RBF.

Table 5.2 Performance of FFNN and RBF to predict compressional wave travel time.

ANN Type	Training Set				Testing Set			
	AAPE	RMSE	CC	R^2	AAPE	RMSE	CC	R^2
Feed Forward Network (FFNN)	2.584	1.918	0.979	**0.959**	2.478	1.811	0.983	**0.967**
Radial Basis Function (RBF)	4.415	3.636	0.924	0.853	4.66	3.46	0.938	0.879

The performance of FFNN highly depends upon the type of learning algorithm. Table 5.3 shows the comparison of the performances of various learning algorithms in FFNN for the prediction of compressional wave travel time. It is evident from Table 5.3 that Levenberg Marquardt learning algorithm in FFNN gave less AAPE, less RMSE and the highest coefficient of determination.

Table 5.3 Performance of different types of learning algorithm in FFNN.

Training Algorithm		Training Set				Testing Set			
Name	Syntax	AAPE	RMSE	CC	R^2	AAPE	RMSE	CC	R^2
Gradient descent	traingdx	5.00	4.23	0.90	0.80	4.76	4.07	0.91	0.83
Quasi Newton	trainbfg	4.37	3.53	0.93	0.86	4.27	3.42	0.94	0.88
Resellient Propagation	trainrp	3.54	2.78	0.96	0.91	3.31	2.49	0.97	0.94
Levenberg Marquardt	trainlm	2.58	1.92	0.98	0.96	2.48	1.81	0.98	0.97
FP Conjugate gradient	traincgf	3.48	2.76	0.96	0.92	3.27	2.58	0.97	0.93
PR Conjugate gradient	traincgp	3.68	2.89	0.95	0.91	3.44	2.67	0.96	0.93
One Step Secant	trainoss	3.80	3.03	0.95	0.90	3.62	2.83	0.96	0.92

Apart from the learning algorithm, the performance of FFNN also depends upon the number of neurons in the hidden layer. Table 5.4 shows the results of sensitivity to the number of neurons from 5 to 20. It also shows that when the number of neurons was set to be 20, the model gave the highest R2 with minimum AAPE as well as RMSE, during both the training and testing phases.

Table 5.4 Sensitivity of neurons used in FFNN to predict compressional wave travel time.

Number of Neurons	Training Set				Testing Set			
	AAPE	RMSE	CC	R^2	AAPE	RMSE	CC	R^2
5	3.005	2.257	0.971	0.944	2.862	2.137	0.977	0.954
6	3.519	2.511	0.965	0.930	3.365	2.341	0.972	0.945
7	2.770	2.046	0.977	0.954	2.693	1.961	0.981	0.962
8	2.765	2.054	0.976	0.953	2.680	1.951	0.981	0.962
9	2.613	1.923	0.979	0.959	2.508	1.814	0.984	0.967
10	2.994	2.171	0.974	0.948	2.894	2.083	0.978	0.957
11	2.521	1.831	0.981	0.963	2.457	1.761	0.985	0.969
12	2.584	1.918	0.979	0.959	2.478	1.811	0.983	0.967
13	2.581	1.898	0.980	0.960	2.551	1.843	0.983	0.966
14	2.598	1.906	0.980	0.960	2.479	1.807	0.984	0.968
15	2.656	1.947	0.979	0.958	2.585	1.897	0.982	0.964
16	2.478	1.815	0.982	0.964	2.403	1.744	0.985	0.970
17	2.633	1.941	0.979	0.958	2.553	1.850	0.983	0.966
18	2.482	1.801	0.982	0.964	2.449	1.753	0.985	0.969
19	2.501	1.862	0.981	0.962	2.482	1.804	0.984	0.968
20	2.388	1.765	0.983	0.966	2.347	1.716	0.985	0.971

After finding the optimum neural network type, learning algorithm, and optimum number of neurons, the next step was to select the optimum number of inputs. Table 5.5 shows the performance of models with different number of input parameters. The model with three input parameters, namely, gamma ray, bulk density, and neutron porosity gave the lowest AAPE, lowest RMSE and highest R^2 both during training and testing phases.

Table 5.5 Model performance with different number of input parameters.

Number of Inputs	Training Set				Testing Set			
	AAPE	RMSE	CC	R^2	AAPE	RMSE	CC	R^2
4(PHIT, GR, RHOB, NPHI)	3.667	5.456	0.951	0.905	3.557	5.276	0.961	0.923
3(GR, RHOB, NPHI)	2.584	1.918	0.979	0.959	2.478	1.811	0.984	0.967
2(RHOB, NPHI)	5.000	4.227	0.896	0.803	4.760	4.071	0.914	0.835

From the sensitivity analysis, the best neural network model type was found to be FFNN with one hidden layer, 20 neurons in the hidden layer, three input parameters, and with levenberg Marquadt as the learning algorithm. This network can be nomenclated as 3-20-

1, where '3' represents number of input parameters, '20' represent number of neurons and '1' represents one output variable.

5.2.2 Results from ANFIS to Predict Compressional Wave Travel Time

Two types of ANFIS techniques were implemented to predict compressional wave travel time, namely, Genfis1 (Grid Partitioning) and Genfis2 (Subtractive Clustering).

Table 5.6. shows the performance of Genfis 1 and Genfis 2.

Table 5.6 Performance of Genfis 1 and Genfis 2 to predict compressional wave travel time.

ANFIS Type	Training Set				Testing Set			
	AAPE	RMSE	CC	R^2	AAPE	RMSE	CC	R^2
Genfis1 (Grid Partitioning)	8.454	6.988	0.833	0.693	9.655	7.898	0.821	0.674
Genfis2 (Subtractive Clustering)	3.396	2.754	0.959	0.919	3.176	2.436	0.967	0.936

Genfis2 was selected as the best ANFIS type to predict compressional wave travel time on the basis of minimum error and highest coefficient of determination. Further, the performance of Genfis 2 depends on the size of cluster radius. Table 5.7 lists the sensitivity results of radius size from very small size of 0.1 to a large size of 0.45 and it was found that the optimum radius size was 0.25.

Table 5.7 Radius size sensitivity to predict compressional wave travel time.

Radius Size	Training Set				Testing Set			
	AAPE	RMSE	CC	R^2	AAPE	RMSE	CC	R^2
0.1	3.8187	3.826396	0.9186	0.8439	3.7319	3.6848	0.9233	0.8526
0.15	2.8523	2.112862	0.9759	0.9524	2.7917	2.0857	0.9761	0.9528
0.2	3.5284	2.779378	0.9579	0.9176	3.3645	2.6252	0.9619	0.9252
0.25	3.3956	2.754169	0.9587	0.9191	3.1764	2.4360	0.9674	0.9358
0.3	3.4261	2.770966	0.9582	0.9181	3.2238	2.4688	0.9664	0.9340
0.35	4.1787	3.194285	0.9440	0.8912	4.0395	2.9792	0.9507	0.9039
0.4	4.2525	3.234904	0.9425	0.8884	4.1104	3.0206	0.9493	0.9011
0.45	4.1406	3.160964	0.9452	0.8934	3.9962	2.9368	0.9522	0.9066

After finding the optimum ANFIS type and the size of cluster radius, the next step was to find the optimum number of inputs. Table 5.8 shows the performances of the models with different number of input parameters and it was found that the optimum number of inputs was three, namely, gamma ray, bulk density, and neutron porosity to predict compressional wave travel time.

Table 5.8 Model performance with different number of input parameters.

Number of Inputs	Training Set				Testing Set			
	AAPE	RMSE	CC	R^2	AAPE	RMSE	CC	R^2
4(PHIT, GR, RHOB, NPHI)	3.667	5.456	0.951	0.905	3.557	5.276	0.961	0.923
3(GR, RHOB, NPHI)	3.39	2.75	0.95	**0.92**	3.17	2.43	0.967	**0.9358**
2(RHOB, NPHI)	5.000	4.227	0.896	0.803	4.760	4.071	0.914	0.835

5.2.3 Results from SVM to Predict Compressional Wave Travel Time

In SVM there are two types of kernel functions, polynomial and Gaussian. Table 5.9 shows the performances of polynomial and Gaussian type kernel functions.

Table 5.9 Performance of different kernel functions in SVM.

SVM Kernel type	Training Set				Testing Set			
	AAPE	RMSE	CC	R^2	AAPE	RMSE	CC	R^2
Polynomial	7.09	10.19	0.86	0.74	7. 93	12.13	0.82	0.672
Gaussian	4.09	7.19	0.92	0.846	4.39	8.13	0.899	0.808

During training of SVM model, 'Gaussian' type kernel function gave 4.09 AAPE, 7.19 RMSE and 0.92 R^2 while 'Polynomial' type kernel function produced high AAPE of 7.09, high RMSE of 10.2 with low R^2 of 0.74. During testing on unseen data 'Gaussian' type kernel function gave 4.39 AAPE, 8.13 RMSE and 0.808 R^2, while 'Polynomial' type kernel function gave 7.93 AAPE, 12.13 of RMSE and 0.672 R^2 value. Based on these results 'Gaussian' type kernel function was selected as the best kernel option in SVM to

predict compressional wave travel time. Furthermore, the performance of SVM model depends upon the size of regularization parameter.

Table 5.10 Sensitivity of regularization parameter used in SVM to predict compressional travel time.

Regularization Parameter C	Training Set				Testing Set			
	AAPE	RMSE	CC	R^2	AAPE	RMSE	CC	R^2
250	3.81	3.82	0.91	0.84	3.73	3.68	0.92	0.85
500	2.85	2.11	0.97	0.95	2.79	2.08	0.97	0.95
1000	3.52	2.77	0.95	0.91	3.36	2.62	0.96	0.92
2500	4.09	7.19	0.92	0.84	4.39	8.13	0.89	0.80
5000	10.42	12.77	0.85	0.72	10.22	12.46	0.86	0.73

Table 5.11 Model performance with different number of input parameters.

Number of Inputs	Training Set				Testing Set			
	AAPE	RMSE	CC	R^2	AAPE	RMSE	CC	R^2
4(PHIT, GR, RHOB, NPHI)	13.667	15.456	0.851	0.705	13.557	15.276	0.861	0.723
3(GR, RHOB, NPHI)	2.85	2.11	0.97	0.95	2.79	2.08	0.97	0.95
2(RHOB, NPHI)	5.000	4.227	0.896	0.803	4.760	4.071	0.914	0.835

From Table 5.10 and Table 5.11 the optimum size of regularization parameter was found out to be 500 with three input parameters, namely, gamma ray, bulk density and neutron porosity.

5.2.4 Comparison of Three AI techniques on prediction of Compressional Wave Travel Time

Fig. 5.3 compares the training and testing performances of optimum models of three artificial intelligence techniques used, namely, ANN, ANFIS and SVM. From this comparison it is apparent that ANN performs better than SVM and ANFIS to predict compressional wave travel time.

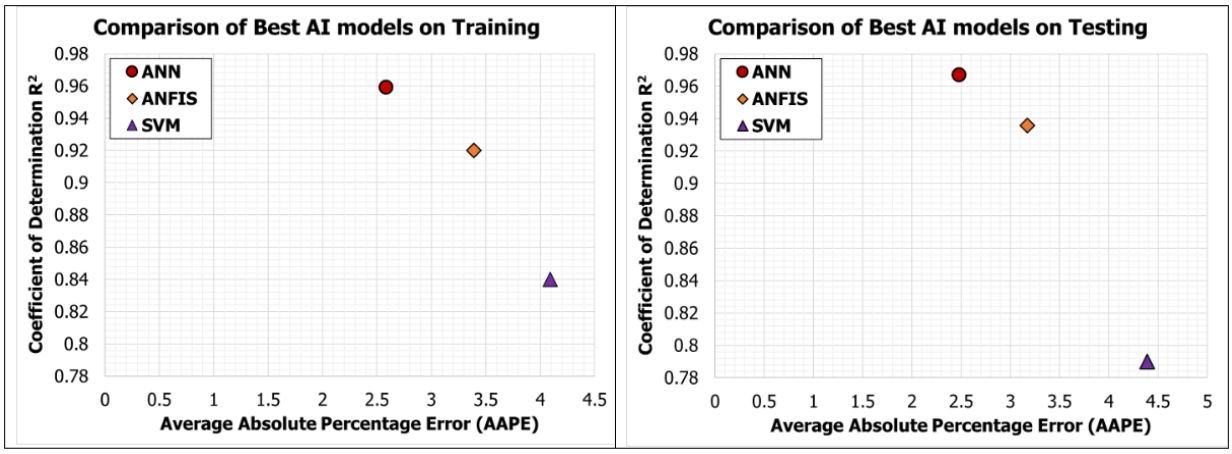

Figure 5.3 Performance Comparison of best AI models for the prediction of Compressional wave travel time.

Fig. 5.4 shows the comparison of three techniques on the complete profile prediction of compressional wave travel time on selected data which is totally unseen by the model. On the basis of minimum AAPE, minimum RMSE and highest coefficient of determination, ANN was proposed as the best AI model to predict compressional wave travel time. The complete architecture of ANN model is given in Table 5.12.

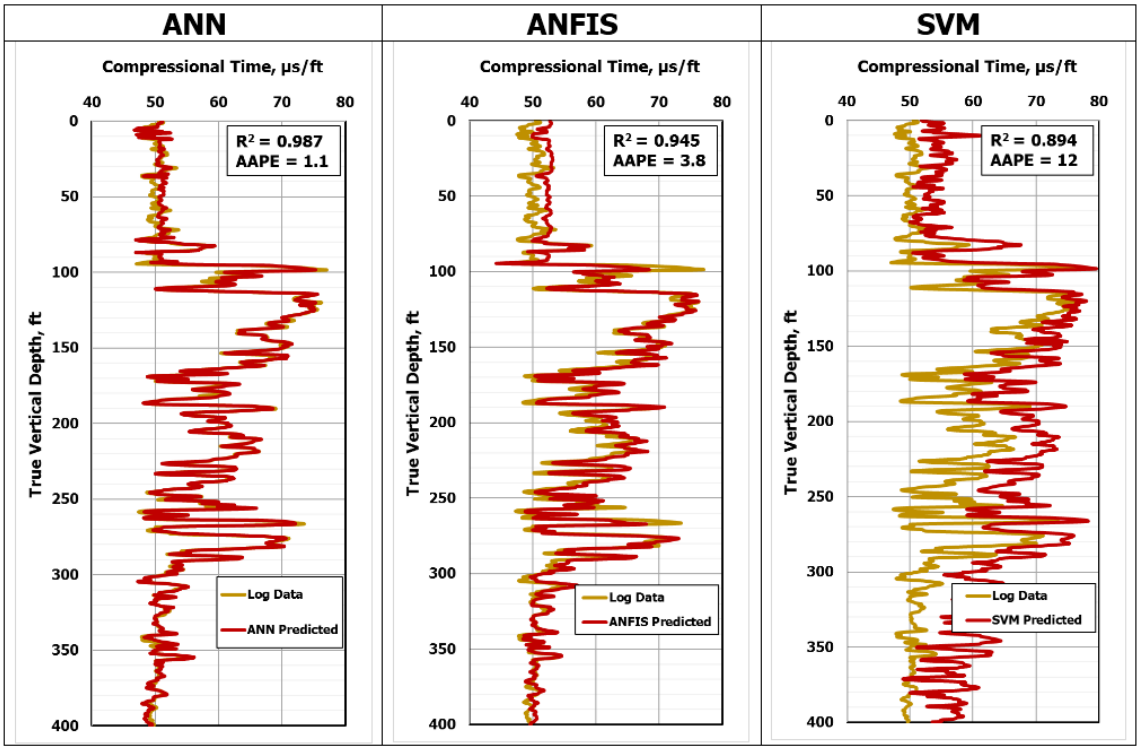

Figure 5.4 Comparison of best AI techniques to predict compressional wave travel time on complete log profile.

Table 5.12 ANN Architecture of Compressional wave travel time model.

Neural Network Parameters	Ranges
Number of Inputs	3
Number of Outputs	1
Number of Neurons	20
Number of Hidden Layer(s)	1
Training Algorithm	Levenberg Marquadt
Learning rate	0.12
Hidden Layer transfer function	Tan-sigmoidal
Outer layer transfer function	pure linear
Training Ratio	0.7
Testing Ratio	0.15
Validation Ratio	0.15

5.2.5 Empirical Model for Compressional Wave Travel Time

The empirical model is derived from the ANN model based on weights and biases associated with input layer/hidden layers and hidden layer/outer layer. The weights

between input layer and hidden layer termed as w_1 and weights between hidden layer and outer layer termed as w_2 are given in Table 5.13. The proposed compressional wave travel time ANN based empirical model is given below

$$\Delta t_{C_n} = \left[\sum_{i=1}^{N} w_{2_i}\left(\frac{2}{1+e^{-2\left(w_{1_{i,1}}\,GR_n + w_{1_{i,2}}\,\varphi_n + w_{1_{i,3}}\rho_n + b_{1_i}\right)}}\right)\right] + b_2 \tag{41}$$

Steps to use New Empirical Model for Compressional Wave Travel Time

Step 1: Normalize the input parameters between the range [-1 1] before using Eq. 41. Normalization is done by point slope form given by Eq. 42 and Eq. 43:

$$\frac{Y - Y_{min}}{Y_{max} - Y_{min}} = \frac{X - X_{min}}{X_{max} - X_{min}} \tag{42}$$

where Ymin = -1, Ymax =1, and X is the input parameter, X_{min} is the input parameter minimum value and X_{max} is the input parameter maximum value.

$$Y = 2 \times \left(\frac{X - X_{min}}{X_{max} - X_{min}}\right) - 1 \tag{43}$$

Step 2: Use Eq. 40 to calculate Δt_{Cn} in normalized form, using the weights given in Table 5.13. The sequence of parameters that goes into the model is given as: gamma ray, neutron porosity, and bulk density.

Step 3: To convert the value of Δt_{Cn} into the real valued form, the result must be de-normalized by applying Eq. 44.

$$\Delta t_C = \frac{(109.392 - 25.467)(\Delta t_{C_n} + 1)}{2} + 25.467 \tag{44}$$

Table 5.13 Weights and biases of ANN based compressional wave travel time empirical model.

Hidden Layer Neurons (N)	Weights between Input and Hidden Layer (w_1)			Weights between Hidden and output Layer (w_2)	Hidden Layer Bias (b_1)	Output Layer Bias (b_2)
1	-0.0375	-1.0995	4.7410	-2.1731	4.3043	-0.3798
2	-1.8232	-3.6434	-0.7333	-0.2977	3.2252	
3	-0.2044	0.5682	-6.1148	-1.6546	-4.9375	
4	-0.3437	2.7500	-3.7933	1.1876	6.5117	
5	2.2407	-5.3837	-8.0596	3.2823	-1.6383	
6	3.9178	10.0096	-2.2949	0.1212	0.0494	
7	-1.3631	0.6755	-3.4047	-0.7403	1.8188	
8	-0.2610	-3.3011	1.3398	-0.6291	-2.2036	
9	6.3474	5.1628	-8.6115	0.1828	-1.9126	
10	4.0993	4.8877	-0.0301	-0.1372	-0.4212	
11	3.0527	-0.8434	0.2768	-1.8622	0.8415	
12	1.9346	-4.8391	-7.9978	3.1392	-0.7600	
13	2.6749	-0.5177	0.6309	2.2400	0.9395	
14	-3.0562	1.2932	-5.9422	0.0875	-2.4007	
15	-0.8546	-5.0713	1.6422	0.3639	-3.5923	
16	-6.2034	1.0298	1.4586	0.4515	-4.9256	
17	-0.5708	1.0649	3.8518	-0.6595	-0.6938	
18	1.0434	0.2768	7.6444	-0.4534	-3.3759	
19	-1.8046	4.4306	7.0072	6.9310	1.0492	
20	-0.4036	3.2168	2.7338	-0.3659	2.3343	

5.3 Modeling for Shear Wave Travel Time Prediction

5.3.1 Results from ANN to Predict Shear Wave Travel Time

Two types of ANN techniques were implemented to predict shear wave travel time, namely, FFNN and RBF. Table 5.14 shows the performance of FFNN and RBF. During training FFNN produced an AAPE of 2.38 and a RMSE of 3.15 while RBF model produced an AAPE of 4.953 and RMSE of 6.875. During testing, FFNN produced AAPE of 2.43 and a RMSE of 3.22 while RBF produced the AAPE of 4.906 and 6.732 RMSE. FFNN produced the R^2 value of 0.97 during training and 0.97 during testing while RBF

gave 0.848 during training and 0.8723 during testing. From this comparison it was obvious that FFNN performed better than RBF in predicting shear wave travel time.

Table 5.14 Performance of FFNN and RBF to predict shear wave travel time.

ANN Type	Training Set				Testing Set			
	AAPE	RMSE	CC	R^2	AAPE	RMSE	CC	R^2
Feed Forward Neural Network (FFNN)	2.38	3.15	0.98	0.97	2.43	3.22	0.99	0.97
Radial Basis Function (RBF)	4.953	6.875	0.921	0.848	4.906	6.732	0.934	0.8723

The performance of FFNN highly depends upon the type of learning algorithm. Table 5.15 shows the comparison of different types of learning algorithms used to train the FFNN model to predict shear wave travel time.

Table 5.15 Performance of different types of learning algorithm in FFNN.

Training Algorithm		Training Set				Testing Set			
Name	Syntax	AAPE	RMSE	CC	R^2	AAPE	RMSE	CC	R^2
Gradient descent	traingdx	5.36	7.84	0.90	0.80	5.30	7.90	0.91	0.83
Quasi Newton	trainbfg	3.60	5.26	0.95	0.91	3.50	5.02	0.96	0.93
Resellient Propagation	trainrp	2.94	4.20	0.97	0.94	2.96	4.03	0.98	0.95
Levenberg Marquardt	trainlm	2.38	3.15	0.98	0.97	2.43	3.22	0.99	0.97
Fletcher Powell Conjugate gradient	traincgf	3.44	4.59	0.97	0.93	3.42	4.57	0.97	0.94
Polak Ribiere Conjugate Gradient	traincgp	3.40	4.52	0.97	0.93	3.45	4.55	0.97	0.94
One Step Secant	trainoss	3.67	5.46	0.95	0.90	3.56	5.28	0.96	0.92

From Table 5.15 it is observed that Levenberg Marquardt learning algorithm gives less AAPE, less RMSE and highest R^2 as compared to other learning algorithms. Apart from learning algorithm, the performance of FFNN is highly dependent upon the number of neurons in the hidden layer. Table 5.16 shows of sensitivity of the number neurons from 5 to 20.

Table 5.16 Sensitivity of number of neurons used in FFNN to predict shear wave travel time.

Number of Neurons	Training Set				Testing Set			
	AAPE	RMSE	CC	R^2	AAPE	RMSE	CC	R^2
5	2.718	3.708	0.978	0.956	2.740	3.694	0.981	0.962
6	2.952	4.046	0.973	0.948	2.984	4.048	0.977	0.954
7	2.835	3.734	0.977	0.955	2.881	3.826	0.979	0.959
8	2.728	3.838	0.976	0.953	2.711	3.847	0.979	0.959
9	2.546	3.371	0.982	0.964	2.614	3.506	0.983	0.966
10	2.410	3.219	0.983	0.967	2.410	3.199	0.986	0.971
11	2.503	3.382	0.982	0.963	2.506	3.477	0.983	0.966
12	2.383	3.150	0.984	0.968	2.431	3.219	0.985	0.971
13	2.491	3.405	0.981	0.963	2.539	3.308	0.985	0.969
14	2.676	4.099	0.973	0.947	2.734	3.778	0.980	0.960
15	2.393	3.201	0.983	0.967	2.413	3.257	0.985	0.970
16	2.427	3.226	0.983	0.967	2.447	3.312	0.985	0.969
17	2.343	3.077	0.985	0.970	2.389	3.200	0.986	0.971
18	2.562	3.457	0.981	0.962	2.644	3.598	0.982	0.964
19	2.229	2.905	0.986	0.973	2.268	2.980	0.988	0.975
20	2.513	3.321	0.982	0.965	2.582	3.455	0.983	0.967

Table 5.16 shows that for 19 neurons the model gave the highest R2 with minimum AAPE and minimum RMSE, during both training and testing phases.

After determining the optimum neural network type, learning algorithm, and optimum number of neurons in the hidden layer, the next step was to select the optimum number of inputs. Table 5.17 shows the performance of the model with different number of input parameters.

Table 5.17 Model performance with different number of input parameters.

Number of Inputs	Training Set				Testing Set			
	AAPE	RMSE	CC	R^2	AAPE	RMSE	CC	R^2
4(PHIT, GR, RHOB, NPHI)	3.600	5.264	0.955	0.911	3.495	5.015	0.964	0.930
3(GR, RHOB, NPHI)	2.383	3.150	0.984	0.968	2.431	3.219	0.985	0.971
2(RHOB, NPHI)	5.362	7.841	0.896	0.804	5.302	7.903	0.909	0.826

Three input parameters, namely, gamma ray, bulk density and neutron porosity produced lowest AAPE, lowest RMSE and highest R^2 both during training and testing.

From the sensitivity analysis, the best neural network model was found to be FFNN with one hidden layer and 19 neurons in the hidden layer, three input parameters and with Levenberg Marquadt as a learning algorithm. This network can be nomenclated as 3-19-1, where '3' represents number of input parameters, '19' represent number of neurons and '1' represents one output variable.

5.3.2 Results from ANFIS to Predict Shear Wave Travel Time

Table 5.18 shows the comparison of Genfis1 and Genfis2 to predict shear wave travel time. Genfis2 produced less AAPE, less RMSE and high R^2 as compared to Genfis1 as shown in Table 5.18. Genfis2 was selected as the best ANFIS type to predict shear wave travel time. Also, the performance of Genfis2 depends upon the sensitivity of radius that is used to make the data clusters. Table 5.19 lists the sensitivity results of the radius from a small size of 0.1 to a large size of 0.45.

Table 5.18 Performance of different ANFIS types to predict shear wave travel time.

ANFIS Type	Training Set				Testing Set			
	AAPE	RMSE	CC	R^2	AAPE	RMSE	CC	R^2
Genfis1 (Grid Partitioning)	12.560	10.789	0.787	0.619	13.560	11.789	0.708	0.501
Genfis2 (Subtractive Clustering)	3.313	4.630	0.967	0.953	3.192	4.386	0.970	0.959

Table 5.19 Radius sensitivity used in Genfis 2 to predict shear wave travel time.

Radius Size	Training Set				Testing Set			
	AAPE	RMSE	CC	R^2	AAPE	RMSE	CC	R^2
0.1	3.537	6.440	0.934	0.872	3.469	6.060	0.942	0.887
0.15	2.888	4.142	0.973	0.947	2.804	3.890	0.977	0.955
0.2	3.243	4.612	0.967	0.935	3.121	4.349	0.971	0.943
0.25	3.313	4.630	0.967	0.935	3.192	4.386	0.970	0.941
0.3	3.147	4.634	0.967	0.935	3.072	4.292	0.971	0.943
0.35	3.162	4.517	0.968	0.937	3.031	4.272	0.972	0.945
0.4	4.286	5.746	0.948	0.899	4.206	5.425	0.954	0.910
0.45	4.084	5.699	0.949	0.901	3.966	5.349	0.955	0.912

From cluster radius sensitivity given in Table 5.19, it was found that the optimum radius size is 0.35. After determining the optimum ANFIS type and the size of cluster radius, the next step was to select the optimum number of inputs. Table 5.20 shows the performance of the model with different number of input parameters.

Table 5.20 Model performance with different number of input parameters.

Number of Inputs	Training Set				Testing Set			
	AAPE	RMSE	CC	R^2	AAPE	RMSE	CC	R^2
4(PHIT, GR, RHOB, NPHI)	3.667	5.456	0.951	0.905	3.557	5.276	0.961	0.923
3(GR, RHOB, NPHI)	3.162	4.517	0.968	0.93	3.031	4.272	0.94	0.88
2(RHOB, NPHI)	5.000	4.227	0.896	0.803	4.760	4.071	0.914	0.835

From Table 5.20 it is clear that the optimum number of inputs were three, namely, gamma ray, bulk density, and neutron porosity

5.3.3 Results from SVM to Predict Shear Wave Travel Time

Table 5.21 compares the performances of polynomial and Gaussian type kernel functions in SVM technique. During training and testing the Gaussian type kernel function, produced less AAPE, less RMSE and high R^2 as compared to the polynomial type kernel function as shown in Table 5.21. Furthermore, the performance of SVM model depends upon the sensitivity of regularization parameter.

Table 5.21 Performance of different kernel functions in SVM.

SVM Kernel type	Training Set				Testing Set			
	AAPE	RMSE	CC	R^2	AAPE	RMSE	CC	R^2
Polynomial	9.09	13.19	0.88	0.76	9. 93	14.13	0.86	0.69
Gaussian	3.09	6.19	0.93	0.85	3.39	7.13	0.9	0.81

Table 5.22 Regularization parameter sensitivity used in SVM to predict shear wave travel time.

Regularization Parameter C	Training Set				Testing Set			
	AAPE	RMSE	CC	R^2	AAPE	RMSE	CC	R^2
250	8.89	9.72	0.86	0.71	8.72	9.68	0.85	0.70
500	12.85	22.11	0.77	0.55	12.79	22.08	0.72	0.50
1000	3.52	2.77	0.85	0.71	3.36	2.62	0.96	0.92
2500	3.09	6.19	0.93	0.85	3.39	7.13	0.9	0.81
5000	4.42	3.77	0.91	0.83	3.2	3.96	0.92	0.86

Table 5.23 Model performance with different number of input parameters.

Number of Inputs	Training Set				Testing Set			
	AAPE	RMSE	CC	R	AAPE	RMSE	CC	R
4(PHIT, GR, RHOB, NPHI)	3.667	5.456	0.951	0.905	3.557	5.276	0.961	0.923
3(GR, RHOB, NPHI)	3.09	6.19	0.93	0.85	3.39	7.13	0.9	0.81
2(RHOB, NPHI)	5.000	4.227	0.896	0.803	4.760	4.071	0.914	0.835

5.3.4 Comparison of Three AI techniques on prediction of Shear Wave Travel Time

Fig 5.5 compares the training and testing performances of optimum models of three artificial intelligence techniques used, namely, ANN, ANFIS and SVM. From this comparison it is apparent that ANN performs better than SVM and ANFIS to predict shear wave travel time. Fig 5.6 shows the comparison of three techniques on the complete profile prediction of shear wave travel time on selected data which is totally unseen by the model. On the basis of minimum AAPE, minimum RMSE and highest coefficient of determination, ANN was proposed as the best AI model to predict shear wave travel time. The complete architecture of ANN model is given in Table 5.24.

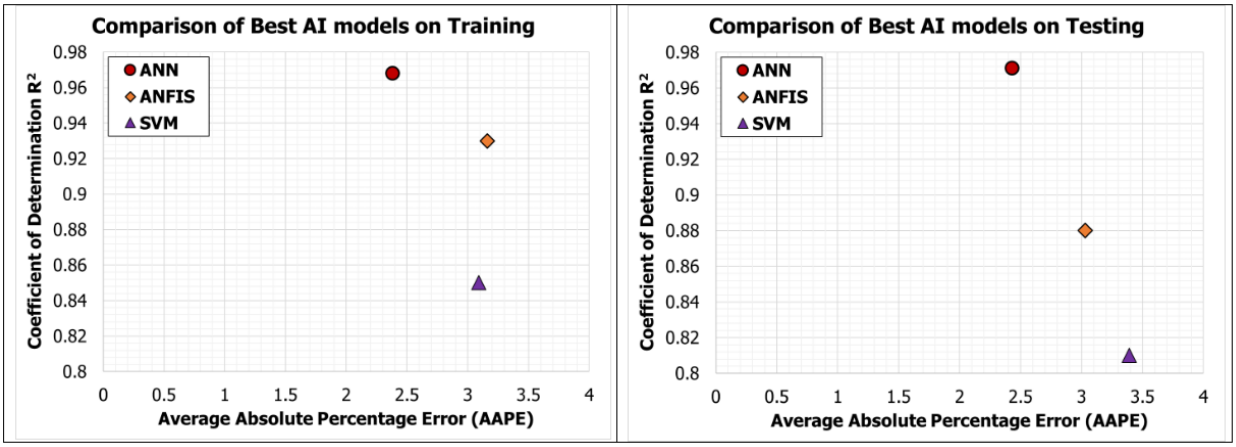

Figure 5. 5 Performance comparison of best AI models for the prediction of shear wave travel time.

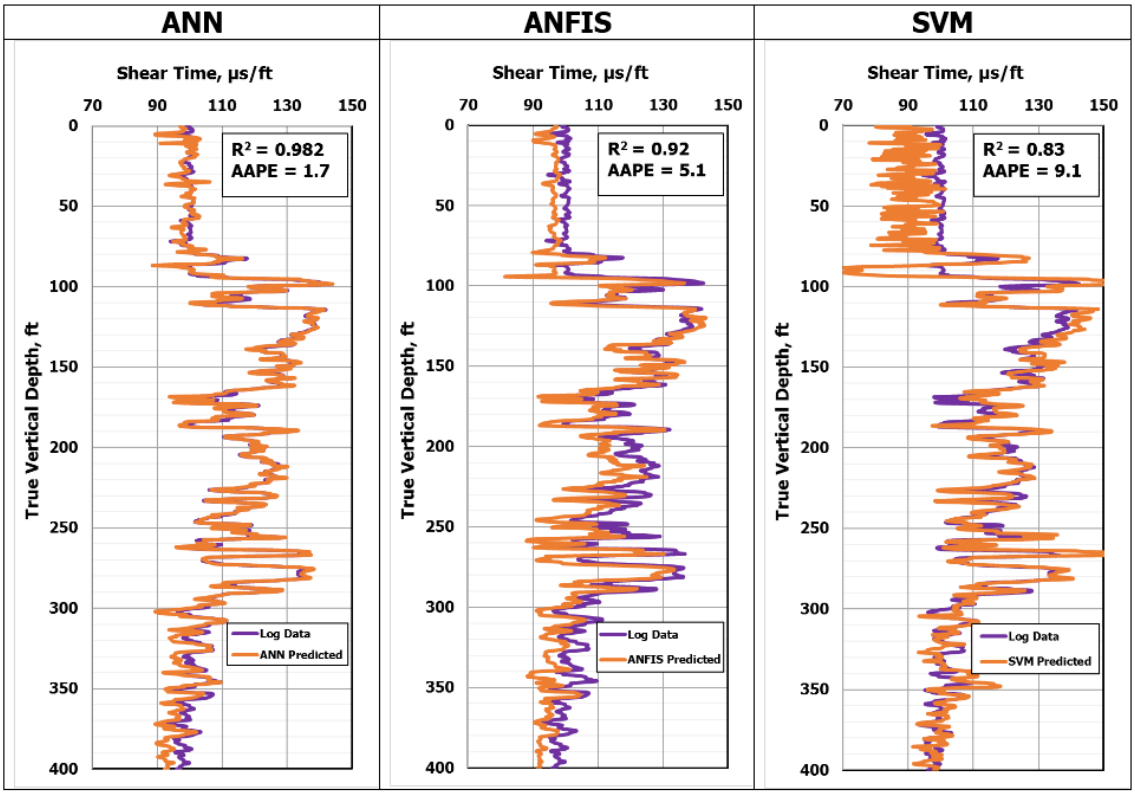

Figure 5.6 Comparison of the best AI techniques to predict shear wave travel time on complete log profile.

The complete architecture of ANN model is given in Table 5.24

Table 5. 24 ANN Architecture of Shear wave travel time model.

Neural Network Parameters	Ranges
Number of Inputs	3
Number of Outputs	1
Number of Neurons	20
Number of Hidden Layer(s)	1
Training Algorithm	Levenberg Marquadt
Learning rate	0.12
Hidden Layer transfer function	Tan-sigmoidal
Outer layer transfer function	pure linear
Training Ratio	0.7
Testing Ratio	0.15
Validation Ratio	0.15

5.3.5 Empirical Model using ANN for Shear Wave Travel Time

The proposed shear wave travel time ANN based empirical model is given by Eq. 45

$$\Delta t_{S_n} = \left[\sum_{i=1}^{N} w_{2_i}\left(\frac{2}{1+e^{-2\left(w_{1_{i,1}}\,GR_n + w_{1_{i,2}}\,\varphi_n + w_{1_{i,3}}\rho_n + b_{1_i}\right)}}\right)\right] + b_2 \tag{45}$$

Steps to use new Artificial Intelligence based empirical correlation for shear wave travel time

Steps 1-2 are same as discussed for compressional wave travel time. Weights for shear wave travel time are given in Table 5.25.

Step 3: The value of Δt_{Sn} obtained from Eq. 45 is in the normalized form, to convert it in the real valued form, the result obtained from Eq. 45 must be de-normalized by applying Eq. 46

$$\Delta t_S = \frac{(176.335 - 71.407)(\Delta t_{S_n} + 1)}{2} + 71.407 \quad (46)$$

Table 5. 25 Weights and biases of ANN based Shear wave travel time empirical model.

Hidden Layer Neurons (N)	Weights between Input and Hidden Layer (w_1)			Weights between Hidden and output Layer (w_2)	Hidden Layer Bias (b_1)	Output Layer Bias (b_2)
1	-3.453	-0.765	2.619	0.487	6.626	-1.498
2	-0.899	1.763	-3.826	-2.514	3.534	
3	-1.224	3.681	-2.392	-0.266	2.714	
4	1.095	2.438	0.036	0.483	0.442	
5	1.370	-1.201	0.407	1.127	1.289	
6	0.821	-1.658	2.709	-3.107	-2.689	
7	-3.533	5.863	7.287	0.155	-0.985	
8	5.201	3.664	-3.315	0.272	-1.860	
9	-2.738	5.725	8.689	-2.920	1.446	
10	-4.287	3.976	-0.019	-0.196	2.047	
11	5.705	3.579	3.323	-0.309	-1.152	
12	6.417	-0.407	0.082	-0.219	1.371	
13	2.542	-0.843	-5.390	0.224	1.692	
14	1.552	0.899	11.050	0.143	-2.211	
15	-2.346	5.077	8.130	6.164	1.158	
16	-3.209	1.098	-0.106	1.078	-2.845	
17	3.357	-3.503	-8.709	0.303	3.717	
18	2.018	-4.355	-7.425	3.158	-0.822	
19	3.482	-1.588	0.441	-0.542	-3.410	

5.3.6 Validation of the Developed Acoustic Models on Real Field Data

Validation of the proposed acoustic wave travel time models was performed on three wells. The data of these three wells was not used in the training of the models. This step is to further test the precision and generalization capabilities of the proposed models.

5.3.6.1 Well No. 1

Fig. 5.7 shows the wireline log data of Well No.1 for an interval of 1000ft. Neutron porosity log values at certain points in the given interval of reservoir section indicated a

tight section. Bulk density average value was 2.7 indicating a limestone section. The complete data description of the input parameters of Well No. 1 is given in Table 5.26.

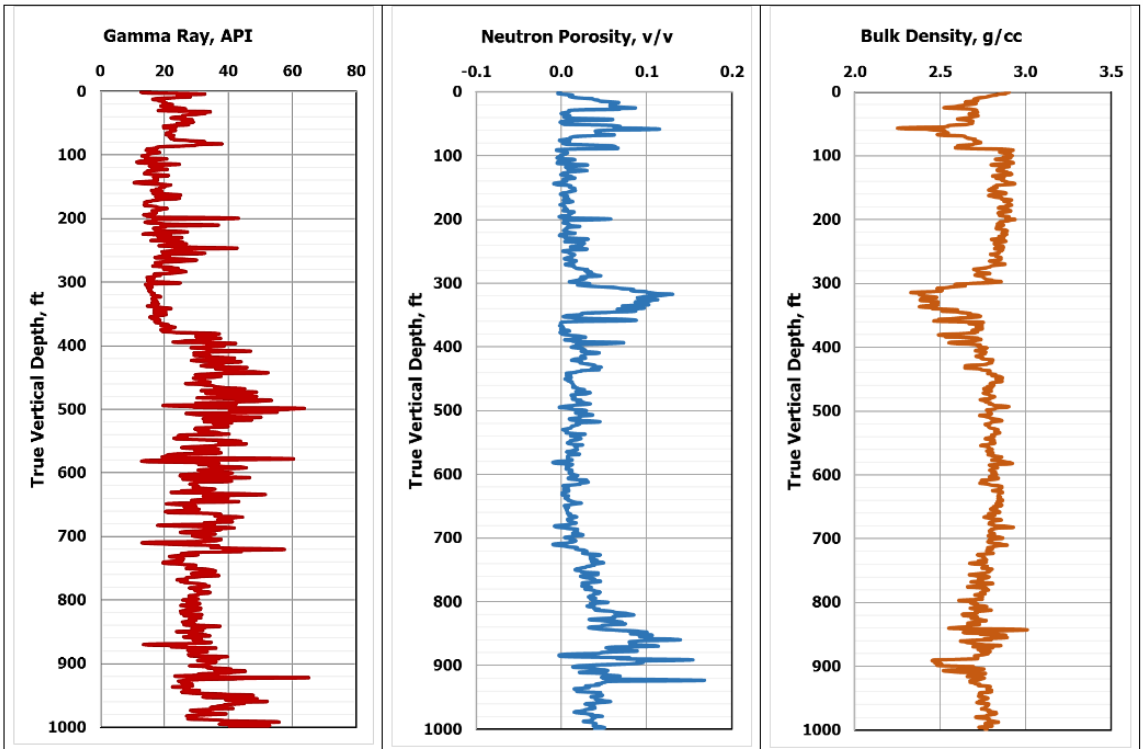

Figure 5.7 Input data for compressional and shear wave model Well No. 1.

Table 5.26 Well No. 1 input data description used for validation of acoustic model.

Parameters	Max	Min	Mean	Range	St. Deviation	Skewness	Kurtosis
Gamma Ray (API)	64.903	10.515	28.184	54.388	9.266	0.517	0.109
Neutron Porosity (V/V)	0.168	-0.010	0.028	0.178	0.027	1.481	2.224
Bulk Density (g/cc)	3.008	2.249	2.755	0.758	0.109	-1.364	2.237

Fig. 5.8 shows the lithology of Well No. 1 by density-neutron porosity cross plot and it shows that the well is present in a limestone region with traces of sandy-lime formation.

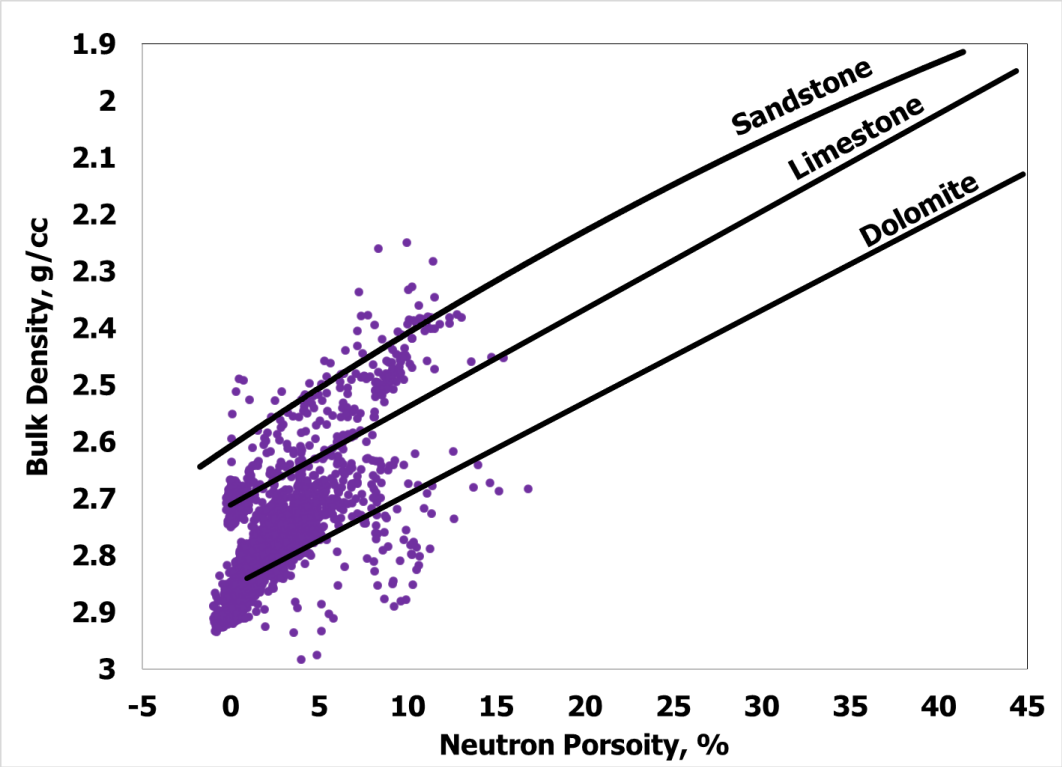

Figure 5.8 Neutron porosity and bulk density cross plot to identify lithology Well No. 1.

Fig. 5.9 shows that the proposed ANN model predicted the compressional time with AAPE of 3% and R^2 of 0.865. Fig. 5.10 shows that the proposed ANN model predicted the shear wave travel time with an AAPE of 4.5 and R2 of 0.80.

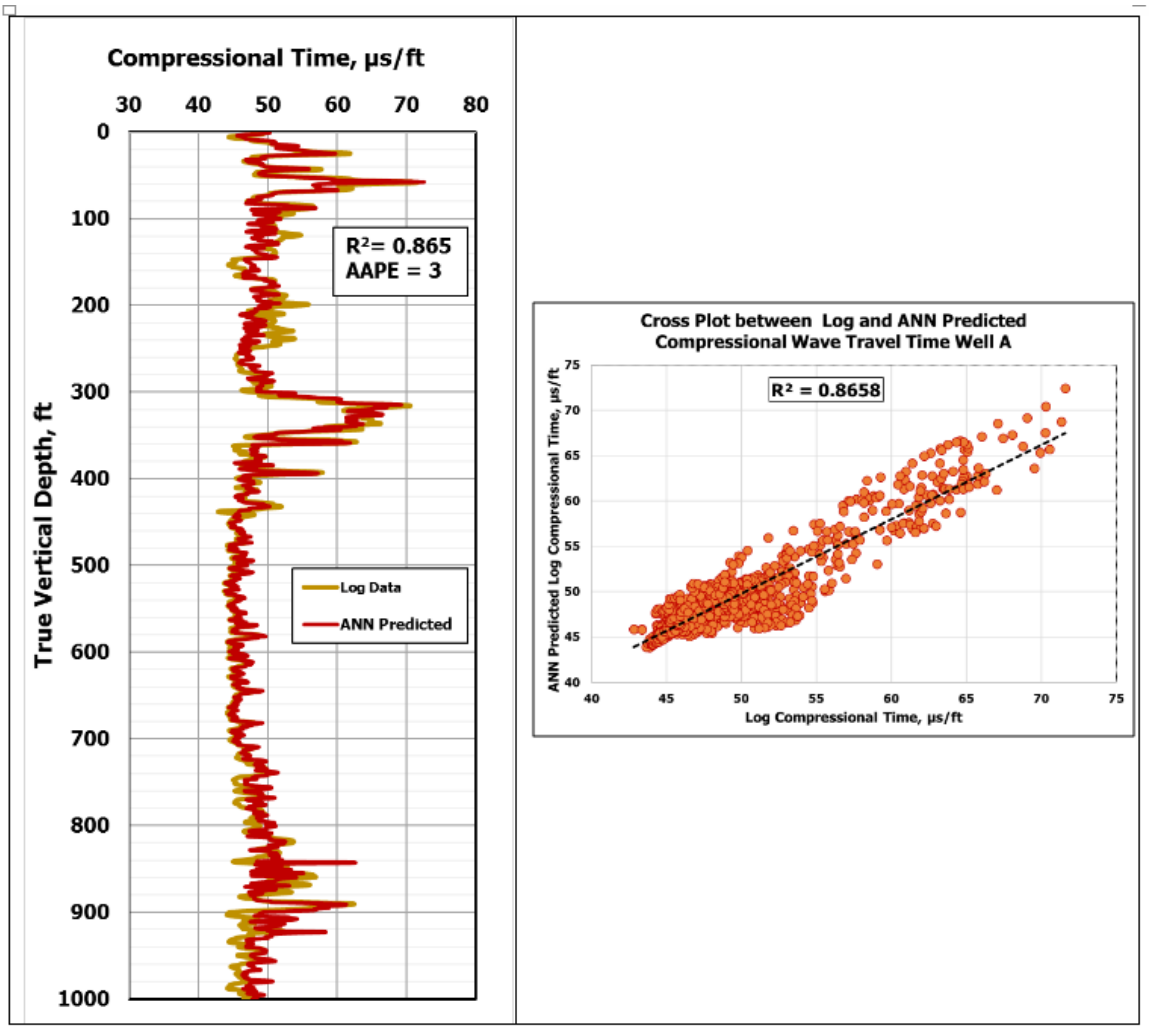

Figure 5.9 Compressional time prediction using ANN Well No. 1.

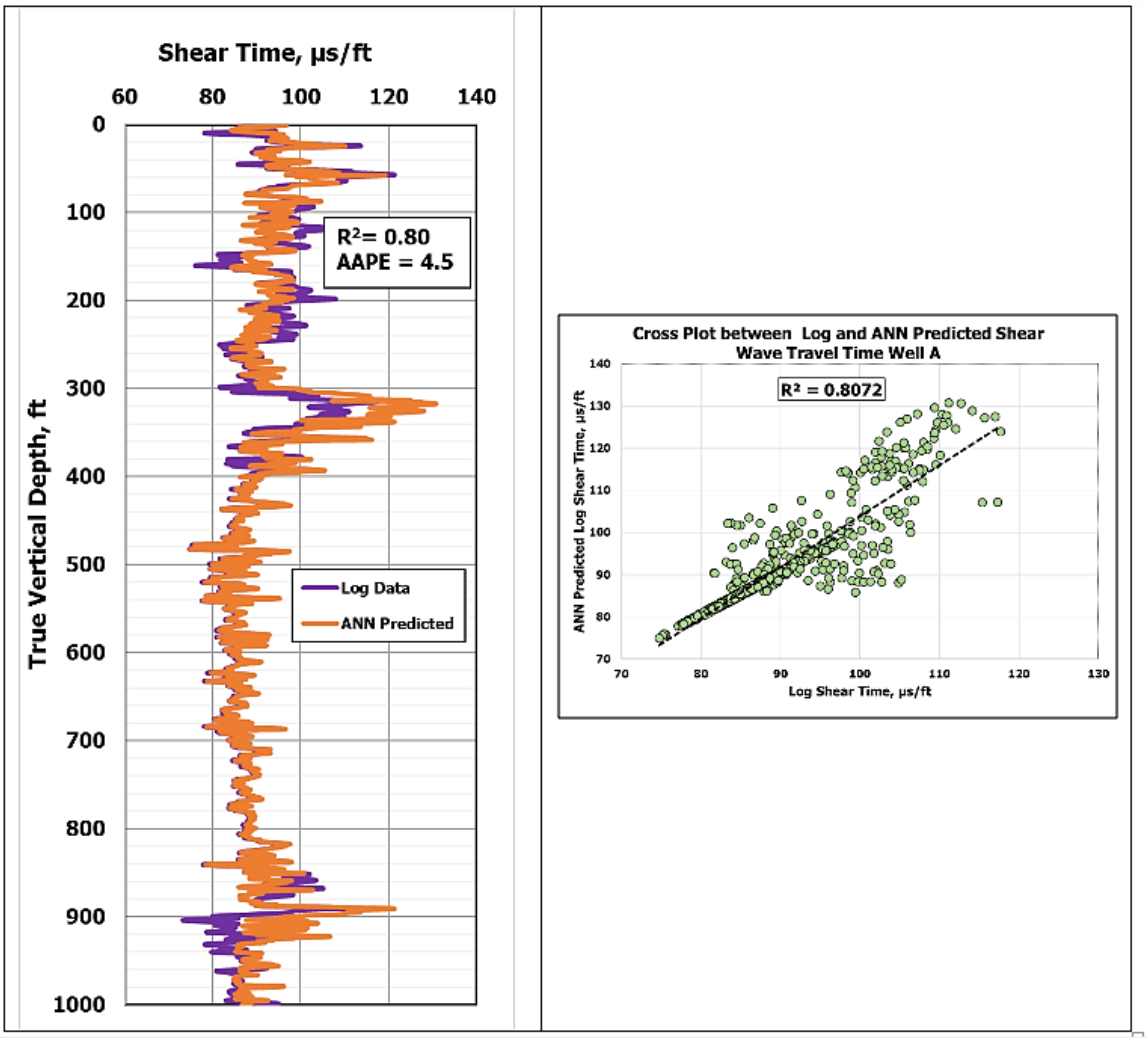

Figure 5.10 Shear wave travel time prediction using ANN Well No. 1.

5.3.6.2 Well No. 2

Fig. 5.11 shows the input data for Well No. 2 which is gamma ray, neutron porosity, and bulk density log for an interval of 1000ft. Fig. 5.12 shows the lithology of Well No. 2 by density-neutron porosity cross plot. Lithology of this well indicates that the major portion lies in a limestone region with dolomitic lime and some traces of anhydrite. Anhydrites are the regions where density is very high but porosity is close to zero. The gamma ray log profile shows mostly low values with some higher values indicating that the reservoir section contains traces of shaly formation. The maximum and minimum values of gamma

ray are within the range of the data on which the model is built. Neutron porosity log shows low values at certain points indicating tight sections. Bulk density log shows the average value of 2.7 indicating a limestone region. The complete data description of the input parameters of Well No. 2 is given in Table 5.27.

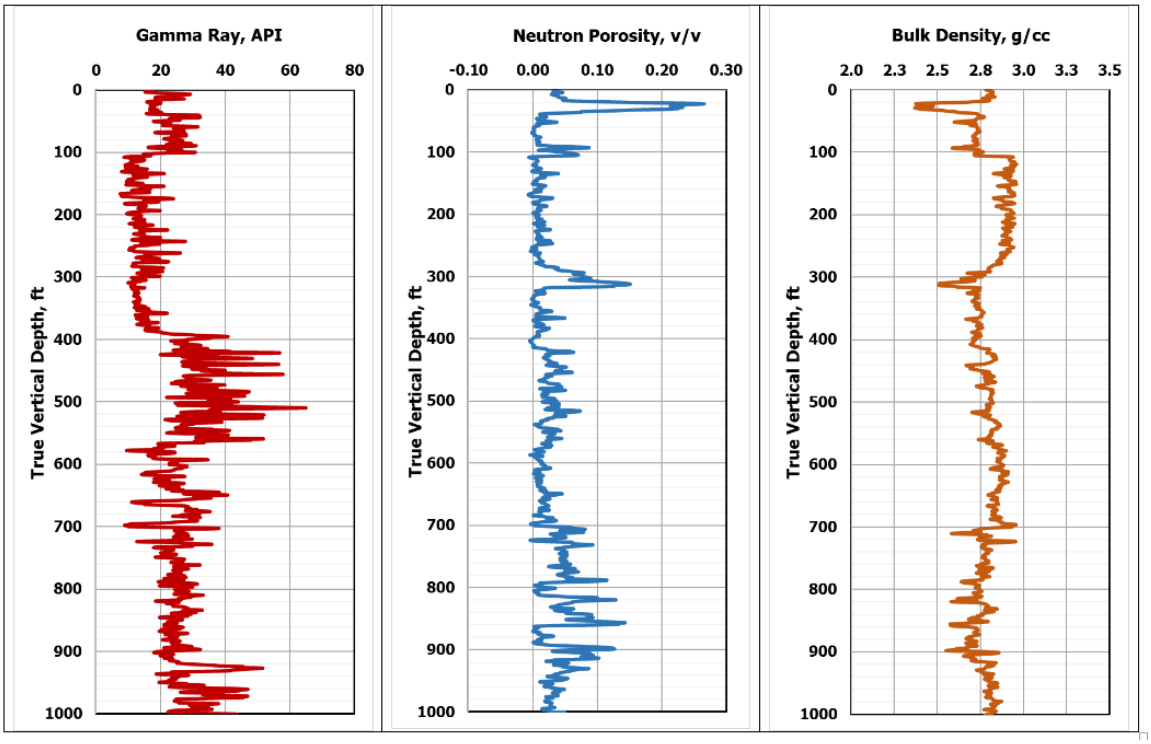

Figure 5.11 Input Data for compressional and shear wave model Well No. 2.

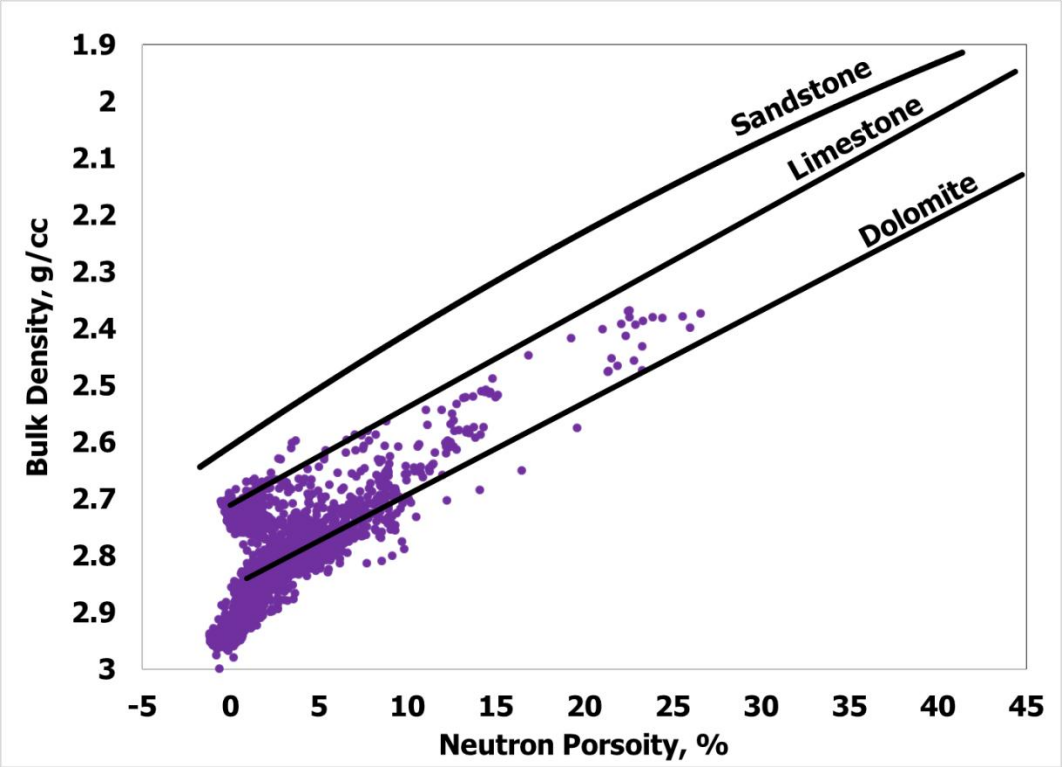

Figure 5.12 Neutron porosity and bulk density cross plot to identify lithology Well No. 2.

Table 5.27 Well No. 2 input data description used for validation of acoustic model.

Parameters	Max	Min	Mean	Range	St. Deviation	Skewness	Kurtosis
Gamma Ray (API)	109.694	7.484	24.128	102.210	10.522	1.899	9.411
Neutron Porosity (V/V)	0.266	-0.012	0.029	0.278	0.034	2.763	11.342
Bulk Density (g/cc)	3.043	2.369	2.797	0.674	0.092	-0.841	2.326

Fig. 5.13 shows that the developed ANN model can be used to predict the compressional time with AAPE of 2.35 and R^2 of 0.853. Similarly proposed ANN model predicted the shear time for Well No. 2 as shown in Fig. 5.14 with AAPE of 1.7 and R2 of 0.895.

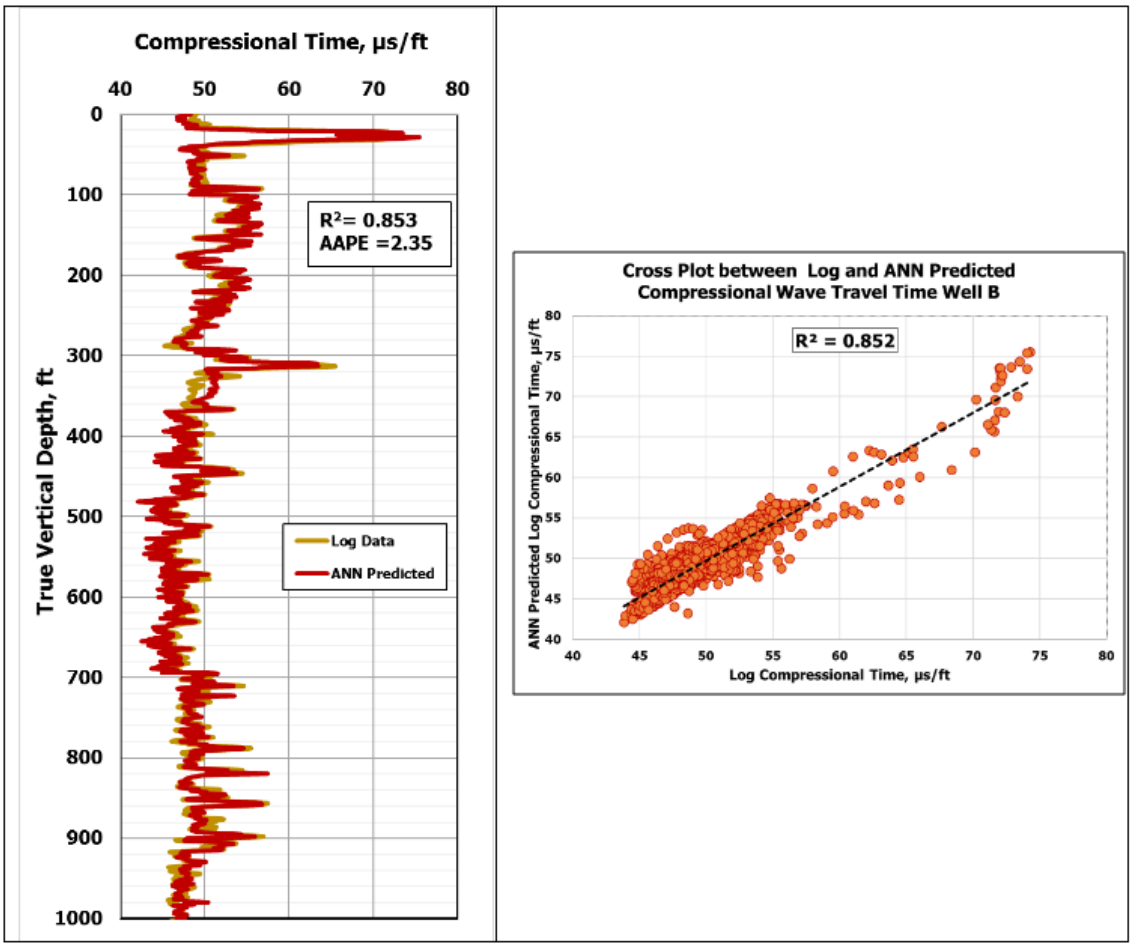

Figure 5.13 Compressional wave travel time prediction using ANN Well No. 2.

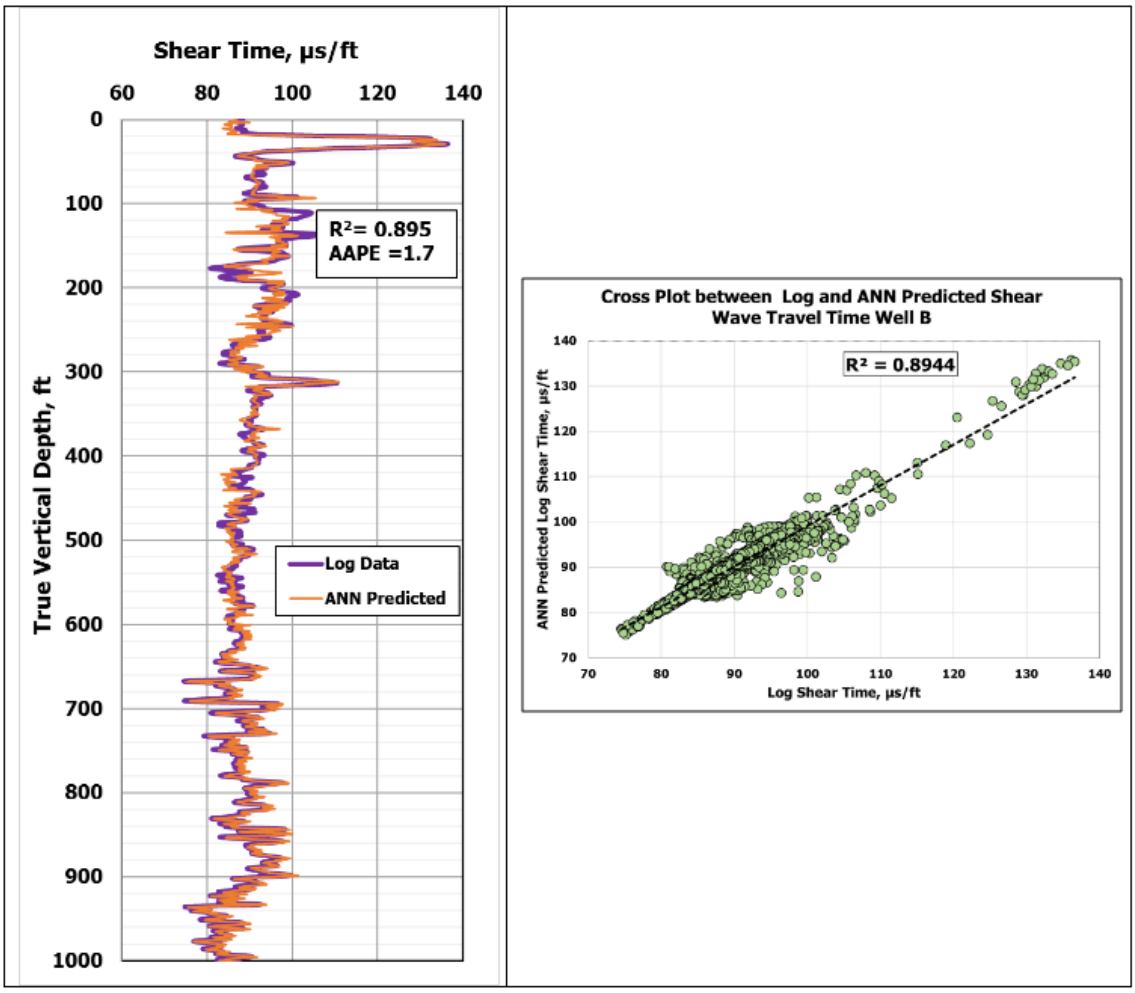

Figure 5. 14 Shear wave travel time prediction using ANN Well No. 2.

5.3.6.3 Well No. 3

Fig. 5.15 shows the wireline log as an input data for Well No. 3 for a reservoir section of an interval 400ft. Fig. 5.16 shows the density-neutron porosity cross plot for Well No. 3. The complete data description of the input parameters of Well No.3 is given in Table 5.28.

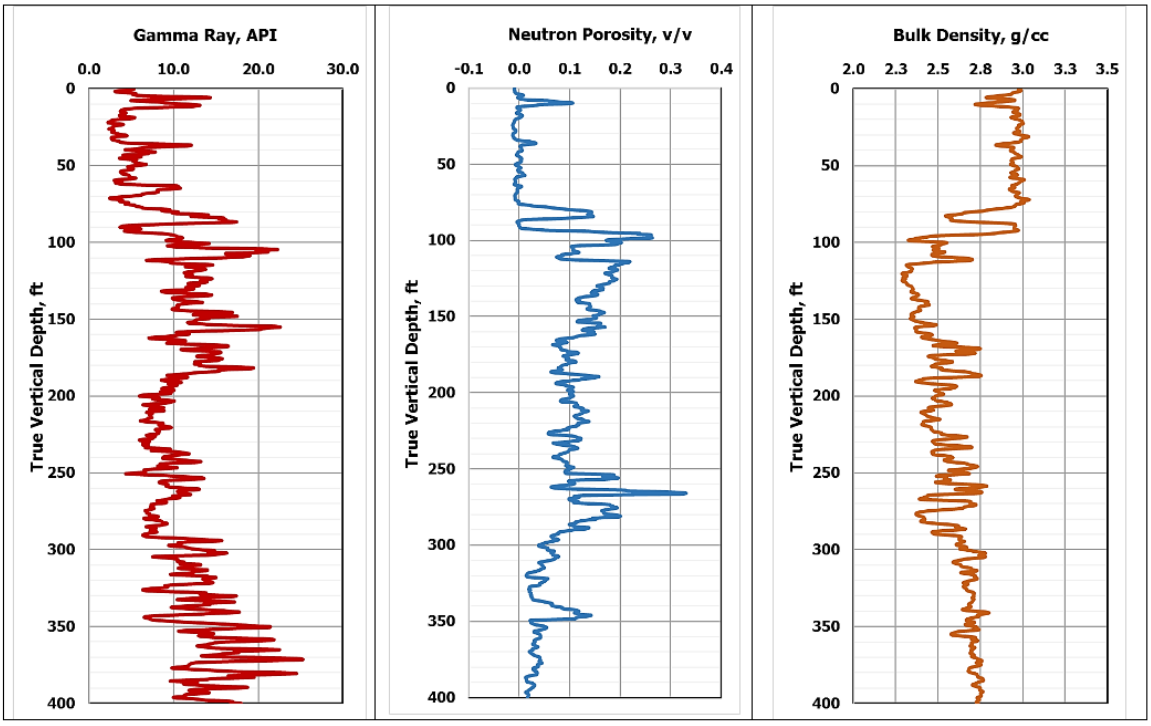

Figure 5.15 Input Data for compressional and shear wave model Well No. 3.

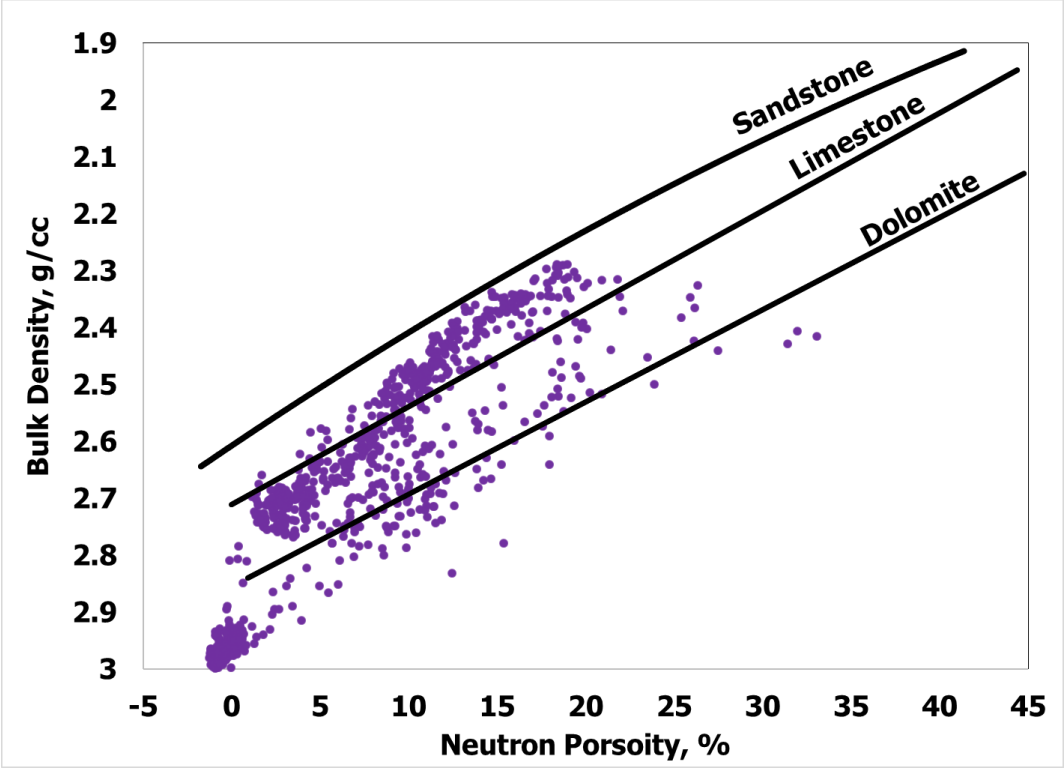

Figure 5.16 Neutron porosity and bulk density cross plot to identify lithology Well No. 3.

Table 5.28 Well No. 3 input data description used for validation of acoustic model.

Parameters	Max	Min	Mean	Range	St. Deviation	Skewness	Kurtosis
Gamma Ray (API)	25.249	2.250	10.404	22.998	4.358	0.460	0.119
Neutron Porosity (V/V)	0.331	-0.013	0.078	0.343	0.064	0.541	-0.043
Bulk Density (g/cc)	3.038	2.289	2.651	0.749	0.199	0.186	-0.938

Fig. 5.17 shows that the developed ANN model can be used to predict the compressional time with AAPE of 1.1 and R^2 of 0.987 and shear time with an AAPE of 1.7 and R^2 of 0.982.

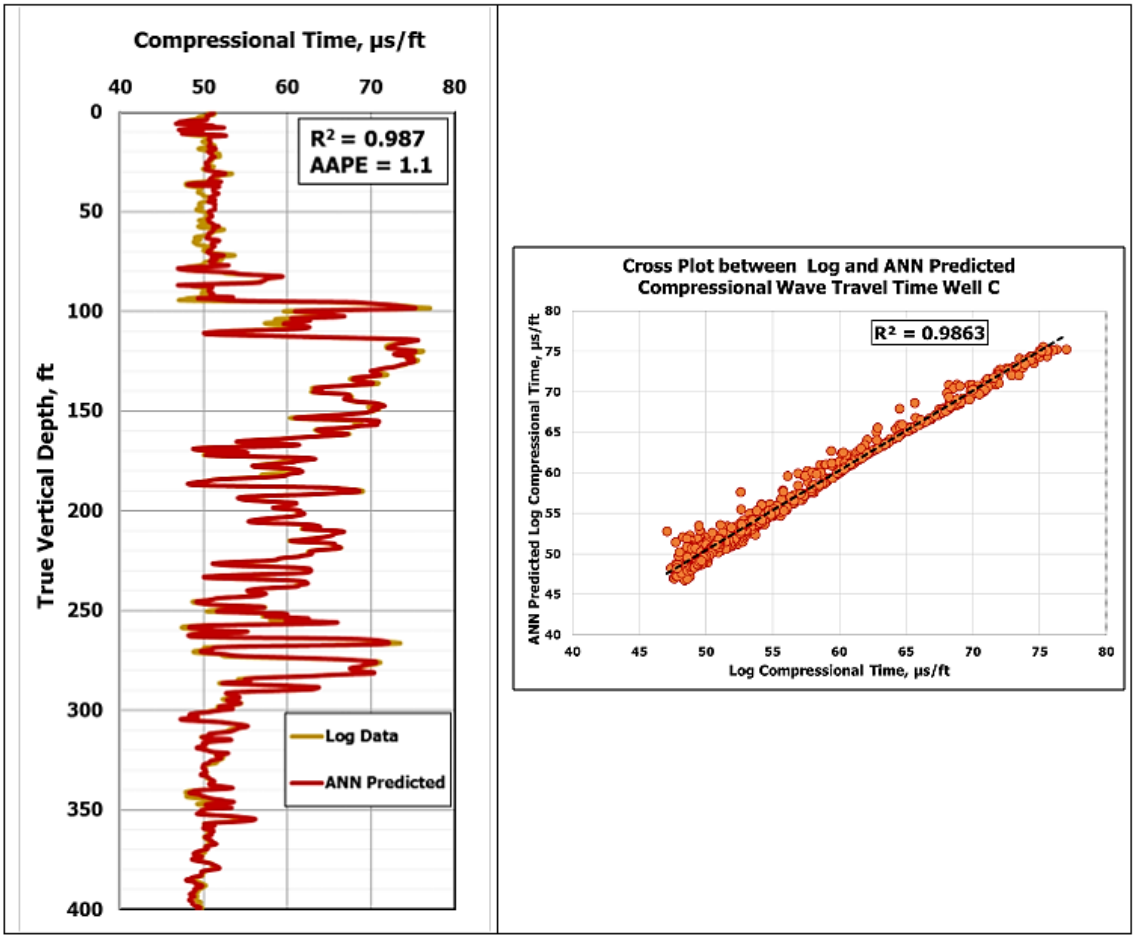

Figure 5.17 Compressional wave travel time prediction using ANN Well No. 3.

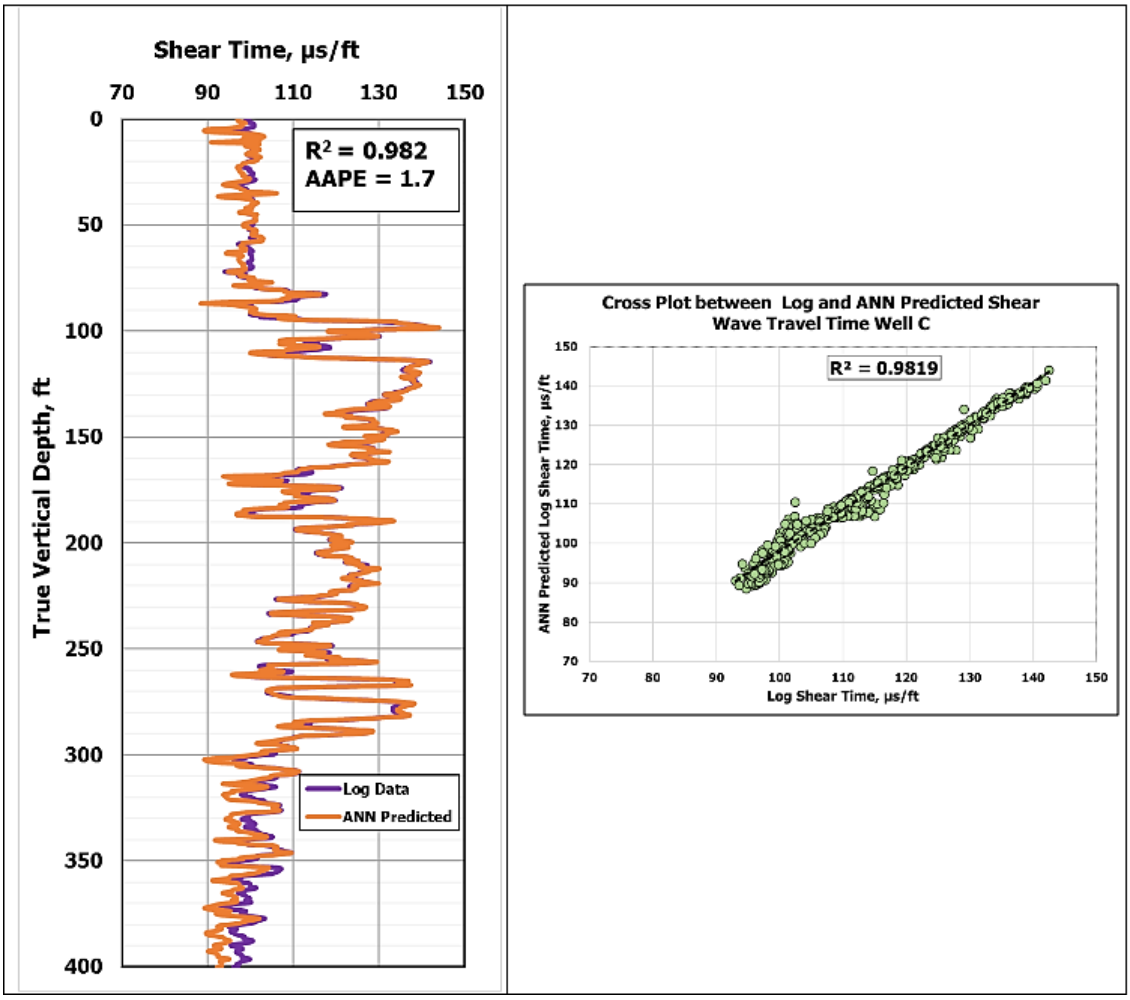

Figure 5.18 Shear wave travel time prediction using ANN Well No. 3.

5.3.7 Model Verification of Shear Wave Travel Time

To check the accuracy and the performance of the proposed shear wave model, it was compared with the commonly used empirical correlations in the oil industry (Caroll 1969, Castagana 1993, Eskandari 2004, Brocher 2008 and Wadhwa 2010) as shown in Fig. 5.19. The proposed ANN model produced highest CC and lowest AAPE between actual and predicted data as shown in Fig. 5.20 while Eskandari 2004 correlation produced lowest CC and highest AAPE.

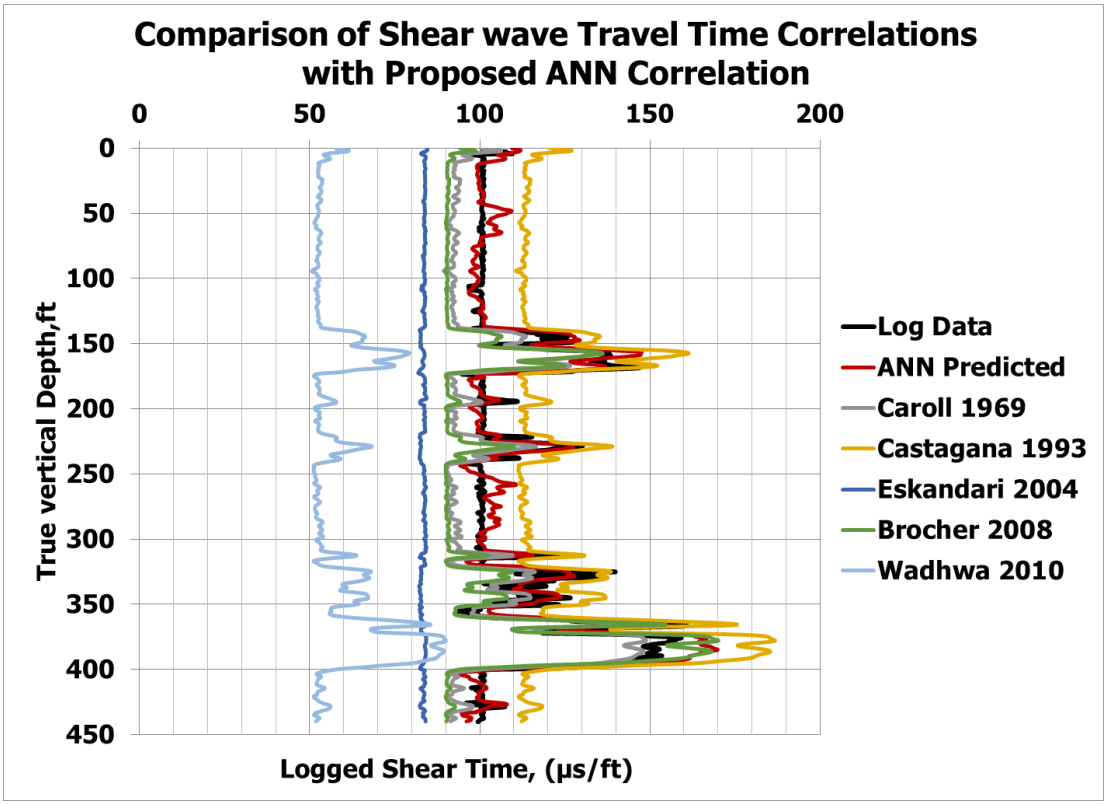

Figure 5.19 Comparison of ANN proposed shear wave travel time model with other correlations.

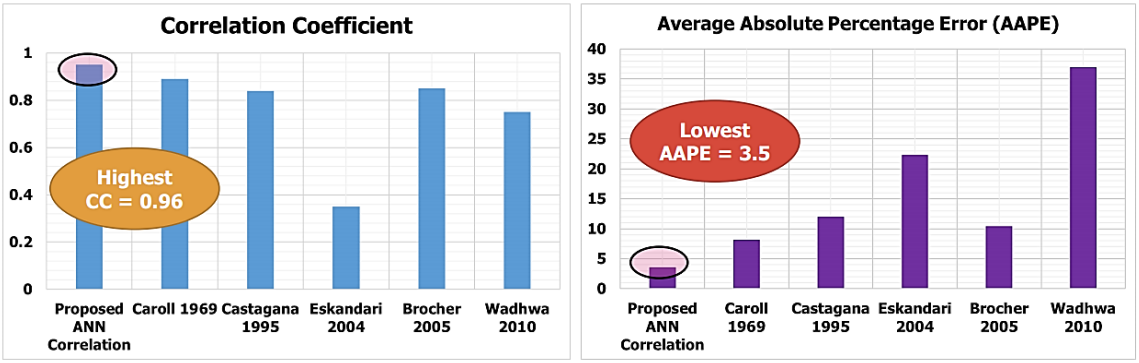

Figure 5.20 Comparison of CC & AAPE of proposed shear wave model with other correlations.

5.4 Prediction of Elastic Parameters

Elastic parameters are Young's modulus and Poisson's ratio.

5.4.1 Data Analysis for Elastic Parameter Models

600 data points were obtained from several wells located in different fields. Most of the data was from limestone formation with a low percentage of sandstone and dolomite and no gas effects as observed in lithology cross plot of neutron porosity and bulk density Fig. 5.21. Wireline log data included gamma ray, neutron porosity, bulk density and compressional and shear time. The core data at corresponding depths comprised of static Young's modulus and static Poisson's ratio. Core data were obtained from the laboratory measurements of triaxial compressional tests. The range of gamma ray was between 7 - 114 API, neutron porosity between -0.0050 – 0.2330 (v/v), bulk density between 2.0 – 3.0 g/cc, compressional wave travel time between 40 – 80 μs/ft, and shear wave travel between 70 – 140 μs/ft. The set of data was randomly divided into two parts, 70% data for training, and 30% for testing the accuracy and generalization capabilities of the model. A complete statistical description of the data used for training and testing is given in Table 5.29.

Table 5.29 Statistical description of the data used for elastic parameters model.

Parameters	Max	Min	Mean	Range	St. Deviation	Skewness	Kurtosis
Gamma Ray (API)	115.133	8.066	22.992	107.067	17.219	3.636	13.845
Neutron Porosity (V/V)	0.233	-0.005	0.044	0.233	0.042	1.513	2.492
Bulk Density (g/cc)	2.98	2.227	2.682	0.753	0.120	-0.326	0.980
Compressional Time (μs/ft)	81.886	44.375	51.683	37.511	5.910	1.946	5.376
Shear Time (μs/ft)	146.496	73.187	95.922	73.309	10.089	1.190	3.491
Estatic (MPsi)	13.456	1.090	7.210	12.366	2.245	0.100	-0.067
Poisson's Ratio	0.45	0.23	0.379	0.22	0.1186	-0.533	.829

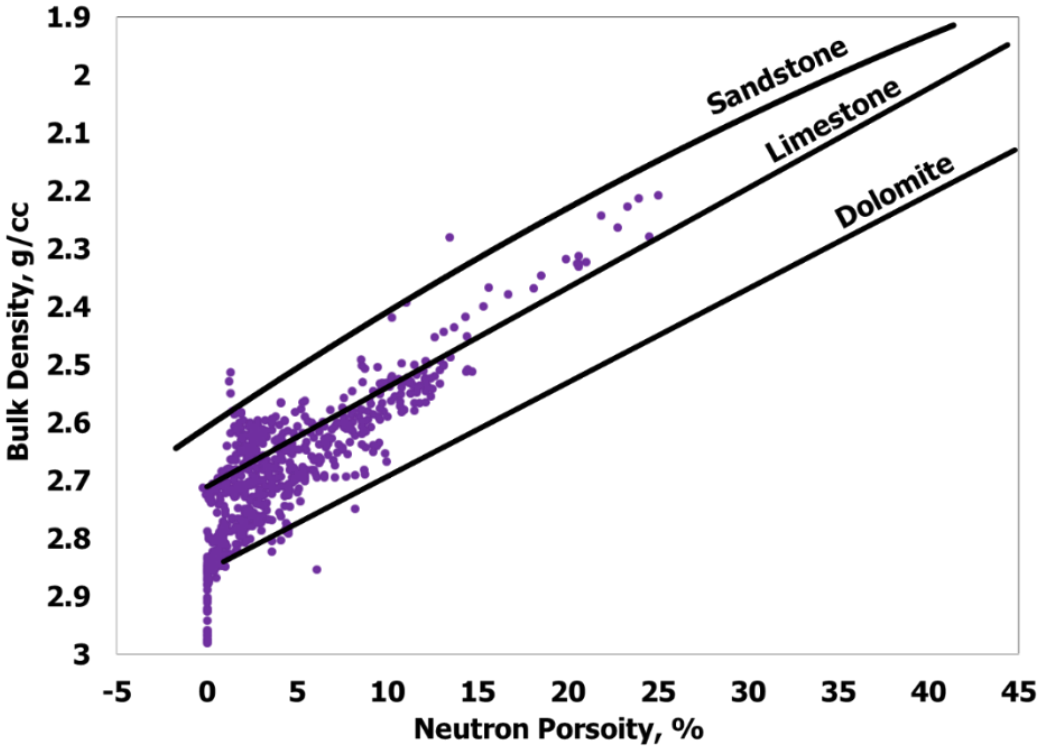

Figure 5.21 Lithology cross plot for elastic parameters model.

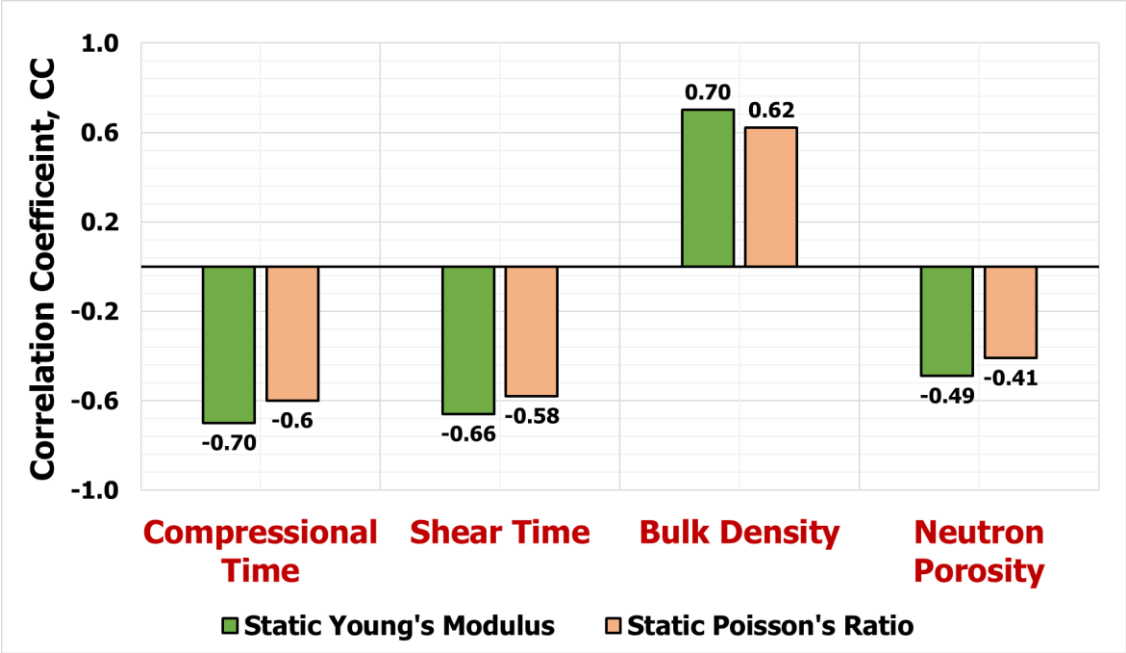

Figure 5.22 Relative importance of basic logs with the elastic parameters.

5.5 Modeling for Static Young's Modulus Prediction

The approach used for prediction of acoustic waves travel time prediction was adopted for the prediction of static Young's modulus. Three AI techniques, ANN, ANFIS, and SVM, were implemented. Sensitivity studies for various AI techniques parameters were done to arrive at the best technique with optimum parameters to predict static Young's modulus. For the sake of simplicity, the performances of only best models results are described here.

5.5.1 Comparison of three AI techniques on prediction of Static Young's Modulus

70% of the total data, selected randomly, was used for training. ANN technique was applied first and it gave the R^2 of 0.92 with AAPE of 5.35between actual and predicted data. The corresponding values for ANFIS were: R^2 of 0.89 and AAPE of 7.71. The SVM model gave R^2 of 0.83 and an AAPE of 4.35. The results for these three models are shown in Fig. 5.23. ANN had the highest R^2 during training phase as shown in cross plot between actual and predicted data in Fig. 5.24.

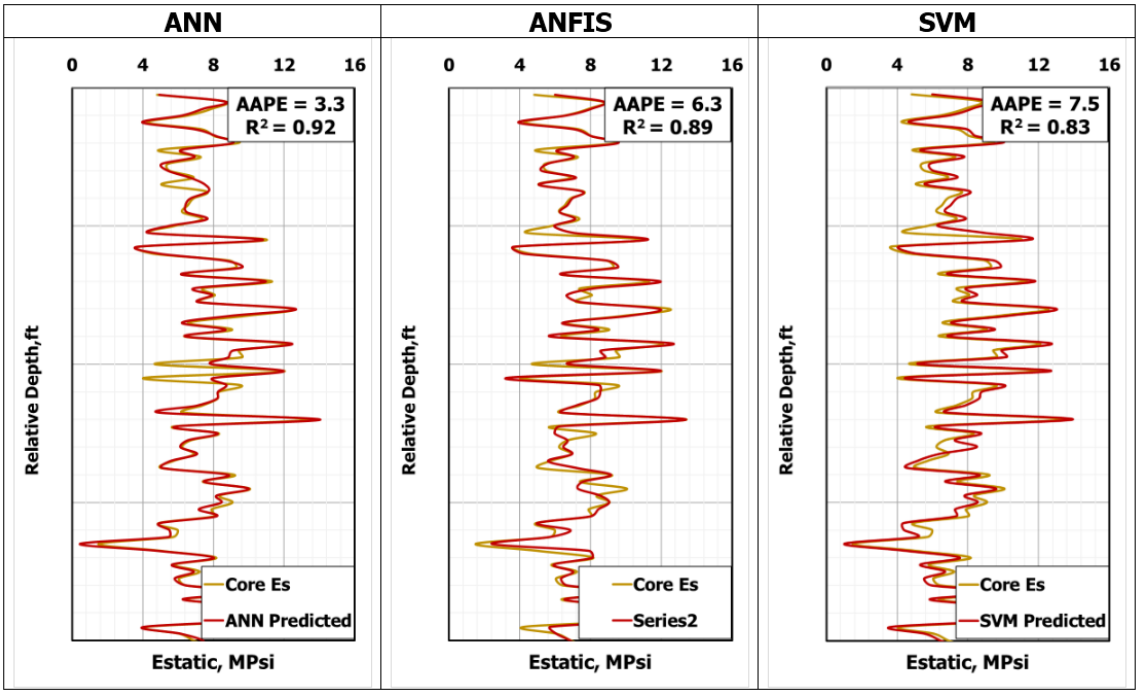

Figure 5.23 Training comparison of static Young's modulus models using ANN, ANFIS and SVM.

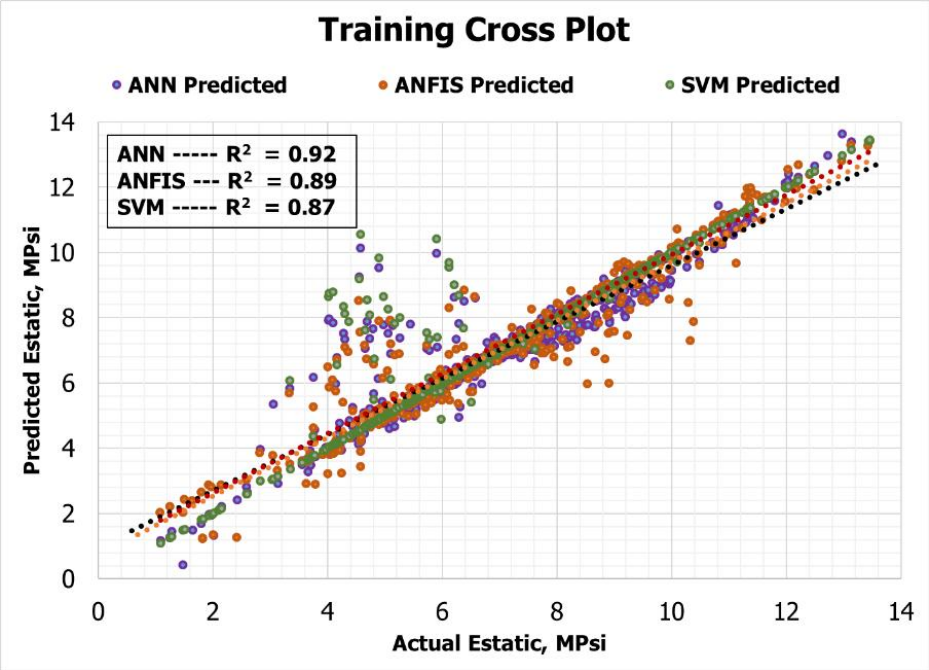

Figure 5.24 Training cross plots comparison of static Young's modulus models.

On a set of 30% random data which was used for testing the accuracy and generalization capabilities of the developed models, ANN gave the R^2 of 0.922 with AAPE of 5.2%,

ANFIS model gave the R^2 of 0.92 with AAPE of 6.31% while SVM gave the R^2 of 0.86 with AAPE of 7.25% as shown in Fig. 5.25. Fig 5.26 shows the performances of three models during testing on unseen data.

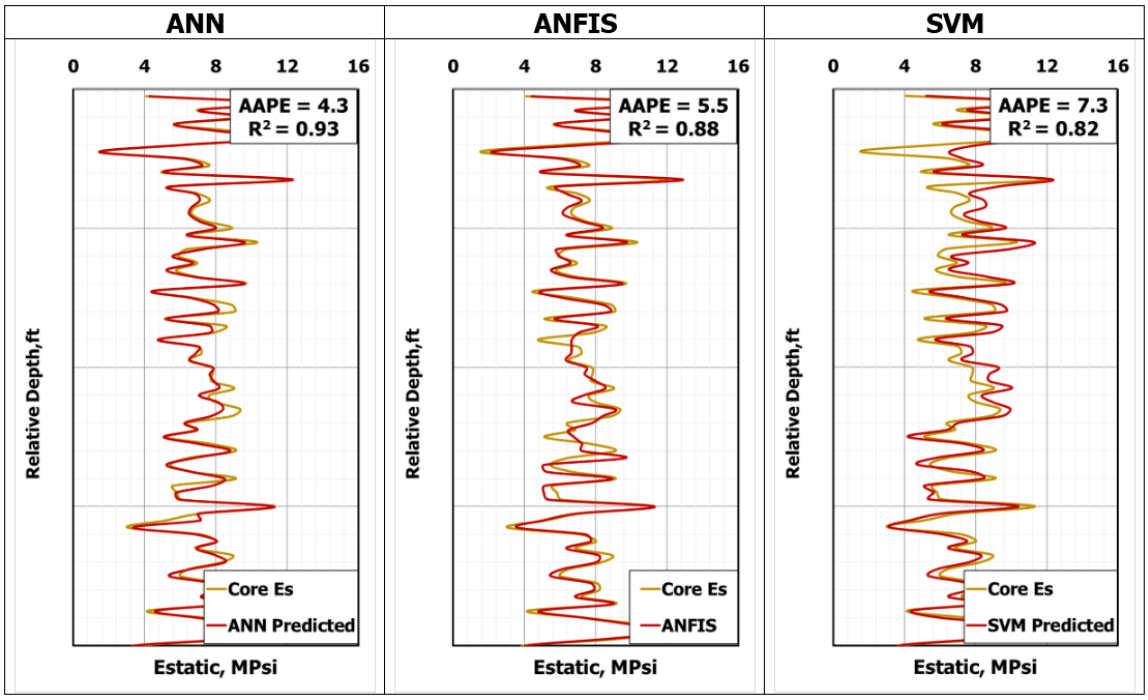

Figure 5.25 Testing comparison of static Young's modulus models using ANN, ANFIS and SVM.

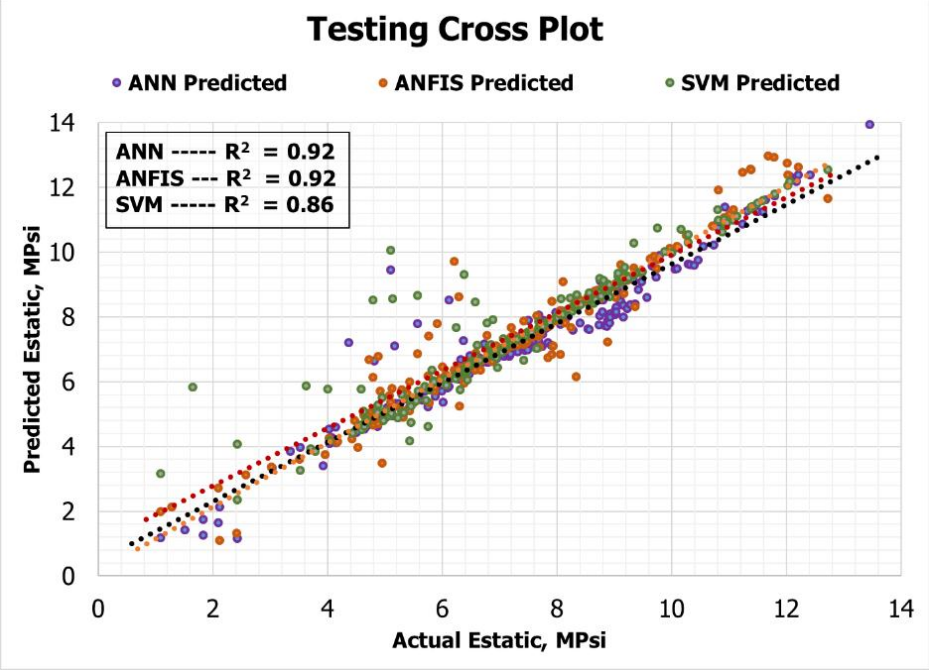

Figure 5.26 Testing cross plots comparison of static Young's modulus model.

On comparing the performance of all three models (ANN, ANFIS and SVM), it was observed that during training SVM model produced less AAPE than ANN and ANFIS, while ANN produced high R^2 than ANFIS and SVM. During the testing on unseen data ANN outperformed ANFIS and SVM by providing less AAPE and highest R^2. It means that on the given set of data the ANN model was very generalized and is capable of giving good results on any unseen data that lies within the boundaries of training data set. Therefore, ANN with three input parameter was suggested as the best model for the prediction of static Young's modulus.

5.5.2 Neural Network Architecture for Predicting Static Young's Modulus

A back propagation neural network algorithm was implemented to model E_{static}. The E_{static} ANN model based on three input parameters, namely, bulk density, compressional time and shear time, one hidden layer and one output parameter which was E_{static}

Table 5.30 Neural network architecture of Estatic Model.

Neural Network Parameters	Ranges
Number of Inputs	3
Number of Outputs	1
Number of Neurons	20
Number of Hidden Layer(s)	1
Training Algorithm	Levenberg Marquadt
Learning rate	0.12
Hidden Layer transfer function	Tan-sigmoidal
Outer layer transfer function	pure linear
Training Ratio	0.7
Testing Ratio	0.15
Validation Ratio	0.15

The neurons in the hidden layer varied between 5 and 20. The optimum neurons were found to be 20 since they produced highest correlation coefficient during training and testing. Tan-sigmoidal type activation function was used as a transfer function between

input and hidden layer and linear type activation functions was used between hidden and output layer. Levenberg-Marquardt back propagation algorithm was implemented as the training algorithm to obtain the weights and biases. Table 5.30 shows the complete anatomy of proposed E_{static} ANN model. In order to avoid the model to stuck on local minima 10,000 realizations were run with the initialization of different weights and biases during training and cross-validation phases of the modeling. After training, the weights and biases from the optimum model were extracted which are given in Table 5.30.

5.5.3 Empirical Model using ANN for Static Young's Modulus

The empirical model is derived from the ANN model based on weights and biases associated with input layer/hidden layers and hidden layer/outer layer. The weights between input layer and hidden layer termed as w_1 and weights between hidden layer and outer layer termed as w_2 are given in Table 5.31. The proposed E_{static} ANN based empirical correlation is given below (Eq.47)

$$E_{static_n} = \left[\sum_{i=1}^{N} w_{2_i}\left(\frac{2}{1+e^{-2\left(w_{1_{i,1}}\rho_n + w_{1_{i,2}}\Delta t_{c_n} + w_{1_{i,3}}\Delta t_{s_n} + b_{1_i}\right)}}\right)\right] + b_2 \quad (47)$$

Steps to use New Empirical Correlation for Static Young's Modulus

Step 1: Normalize the input parameters between the range [-1 1] before using Eq. 47. Normalization is done by two points slope form given by Eq. 48 and Eq. 49

$$\frac{Y - Y_{min}}{Y_{max} - Y_{min}} = \frac{X - X_{min}}{X_{max} - X_{min}} \quad (48)$$

where, Ymin = -1, Ymax =1, X is the input parameters, X_{min} is the input parameter minimum value and X_{max} is the input parameter maximum value.

$$Y = 2 \times \left(\frac{X - X_{min}}{X_{max} - X_{min}}\right) - 1 \tag{49}$$

Step 2: Use Eq. 47 to calculate E_{static} in normalized form. Eq. 47 can be used by using the weights given in Table 5.31. The sequence of parameters that goes into the model is given as: bulk density, compressional time and shear time.

Step 3: The value of E_{static} obtained from Eq. 47 is in the normalized form, to convert it in the real value, the result obtained from Eq. 47 must be de-normalized by applying Eq. 50

$$Estatic = \frac{(13.456 - 1.090)(Estatic_n + 1)}{2} + 1.090 \tag{50}$$

Note: The results obtain using Eq. 50 will be in MPsi.

Table 5.31 Weights and biases of ANN based Estatic empirical model.

Hidden Layer Neurons (N)	Weights between Input and Hidden Layer (W1)			Weights between Hidden and output Layer (W2)	Hidden Layer Bias (b1)	Output Layer Bias (b2)
1	0.42460	0.50130	3.65107	-0.26124	-3.91089	0.576
2	-1.13204	-0.95012	-3.51512	-0.35929	3.40925	
3	0.18488	4.37150	0.57420	-1.51769	5.50504	
4	-0.78986	-3.46964	-2.16191	0.28203	1.93902	
5	0.50731	-1.44761	-1.29409	-0.39904	-3.14061	
6	-0.72229	1.87035	-7.28818	0.37974	-3.29586	
7	-3.68864	-0.01934	-2.84290	-0.22672	0.91400	
8	2.62086	-3.03493	-2.69670	0.03602	0.39281	
9	0.83851	0.49415	4.55257	-0.31010	0.98314	
10	-0.27552	-2.81866	-2.66761	-0.05683	-0.26209	
11	0.80986	-4.14568	0.71475	0.18145	0.85250	
12	-2.49842	0.68699	3.34146	0.31962	-1.47316	
13	-1.52355	2.86050	1.67209	-0.10313	-1.23057	
14	-3.11042	1.27834	-3.21127	-0.26785	-1.48941	
15	-2.10242	0.98924	3.71904	-1.07362	-2.60650	

16	2.46970	0.17189	-2.74226	0.14159	2.19564
17	-2.39073	2.58597	1.66841	1.26722	-2.71472
18	-3.26356	0.30545	-1.47078	0.49576	-2.73382
19	-0.10389	2.74913	-2.59456	0.11253	-3.45066
20	-1.20784	2.69784	-2.21499	-1.07450	-4.07682

5.5.4 Validation of the Developed Empirical Model for E_{static}

In order to validate the accuracy and generalization power of the ANN based empirical model it was compared with the real field data of Well No.1, 2 and 3. All three wells were located in limestone formation. Figs. 5.27 - 5.29 shows the wireline log input data for three Wells. These three wells contain the data of certain laboratory measured static Young's modulus on core plugs.

Fig. 5.27 shows the wireline log data of Well No. 1 for an interval of 1000ft which consists of bulk density, compressional wave travel time and shear wave travel time. The range of bulk density was in between 2.4 – 2.9 g/cc, the range of compressional wave travel time was in between 40 - 80 µs/ft. while for shear wave travel time the range was in between 80 - 120 µs/ft. as shown in Fig. 5.27. The maximum and minimum values of three log input parameter for static Young's modulus were in between the range of values on which model was built.

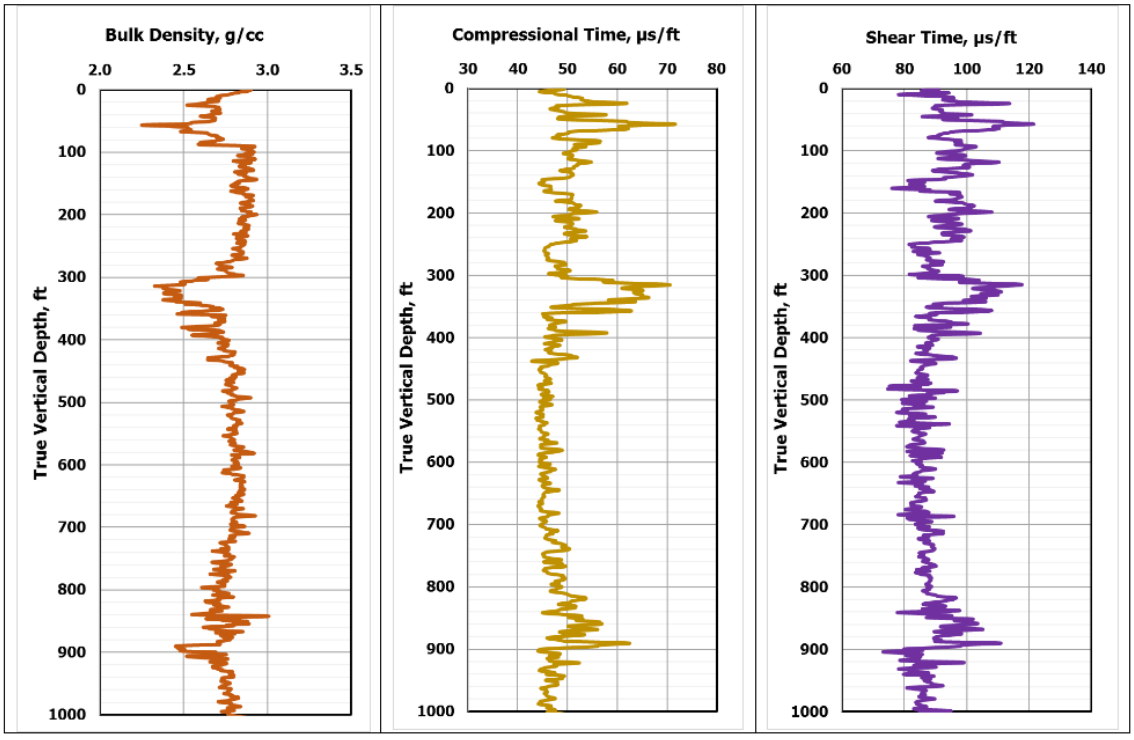

Figure 5. 27 Real field wireline log input data for E_{static} model Well No. 1.

Fig. 5.28 shows the input data for Well No. 2 for an interval of 1000ft. The minimum and maximum values of bulk density was in between 2.4 – 2.9 g/cc, compressional wave travel time between 45 – 70 µs/ft., while shear wave travel time between 90 – 138 µs/ft.

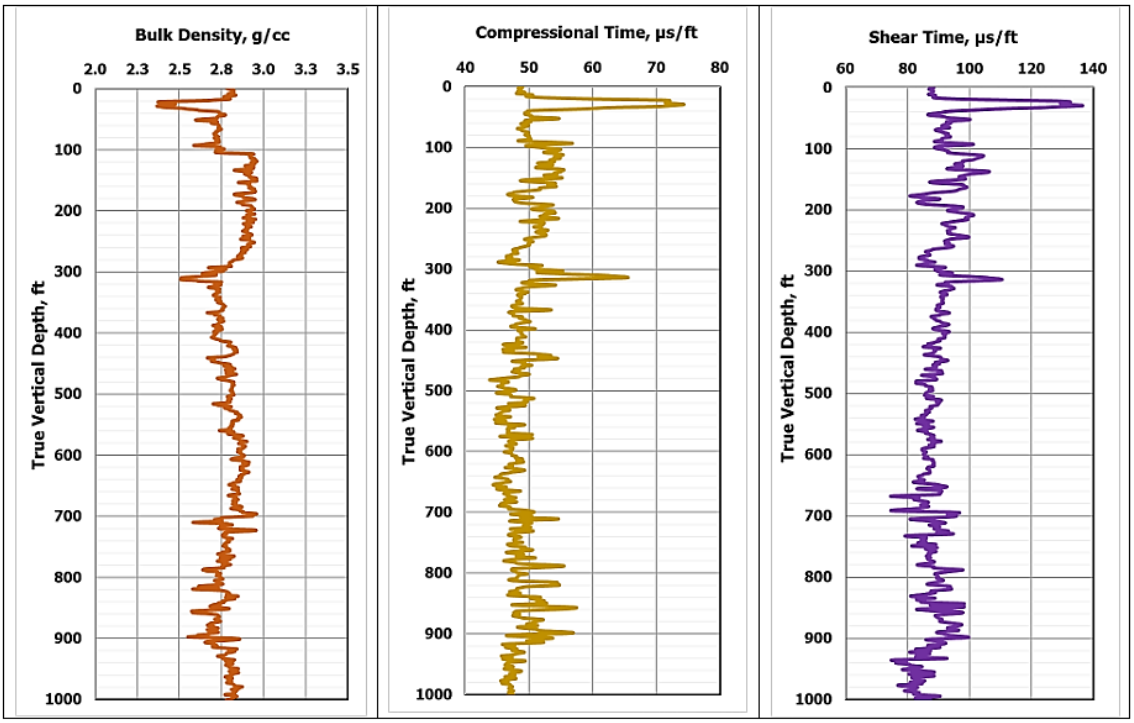

Figure 5. 28 Real field wireline log input data for E_{static} model Well No. 2.

Fig. 5.29 shows the wireline log input data for Well No. 3 for an interval 400ft. The range of bulk density log was in between 2.3 – 3.0 g/cc, compressional time between 50 – 75 µs/ft, while shear wave travel time between 100 – 138 µs/ft.

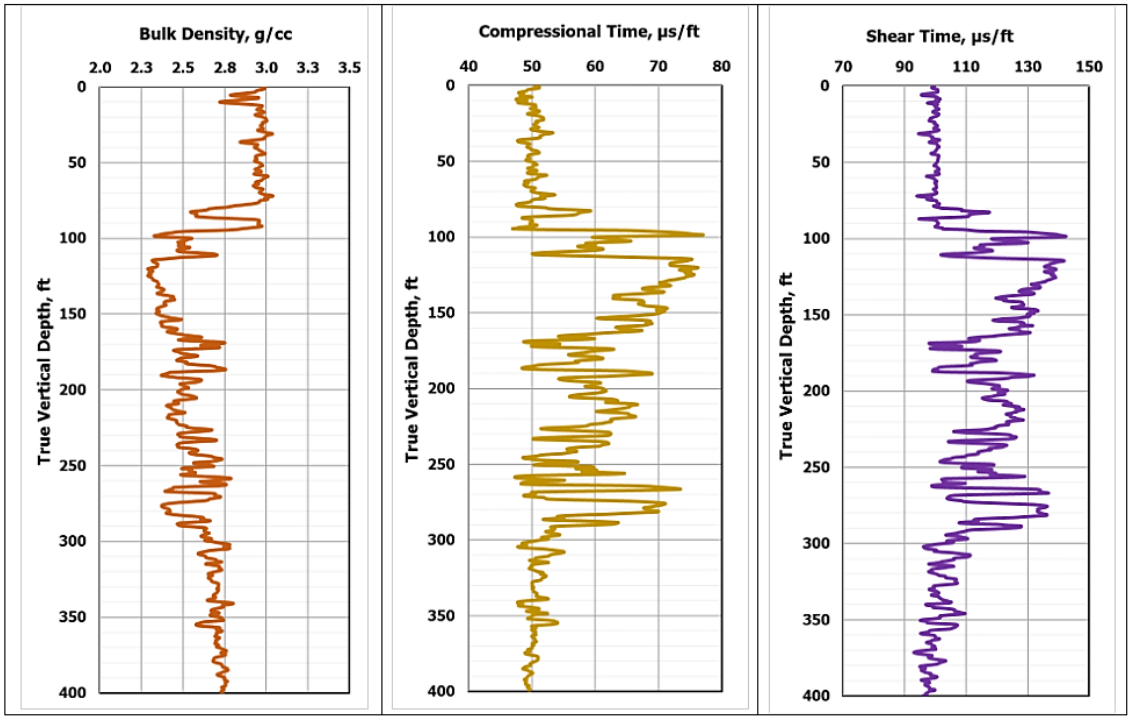

Figure 5. 29 Real field wireline log input data for E_{static} model Well No. 3.

5.5.4.1 Well No. 1

Fig. 5. 30 shows the ANN predicted E_{static} for an interval of 1000 ft. This well contain 13 actual laboratory measured static Young's modulus values from triaxial compressional tests. The $E_{dynamic}$ profile in Fig. 5.30 is the dynamic Young's modulus which was calculated using Eq. 1. The value of dynamic Young's modulus is always 1.5 - 3 times greater than static Young's modulus. This criterion suggest that the values of static Young's modulus can never be higher than dynamic Young's modulus and can never be lower than (1/3) times of dynamic Young's modulus.

Right side of Fig. 5.30 shows the cross plot between laboratory measured static Young's modulus and ANN predicted static Young's modulus values on the same depth from where these core samples were retrieved. Cross plot shows the R^2 value of 0.956. The E_{static} profile in Fig. 5.30 and cross plot clearly indicates that the developed model based

on ANN is fully capable of predicting E_{static} using three input, namely, bulk density, compressional and shear wave travel time.

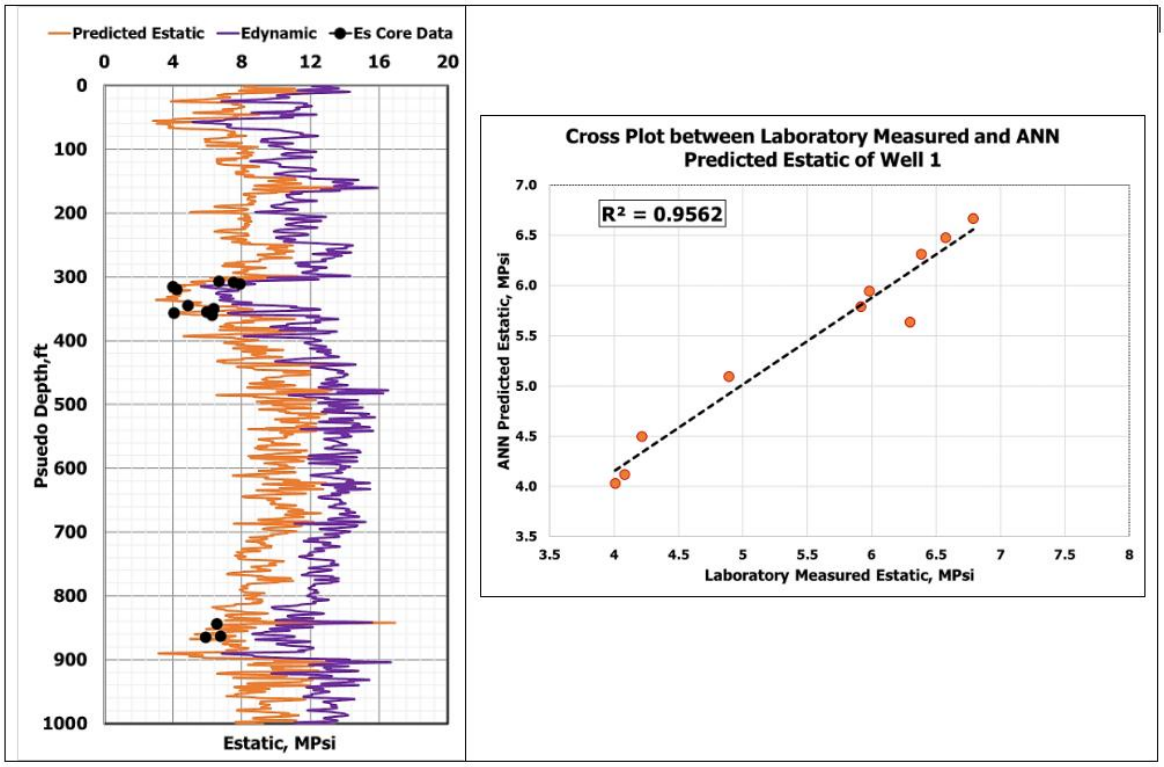

Figure 5.30 Static Young's modulus prediction using proposed ANN model on Well No. 1.

5.5.4.2 Well No. 2

Fig. 5.31 shows the ANN predicted E_{static} for an interval of 1000 ft. R^2 of 0.895 indicates that the new developed correlation is giving the close results similar to laboratory measured static values.

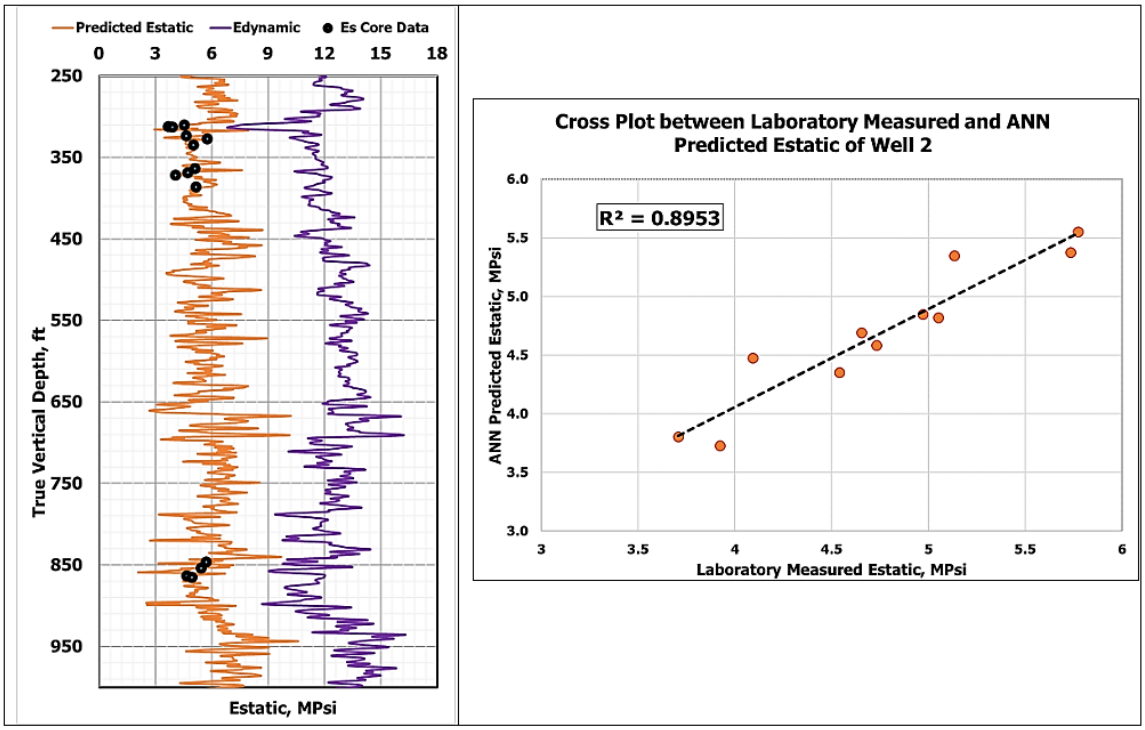

Figure 5.31 Static Young's modulus prediction using proposed ANN model on Well No. 2.

5.5.4.3 Well No. 3

This well contains four triaxial compressional test static Young's modulus values. Fig. 5.32 shows the ANN predicted E_{static} for a reservoir section of 400ft.

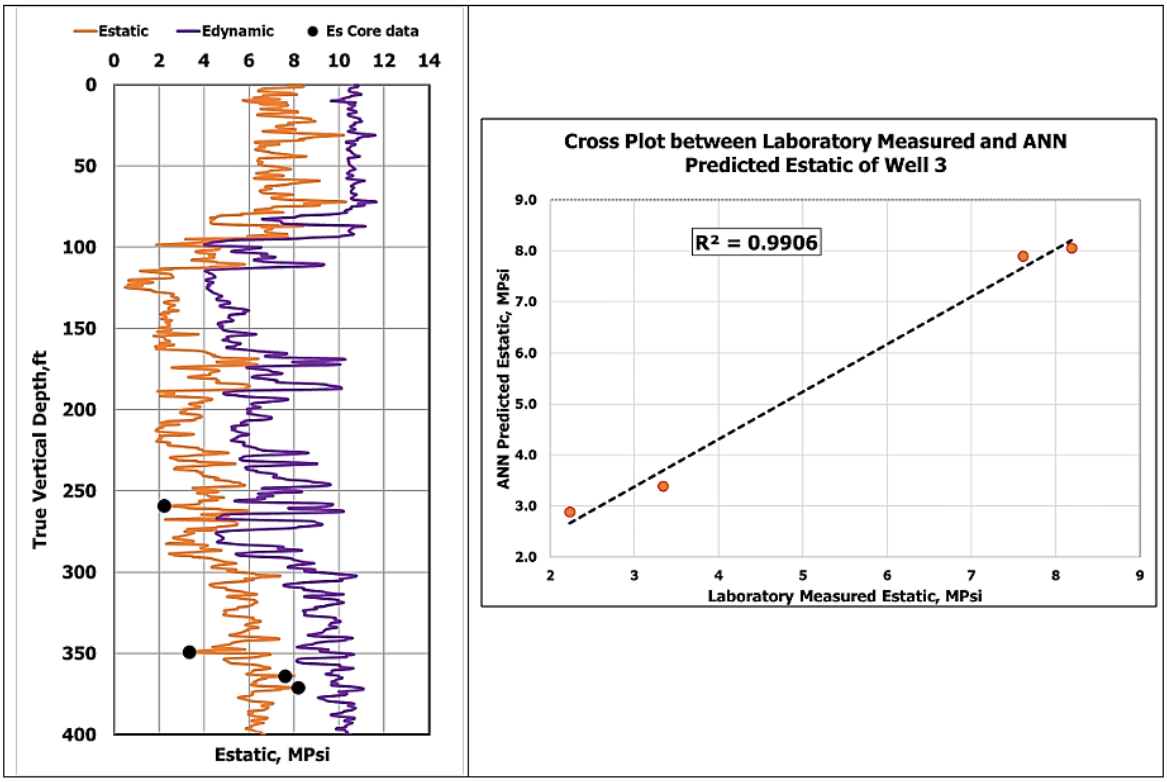

Figure 5.32 Static Young's modulus prediction using proposed ANN model on Well No. 3.

5.5.5 Comparison of proposed model with the commonly used correlations in oil and gas industry

To check the accuracy and the performance of the proposed model, it was compared with the commonly used empirical correlations in the oil industry to predict E_{static} (Kings 1983, Eissa & Kazi 1988, Wang 2000, Canady 2011 and Najeibi 2015). This comparison was made on Well No. 1 data whose complete input wireline log data is given in Fig. 5.27. Fig. 5.33 shows the comparison of ANN predicted and other correlations predicted E_{static} values. The E_{static} prediction from Eissa and Kazi using Eq 15 shows very poor match only few data points were matched with actual laboratory measured E_{static} values. The E_{static} prediction from Canady correlation using Eq 17 also shows very poor match, only two data points were matched with actual laboratory measured values. Kings, and Wang correlations Eq 14 and Eq 16 captured the non-linearity of the data but their correlations

also did not match with any lab measured data points. The E_{static} predicted using Najeibi correlation from Eq. 7 matched with only one actual data point. The static Young's modulus predicted using proposed ANN correlation gave the best match with all data points.

The complete statistical comparison of the ANN predicted and other correlation prediction on Well No. 1 is given in Table 5.32.

Table 5. 32 Comparison of proposed E_{static} ANN model with commonly used E_{static} Empirical Correlations.

CORRELATIONS	AAPE	RMSE	R^2	Emin	Emax
Kings (1983)	40	1.97	0.9	3.75	648
Eissa & Kazi (1988)	25.8	2.25	0.87	0.0043	283
Wang (2000)	54.25	3.95	0.89	1.138	187
Canady (2011)	60	7.48	0.81	80	97
Najeibi (2015)	30.4	3.15	0.84	2.5	110
Proposed ANN Model	6.2	0.3535	0.96	0.043	47

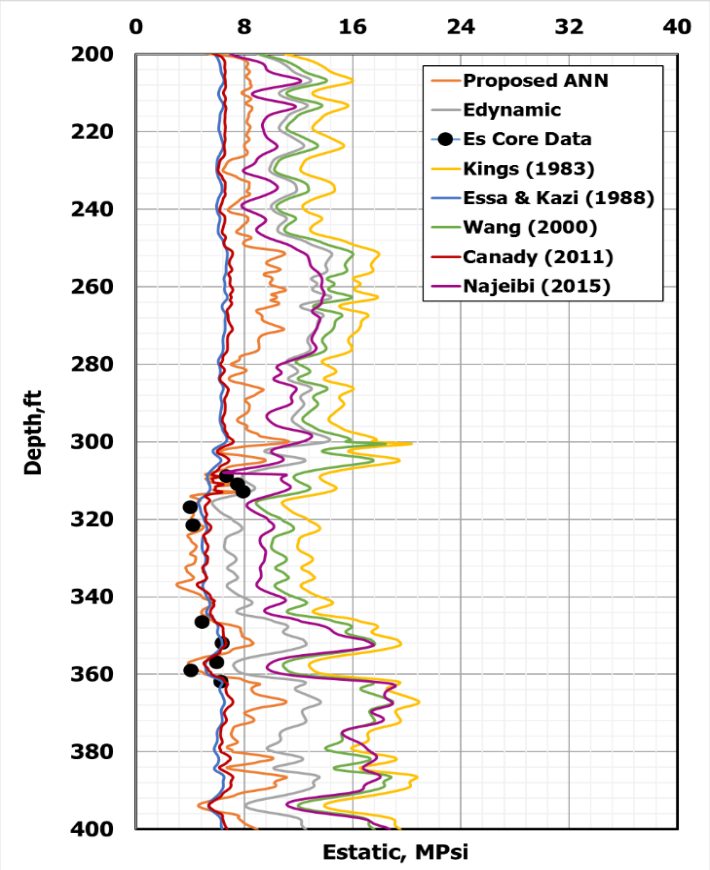

Figure 5.33 Comparison of ANN predicted E_{static} with other correlations on Well No. 1 interval (200-400) ft.

5.6 Modeling for Static Poisson's Ratio Prediction

Three AI techniques, namely, ANN, ANFIS and SVM were implemented to predict static Poisson's ratio.

5.6.1 Comparison of Three AI Techniques for Predicting Poisson's Ratio

On comparing the individual performances of three best AI models, ANN on a set of 70% random data dedicated for training, produced R^2 of 0.97 and an AAPE 1.3, ANFIS produced R^2 of 0.93 and an AAPE of 3.5 and SVM produced R^2 0.81 and an AAPE of 8.3, while on testing ANN produced R^2 of 0.96 and an AAPE 1.4, ANFIS produced R^2 of 0.92 and an AAPE of 3.3 and SVM produced R^2 0.8 and an AAPE of 8.3 as shown in

Figs 5.34 - 5.35. ANN outperformed all other techniques on prediction of Poisson's ratio during on both training and testing phases.

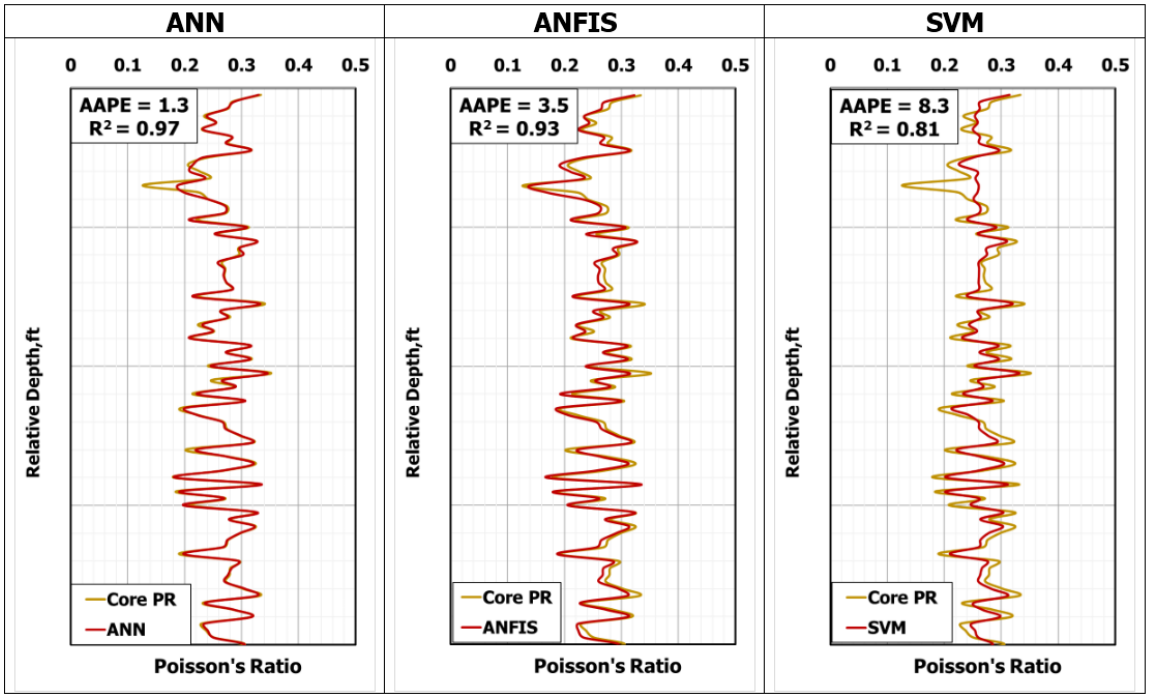

Figure 5. 34 Training comparison of static Poisson's ratio models using ANN, ANFIS and SVM.

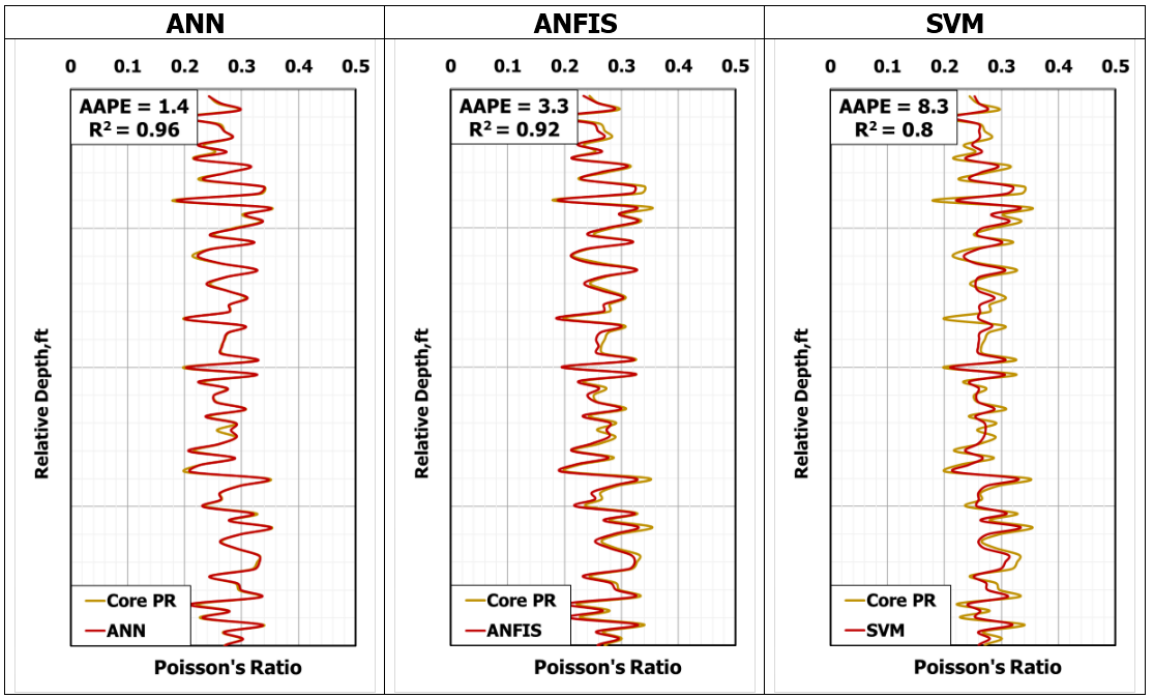

Figure 5. 35 Testing comparison of static Poisson's ratio models using ANN, ANFIS and SVM.

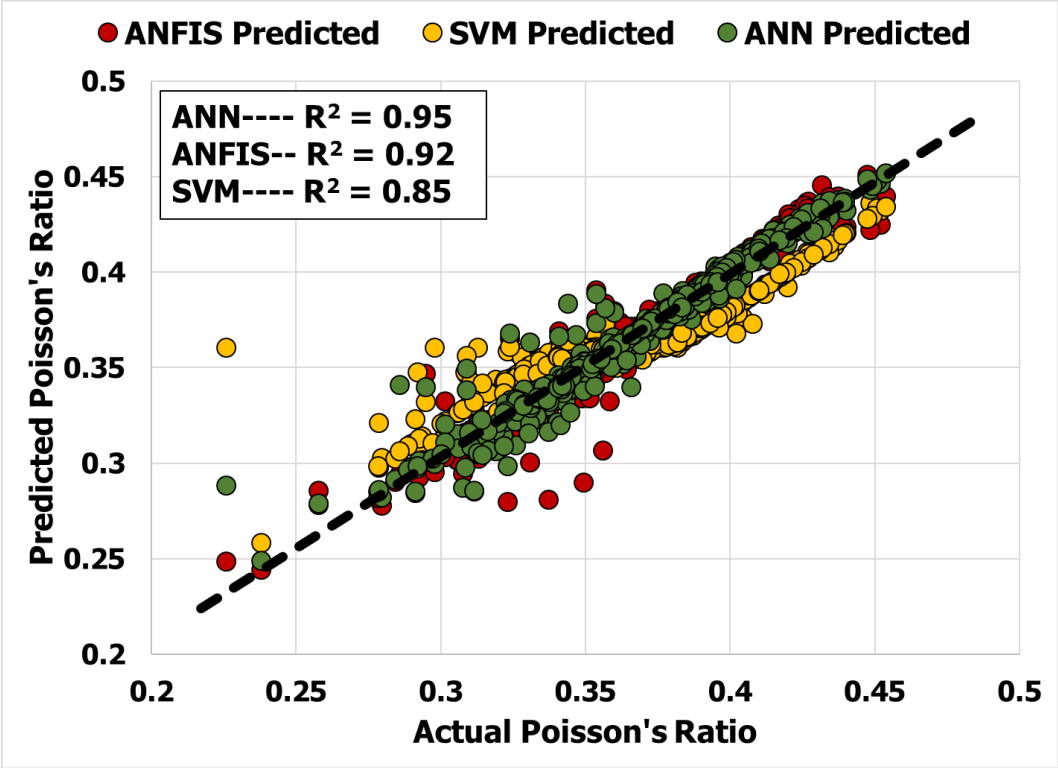

Figure 5. 36 Cross plot comparison of three techniques on overall data.

5.6.2 Neural Network Architecture for Predicting Static Poisson's Ratio

A back propagation neural network algorithm was implemented to predict static Poisson's ratio. The static Poisson's Ratio ANN model based on three input parameters, namely, bulk density, compressional time and shear time, one hidden layer and one output parameter. The neurons in the hidden layer varied between 5 and 20. The optimum neurons were found to be 20 since they produced highest R^2 for unseen data simultaneously with seen data. Tan-sigmoidal transfer function was used between input and hidden layer and linear type transfer functions was used between hidden and output layer. Table 5.33 shows the complete anatomy of proposed static Poisson's Ratio ANN model.

Table 5.33 Neural network architecture of static Poisson's Ratio model.

Neural Network Parameters	Ranges
Number of Inputs	3
Number of Outputs	1
Number of Neurons	20
Number of Hidden Layer(s)	1
Training Algorithm	Levenberg Marquadt
Learning rate	0.12
Hidden Layer transfer function	Tan-sigmoidal
Outer layer transfer function	pure linear
Training Ratio	0.7
Testing Ratio	0.15
Validation Ratio	0.15

5.6.3 Validation of the Developed Empirical Model for static Poisson's Ratio

To validate the accuracy and generalization power of the ANN based proposed model for Poisson's Ratio it was compared with the real field data of Well No. 1, 2 and 3. All three wells were located in limestone formation. These three wells have certain laboratory measured values of static Poisson's ratio.

5.6.3.1 Well No. 1

Input data and complete statistics of Well No. 1 is given in Fig 5.27.

Fig. 5.37 shows the ANN predicted Poisson's ratio for an interval of 1000 ft. This well's data contain 13 actual laboratory measured static Poisson's ratio values using triaxial compressional tests. Right side of Fig. 5.37 shows the cross plot between laboratory measured static Poisson's ratio and ANN predicted Poisson's ratio. Cross plot shows the R^2 value of 0.83. The PR profile in Fig. 5.37 and cross plot clearly indicates that the developed model and correlation based on ANN is fully capable of predicting Poisson's ratio using three input, namely, bulk density, compressional and shear wave travel time.

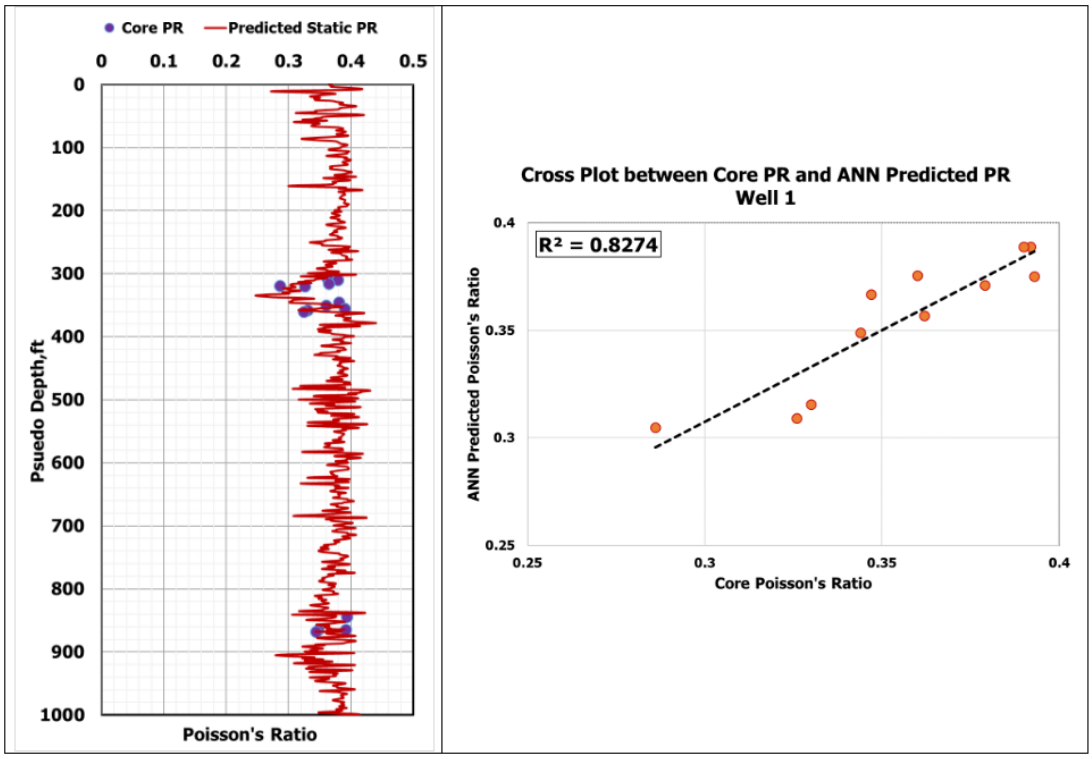

Figure 5. 37 Static Poisson's ratio prediction using proposed ANN model on Well No. 1.

5.6.3.2 Well No. 2

Input data of Well No. 2 is given in Fig 5.38. Fig. 5.39 shows the ANN predicted PR for a reservoir section of 400ft. This well contain five triaxial compressional test measured static Poisson's ratio values. R^2 of 0.8 between actual and ANN predicted results shows the perfect match and it clearly confirms the robustness of the proposed model.

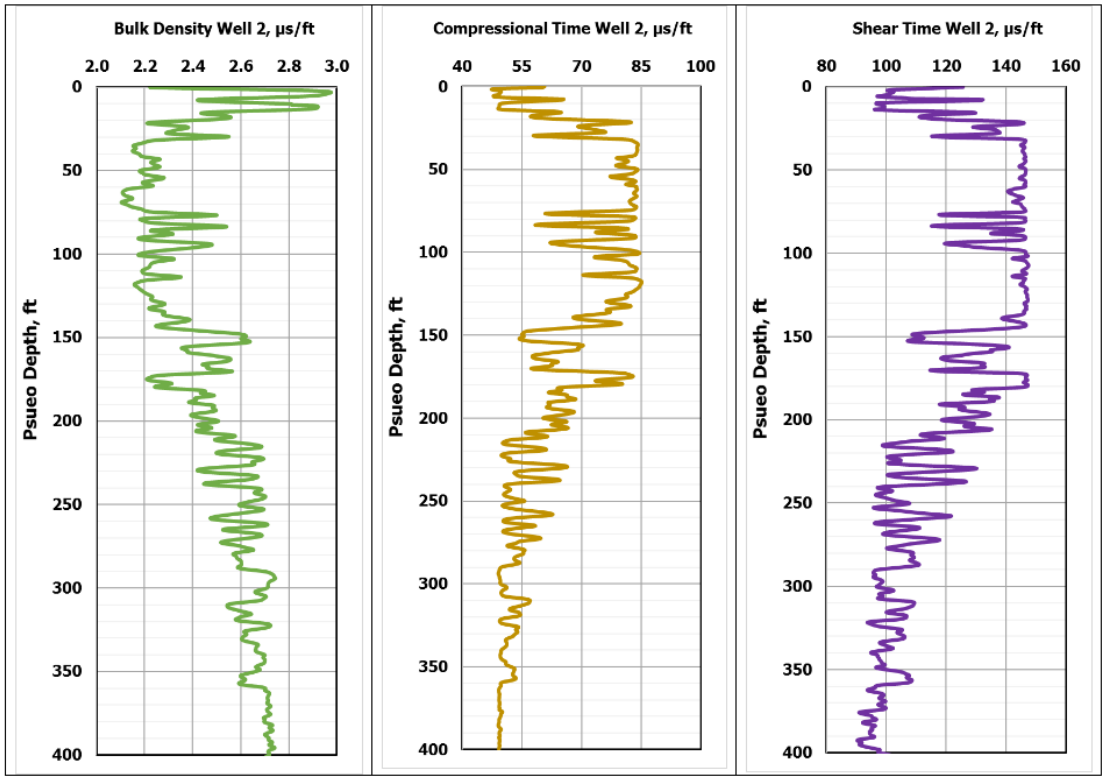

Figure 5. 38 Real field wireline log input data for static Poisson's ratio model Well No. 2.

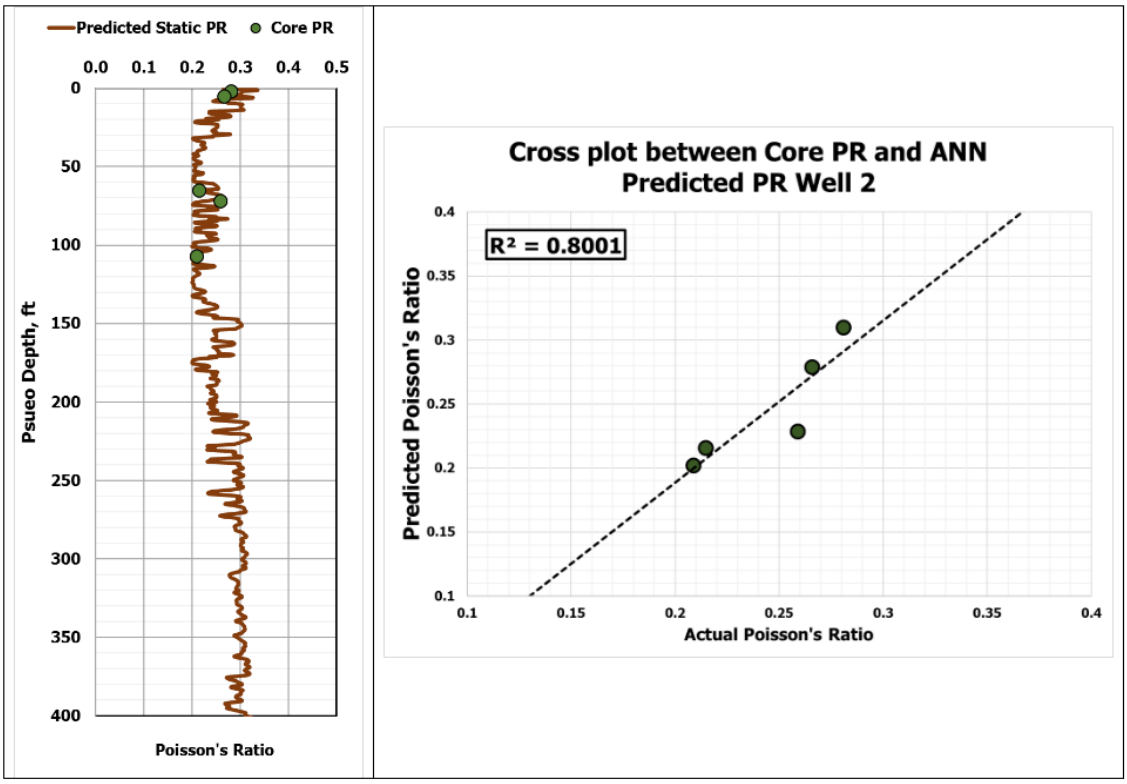

Figure 5. 39 Static Poisson's ratio prediction using proposed ANN model on Well No. 2.

5.6.3.3 Well No. 3

Fig. 5.39 shows the wireline log input data for Well No. 3 for reservoir section of an interval 400ft. Fig. 5.40 shows the ANN predicted PR with the cross plot between actual and ANN predicted data set. This well contain four triaxial compressional test measured static Poisson's ratio values. R^2 of 0.81 shows the perfect match and it clearly confirms the robustness of the proposed model.

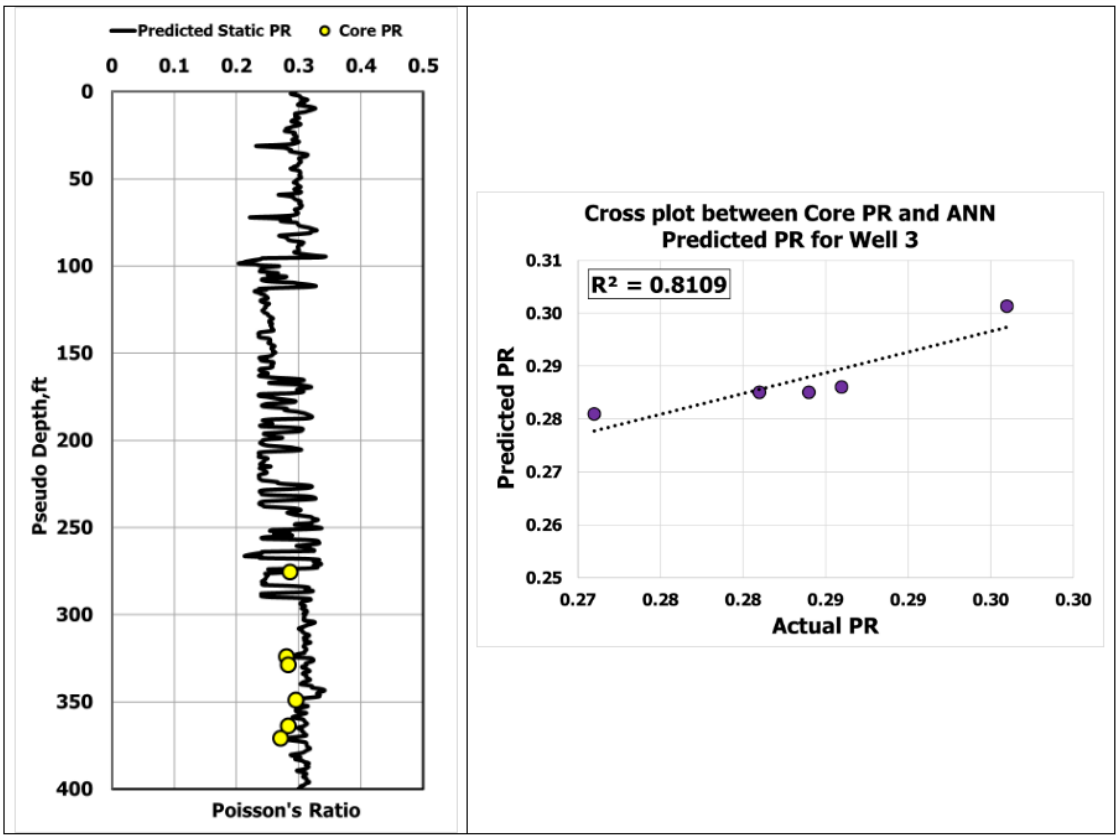

Figure 5. 40 Static Poisson's ratio prediction using proposed ANN model on Well No. 3.

5.6.4 Empirical Model for Poisson's Ratio

The empirical model is derived from the ANN model based on weights and biases associated with input layer/hidden layers and hidden layer/outer layer. The weights between input layer and hidden layer termed as w1 and weights between hidden layer and outer layer termed as w2 are given in Table 5.34. The proposed static Poisson's ratio ANN based empirical correlation is given below

$$PR_{static_n} = \left[\sum_{i=1}^{N} w_{2_i}\left(\frac{2}{1+e^{-2\left(w_{1_{i,1}}\rho_n + w_{1_{i,2}}\Delta t_{c_n} + w_{1_{i,3}}\Delta t_{s_n} + b_{1_i}\right)}}\right)\right] + b_2 \quad (51)$$

5.6.4.1 Steps to use new empirical correlation for static Poisson's Ratio

Step 1: Normalize the input parameters between the range [-1 1] before using Eq. 51. Normalization is done by two points slope form given by Eq. 52 and Eq. 53

$$\frac{Y - Y_{min}}{Y_{max} - Y_{min}} = \frac{X - X_{min}}{X_{max} - X_{min}} \tag{52}$$

where, Ymin = -1, Ymax =1, X is the input parameters, X_{min} is the input parameter minimum value and X_{max} is the input parameter maximum value.

$$Y = 2 \times \left(\frac{X - X_{min}}{X_{max} - X_{min}}\right) - 1 \tag{53}$$

Step 2: Use Eq. 51 to calculate PR_{static} in normalized form. Eq. 51 can be used by using the weights given in Table 5.34. The sequence of parameters goes in to the model given as: bulk density, compressional time and shear time.

Step 3: The value of PR_{static} obtained from Eq. 51 is in the normalized form, to convert it in the real value form, the result obtained from Eq. 51 must be de-normalized by applying Eq. 54

$$PR_{Static} = \frac{(0.45-0.23)(PRstatic_n+1)}{2} + 0.23 \tag{54}$$

$$PR_{Static} = 0.11 * PRstatic_n + 0.34 \tag{55}$$

Table 5.34 Weights and biases of ANN based static Poisson's Ratio empirical model.

Hidden Layer Neurons (N)	Weights between Input and Hidden Layer (W1)			Weights between Hidden and output Layer (W2)	Hidden Layer Bias (b1)	Output Layer Bias (b2)
1	-1.2314	-2.9794	2.0121	0.3913	3.8005	-0.0967
2	1.3902	2.5859	-2.4137	-0.2448	-3.3980	
3	3.4145	-0.1898	1.4337	-0.0680	-3.0697	
4	-2.5968	0.9273	2.7916	0.1152	2.2065	
5	-3.3914	0.4693	-1.6750	0.0649	2.1876	
6	2.8713	2.1071	-1.1225	0.4812	-2.1325	
7	-0.4226	-2.0808	3.2887	0.8226	0.8938	
8	2.0472	-1.6680	2.0529	0.5568	-0.6840	
9	-2.1682	-3.1313	-0.3281	0.7791	1.0094	
10	2.5987	-0.8754	-2.6584	-0.1450	-0.3550	
11	2.4961	-0.3705	2.7577	-0.2773	0.4325	
12	3.6297	0.7305	0.2771	0.1844	0.7534	
13	2.4701	-2.4706	-1.6484	0.2709	0.7058	
14	1.3511	-2.2715	-2.5952	-0.3211	1.8720	
15	2.4343	2.7492	-0.1814	-0.2044	2.2261	
16	1.2946	2.9277	2.1830	-0.0862	2.0350	
17	2.2039	-1.0213	3.0066	0.3858	2.4757	
18	-2.8993	-1.4603	-1.6259	0.1591	-3.1477	
19	0.9094	-2.9271	2.2723	-0.4253	3.3760	
20	0.5098	-3.0616	1.5846	-0.7362	4.1947	

5.7 Failure Parameters Prediction

Failure parameters are:

1. Unconfined Compressive strength (UCS),
2. Cohesion, and
3. Friction Angle (FANG).

5.7.1 Data Analysis for Failure Parameter Models

The data used to develop models for failure parameters were obtained from several wells located in different fields. Most of the data were from limestone formation with low

percentage of sandstone and dolomite and no gas effects as shown in Fig. 5.41. Wireline log data included gamma ray, neutron porosity, bulk density and compressional and shear wave travel times. The core data at corresponding depths comprised of UCS, FANG and cohesion. Core data were obtained from the laboratory measurements of triaxial compressional tests. The set of data were randomly divided in to two parts; 70% of the data were used for training while 30% of the data were used for testing the accuracy and generalization capabilities of the model. A complete statistical description of the data used for training and testing is given in Table 5.35.

Table 5.35 Statistical description of the data used for training/testing of failure parameters.

Parameters	Max	Min	Range	Mean	Std. Deviation	Variance	Skewness	Kurtosis
Static Young's modulus E_s, Mpsi	13.05	0.608	12.446	3.911	2.560	6.554	1.231	0.870
Compressional wave velocity, km/s	6.719	1.988	4.731	5.009	1.090	1.187	-0.367	-0.821
Shear wave velocity, km/s	3.614	1.055	2.559	2.744	0.510	0.261	-0.517	-0.231
Bulk Density g/cc	2.939	2.170	0.770	2.578	0.177	0.031	-0.347	-0.520
Unconfined Compressive Strength, Ksi	26.11	3.394	22.713	10.81	5.184	26.875	0.982	0.483
Cohesion, Ksi	8.69	0.26	8.95	2.377	1.23271	1.52	1.628	5.733

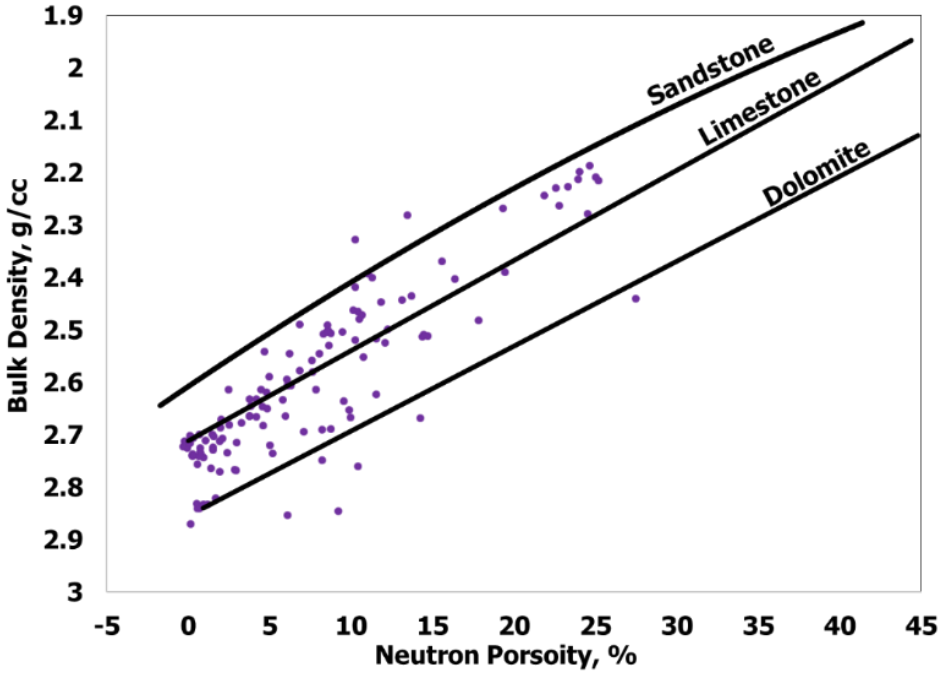

Figure 5.41 Lithology cross plot for data used to model failure parameters.

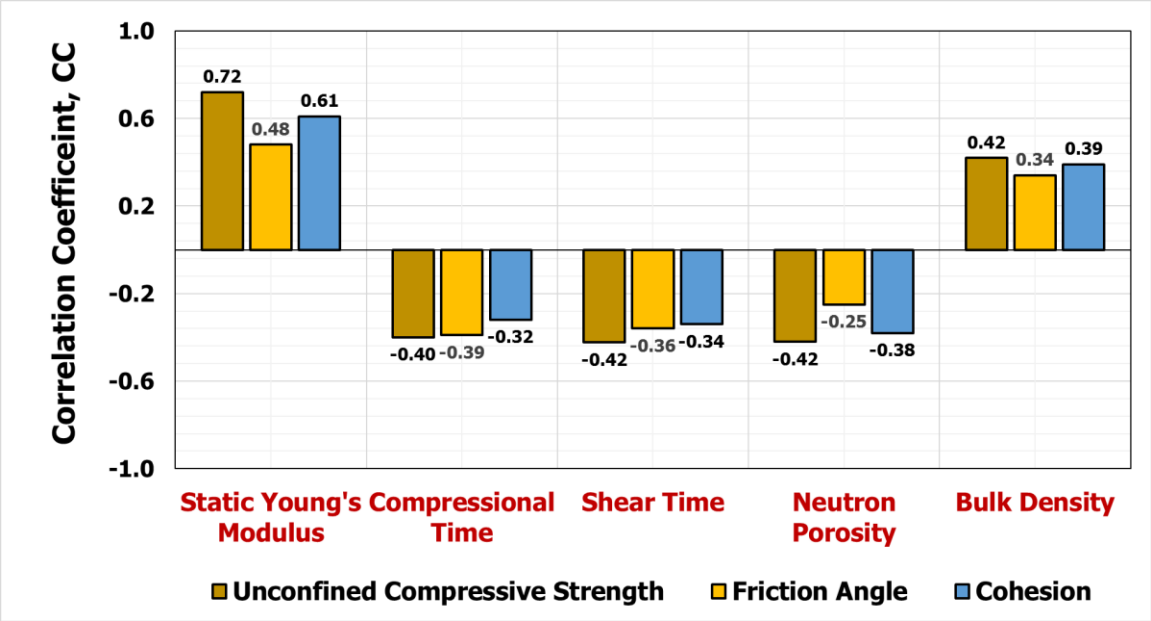

Figure 5. 42 Relative importance of input parameters with respect to failure parameters.

5.8 Modeling for the Prediction of Unconfined Compressive Strength (UCS)

To find the optimal input parameters for UCS prediction, five cases were designed:

1. Case 1: Three inputs (Bulk Density, Compressional wave velocity and Shear wave velocity)
2. Case 2: Four inputs (Bulk Density, Neutron porosity, Compressional wave velocity and Shear wave velocity)
3. Case 3: Four inputs (Static Young's Modulus, Bulk Density, Neutron porosity, Compressional wave velocity and Shear wave velocity)
4. Case 4: Four inputs (Static Young' s Modulus, Bulk Density, Compressional wave velocity and Shear wave velocity)
5. Case 5: Two inputs (Static Young' s Modulus and Bulk Density)

In all of the above cases, static Young's modulus was used as an input as was used by earlier researchers (Najebi et al. 2014, Bradford et al. 1998, Chang et al. 2006). However, the end of this section shows a two-step approach to prediction of failure parameters, viz., prediction of static Young's modulus using AI techniques, and the use of the predicted value in addition to others to predict failure parameters.

5.8.1 Results from ANN to Predict UCS

Fig 5.43 shows the performance of ANN on different cases. It is evident that case 4 produced the best results by giving high R^2 and low AAPE. Further improvement in the model was achieved by performing parametric study. Final ANN model for UCS prediction was found to be based on back propagation neural network algorithm with 20 neurons. Fig 5.44 shows the overall prediction performance of the best ANN model.

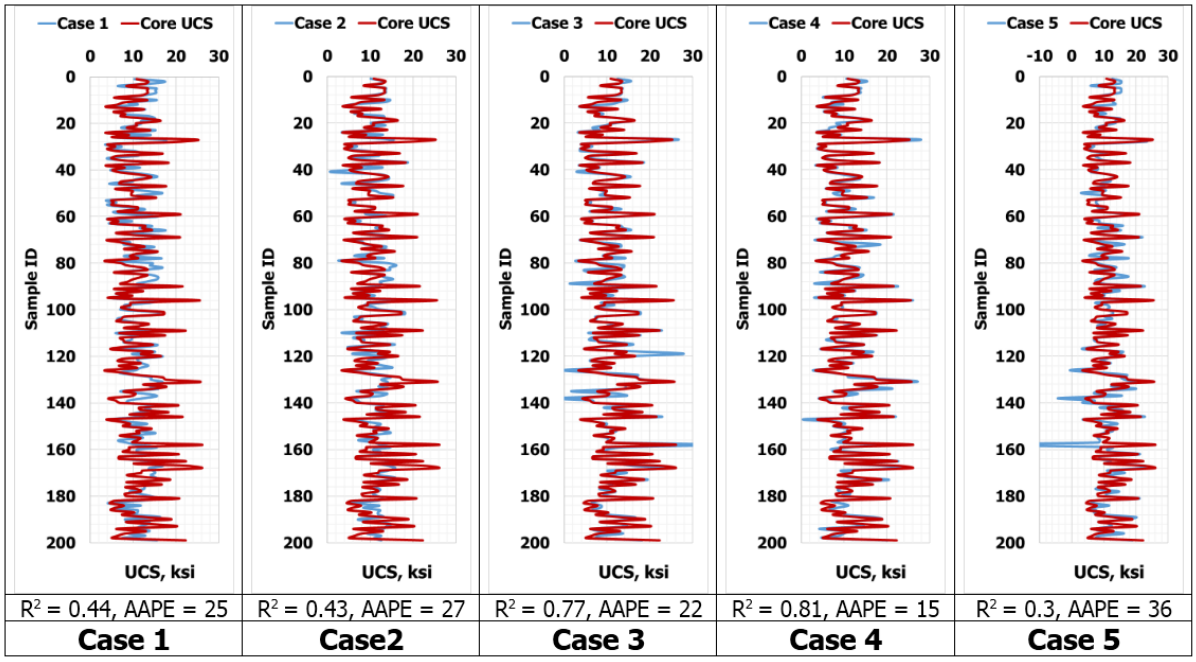

Figure 5.43 Comparison of different cases for the prediction of UCS using ANN.

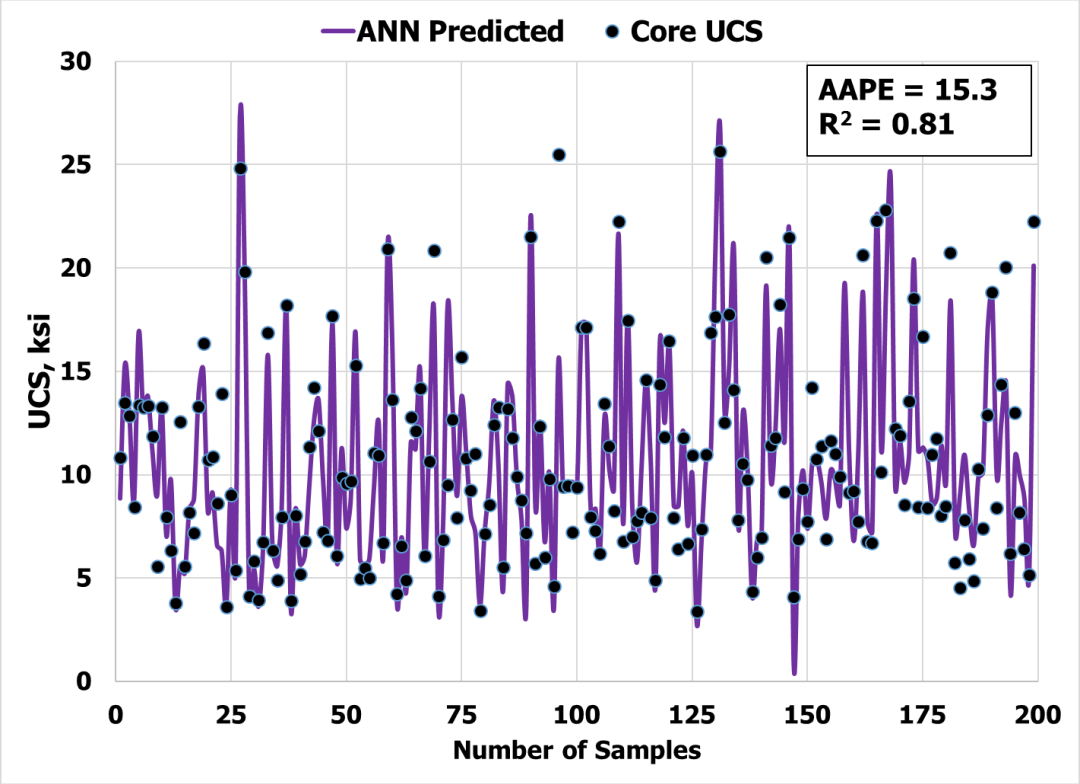

Figure 5.44 Overall prediction performance of ANN based model for UCS prediction.

5.8.2 Results from ANFIS to Predict UCS

Using ANFIS five cases defined above were studied and their performances are shown in Fig 5.45. Case 4 which is based on four input parameters, namely, Static Young's modulus, Bulk density, compressional and shear wave velocities was selected as the best case.

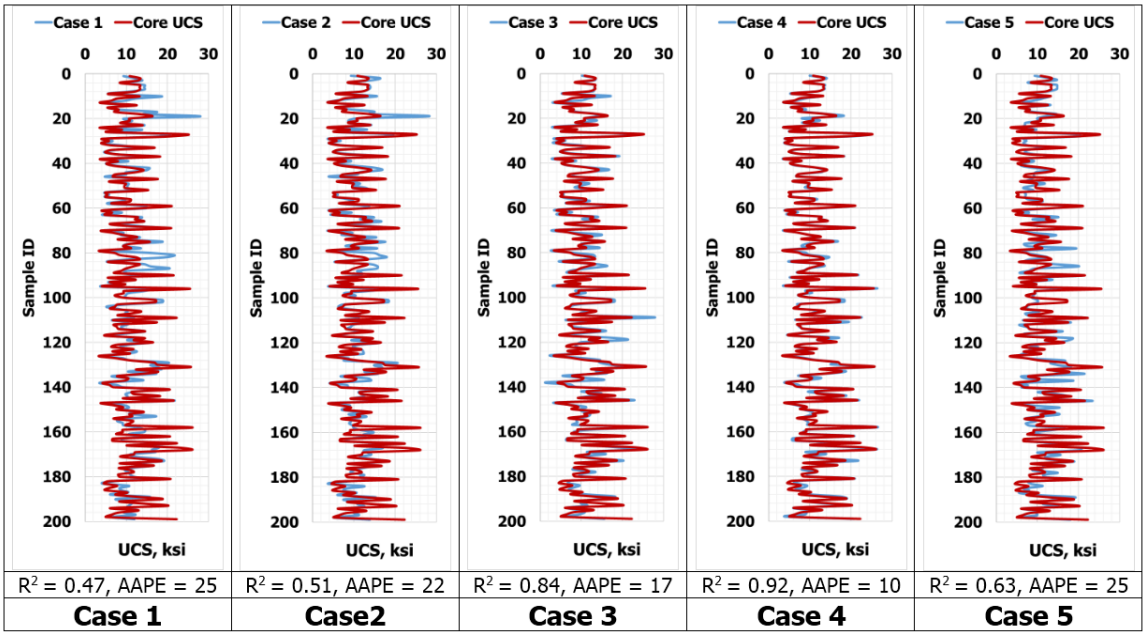

Figure 5.45 Comparison of different cases for the prediction of UCS using ANFIS.

Further improvement in the ANFIS model was achieved by performing parametric study. Final ANFIS model was based on Genfis2 with a cluster radius size of 0.5. Optimum cluster radius size was found by varying the cluster radii between 0.1 – 1. Fig 5.46 shows the performance of optimum ANFIS model to predict UCS.

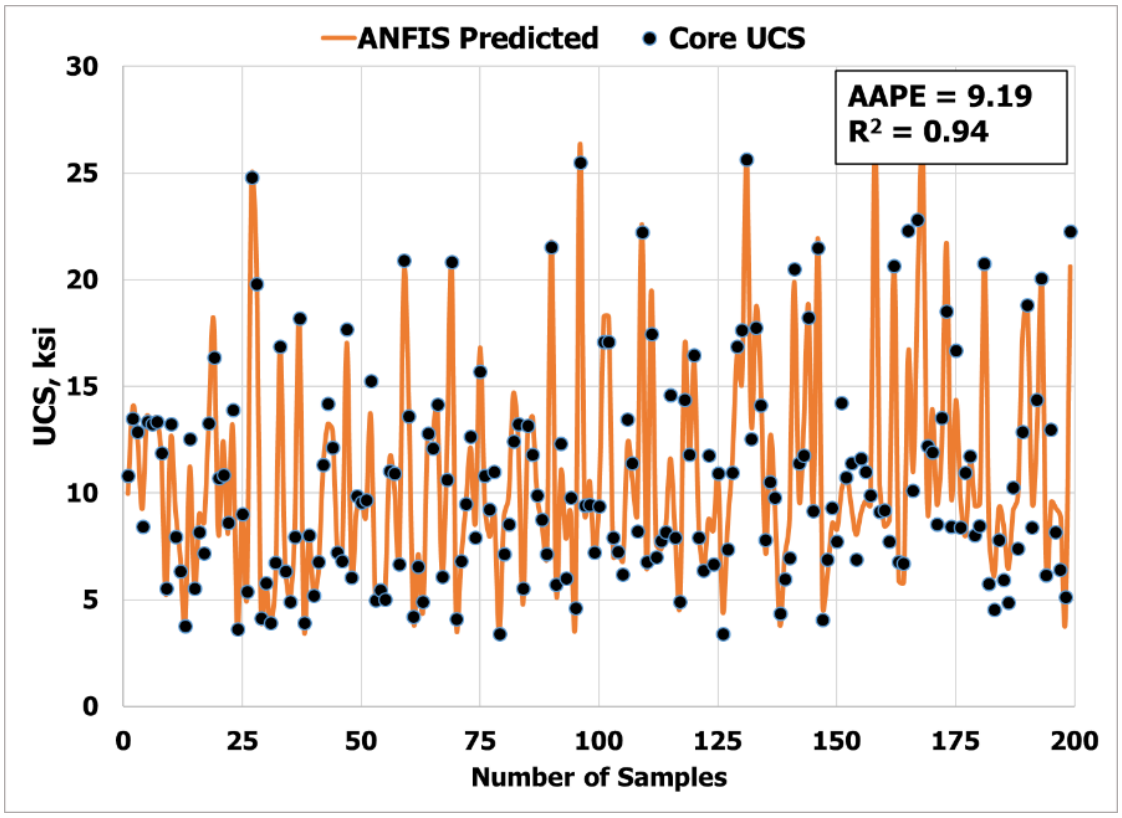

Figure 5.46 Overall prediction performance of ANFIS based model for UCS prediction.

5.8.3 Results from SVM to Predict UCS

From Fig 5.47, it is observed that case 4 gives the best results by giving high R^2 and low AAPE. Further improvement in the model was achieved by performing parametric study. Final SVM model for predicting UCS was based upon Gaussian type kernel function. Final SVM model to predict UCS is shown in Fig 5.48.

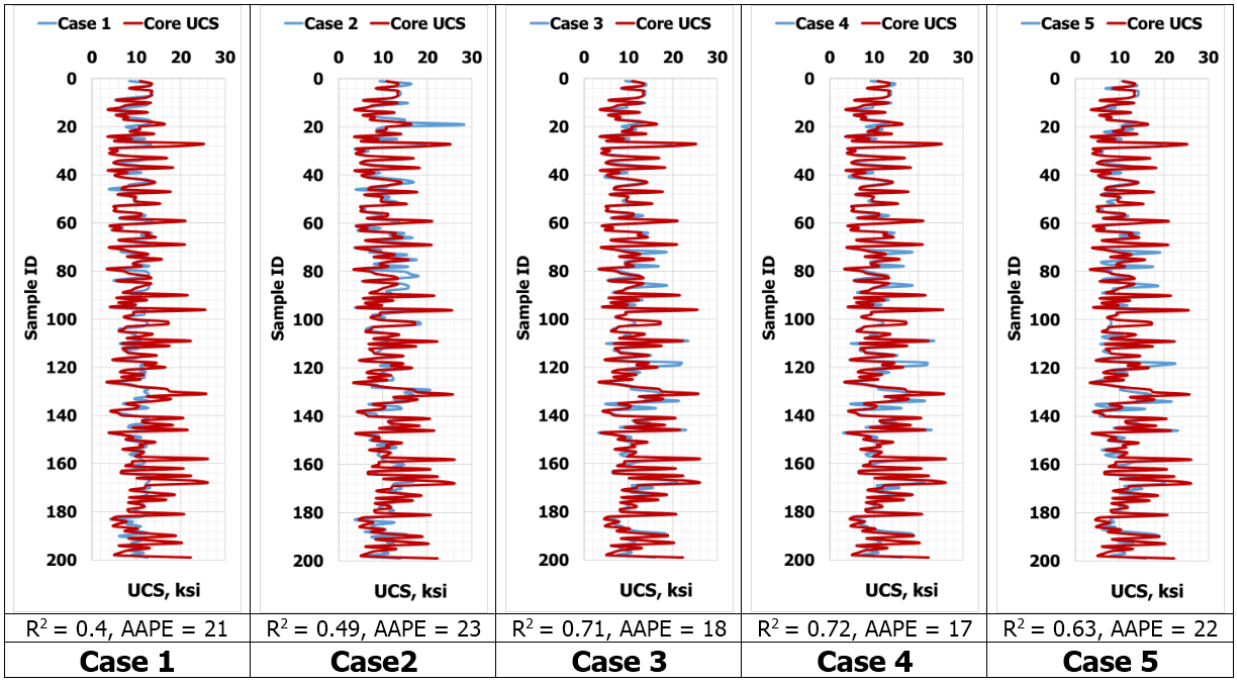

Figure 5.47 Comparison of different cases for the prediction of UCS using SVM.

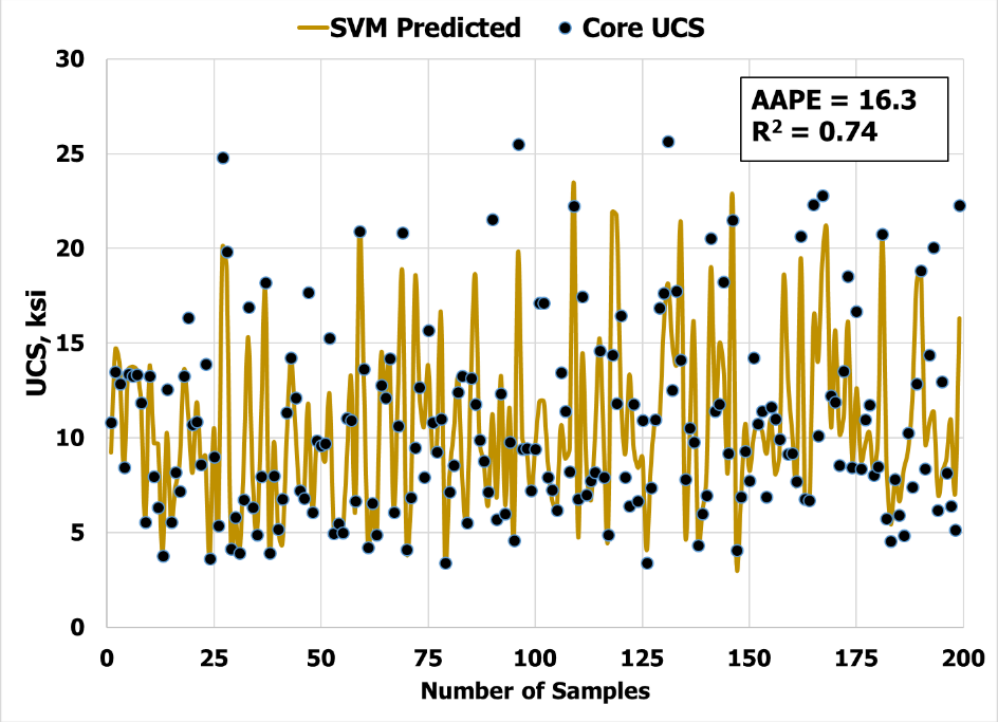

Figure 5.48 Overall prediction performance of SVM based model for UCS prediction.

5.8.4 Comparison of Three AI techniques on prediction of UCS

Figs 5.49 – 5.51 shows the performance of three best AI models on overall data. ANN gave R^2 of 0.81 and an AAPE 15, ANFIS gave R^2 of 0.94 and an AAPE of 9.2, and SVM

gave R^2 0.74 and an AAPE of 16.3. From this comparison it is clear that on a given set of data, ANFIS with four input parameters (static Young's modulus, bulk density, compressional and shear wave velocities) is the best model to predict UCS.

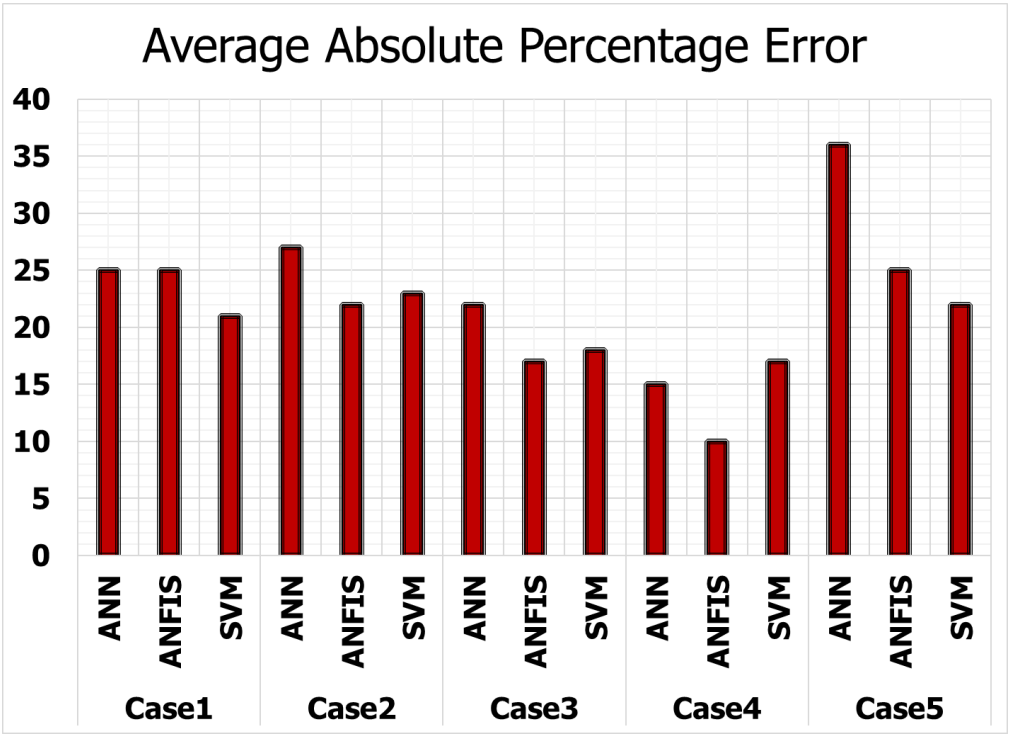

Figure 5.49 AAPE comparison of all cases.

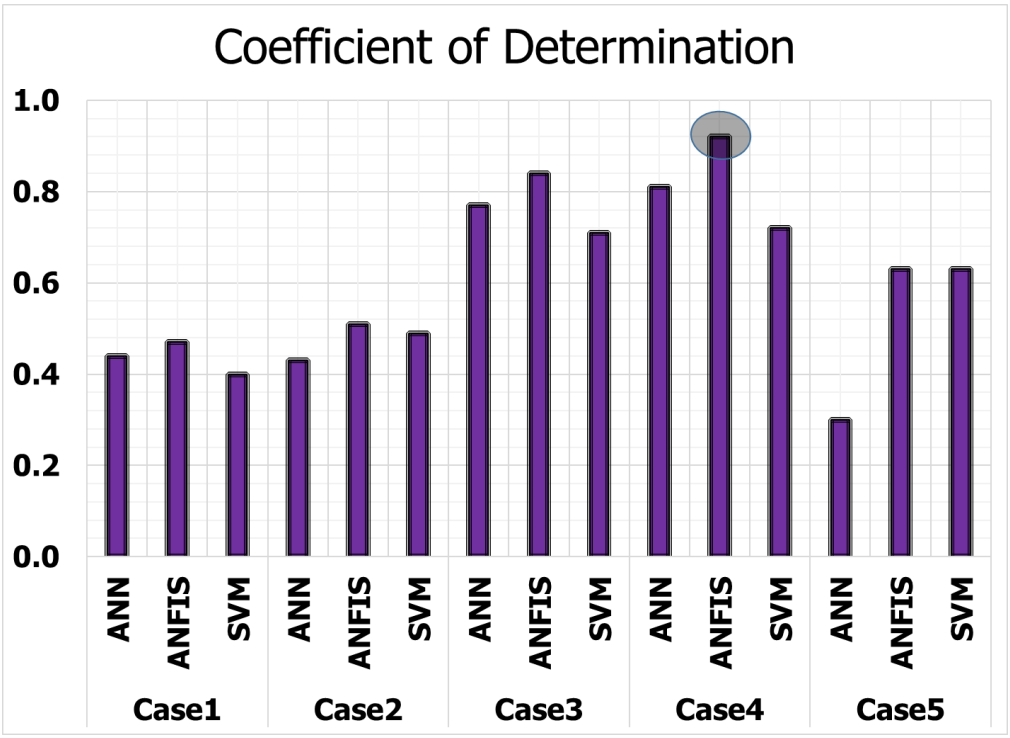

Figure 5. 50 Coefficient of determination comparison of all cases.

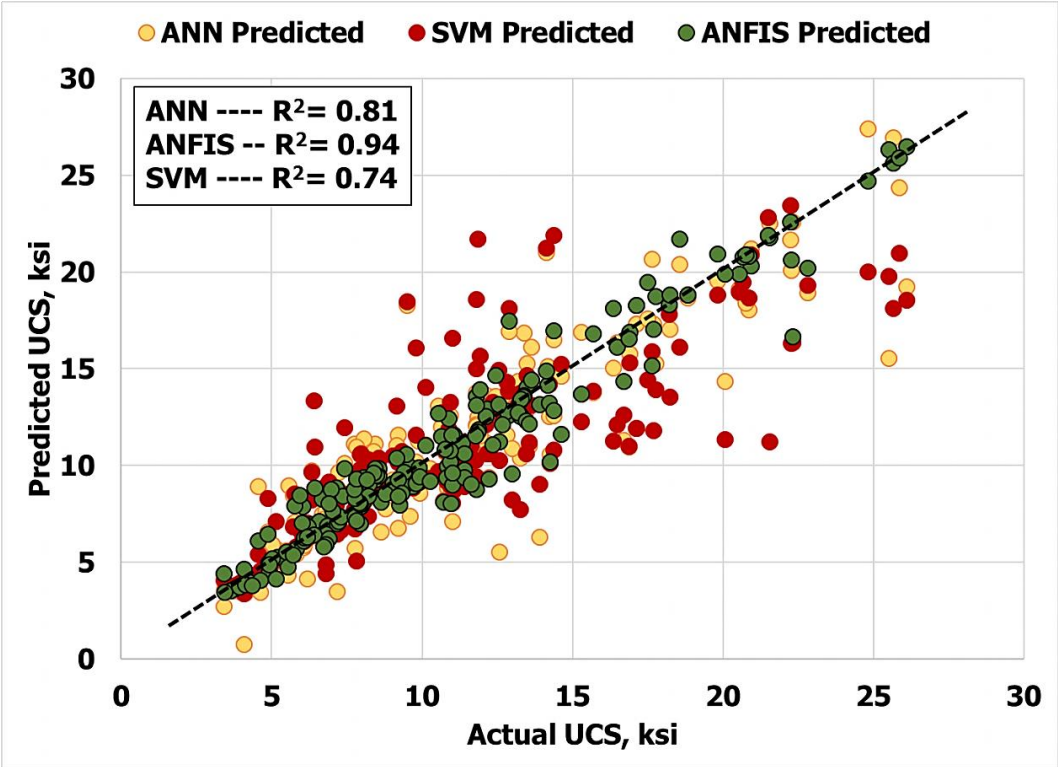

Figure 5. 51 Comparison of best AI models for the prediction of UCS.

5.8.5 Two Step Prediction of UCS using Optimized Model

Fig 5.52 shows the two step prediction of optimized ANFIS model on overall data. In two-step prediction approach, first, the static Young's modulus is predicted by using basic well logs, namely, bulk density, compressional time and shear time as given in section 5.5, and in second step the UCS is predicted using the predicted static Young's modulus along with other parameters, namely, bulk density, compressional and shear wave travel times. From this approach it is clearly evident that model is capable of predicting UCS using aforementioned parameters.

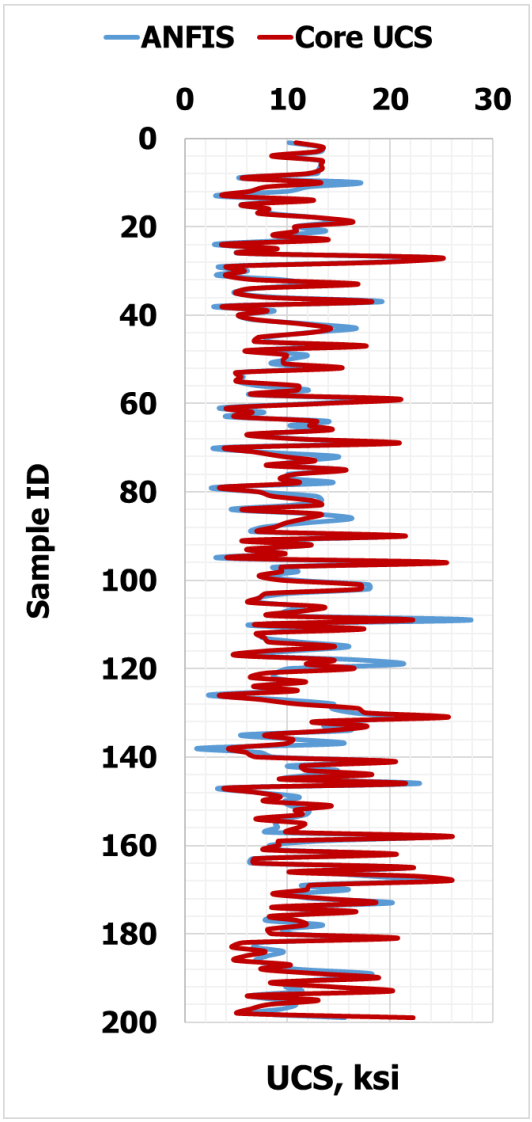

Figure 5. 52 Optimized two step ANFIS model prediction on overall data.

5.8.6 Validation of the Proposed Model

5.8.6.1 Well No. 1

Input Data of Well No. 1 is given in Fig 5.53. Fig. 5.54 shows the ANFIS predicted UCS for Well No. 1. This Well contains 13 actual laboratory measured UCS test points on selected cores using triaxial compressional test. Right side of Fig. 5.54 is the cross plot which shows the R^2 value of 0.91 between laboratory measured UCS values and ANFIS

predicted UCS values on the same depth from where these core plugs were retrieved. Cross plot clearly indicates that the developed model based on ANFIS is fully capable of predicting UCS using four inputs, namely, predicted static Young's modulus, bulk density, compressional and shear wave travel times.

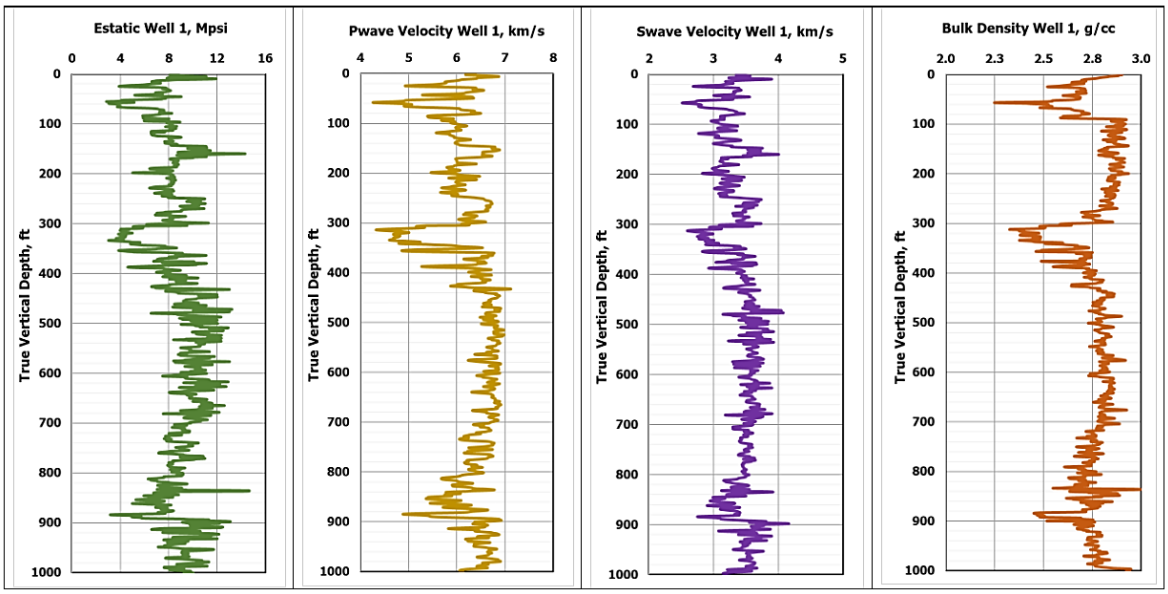

Figure 5.53 Real field wireline log input data for UCS model Well No. 1.

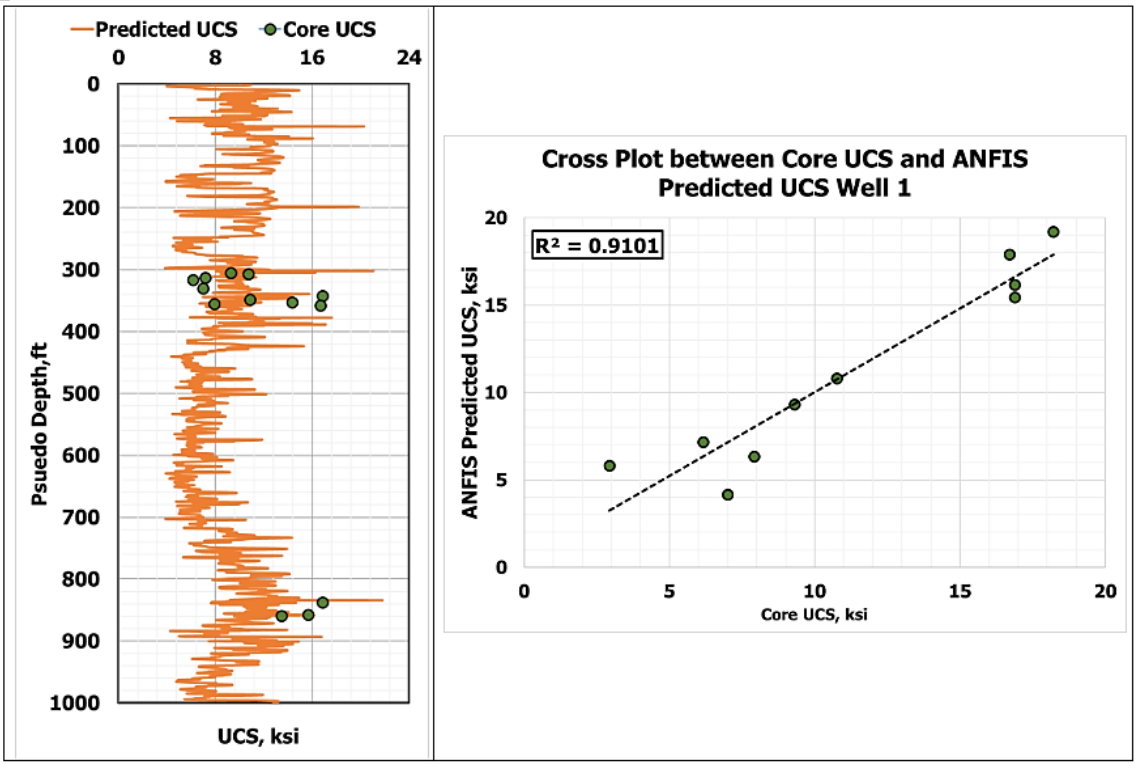

Figure 5.54 UCS prediction using proposed ANFIS model on Well No. 1.

5.8.6.2 Well No. 2

Input Data of Well No. 2 for an interval of 400 ft is given in Fig 5.55. Fig. 5.56 shows that the proposed ANFIS model prediction gives perfect results on comparing with actual laboratory measured UCS.

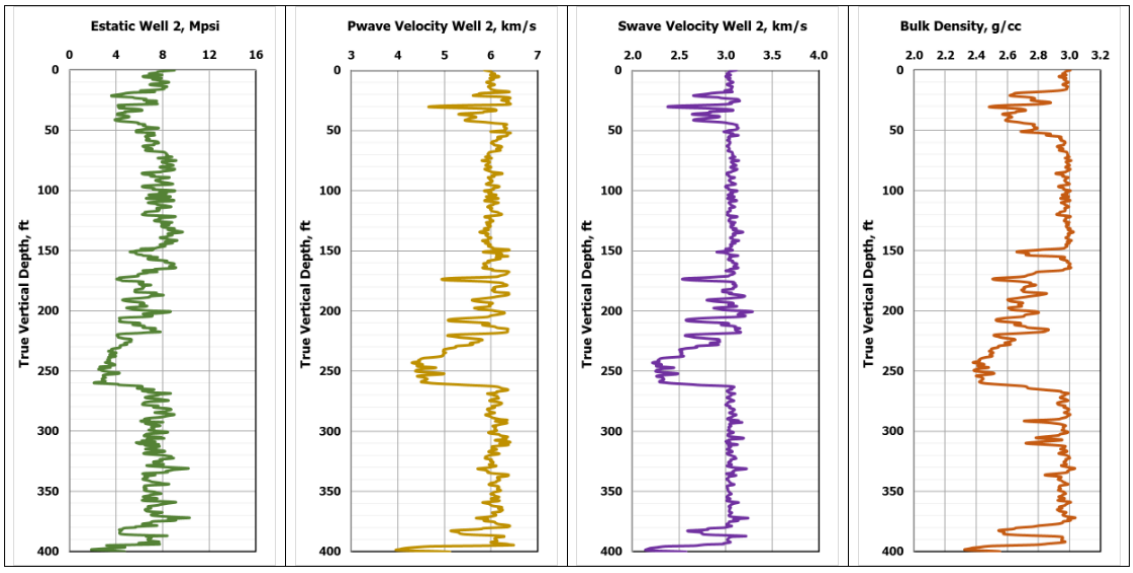

Figure 5.55 Real field wireline log input data for UCS model Well No. 2.

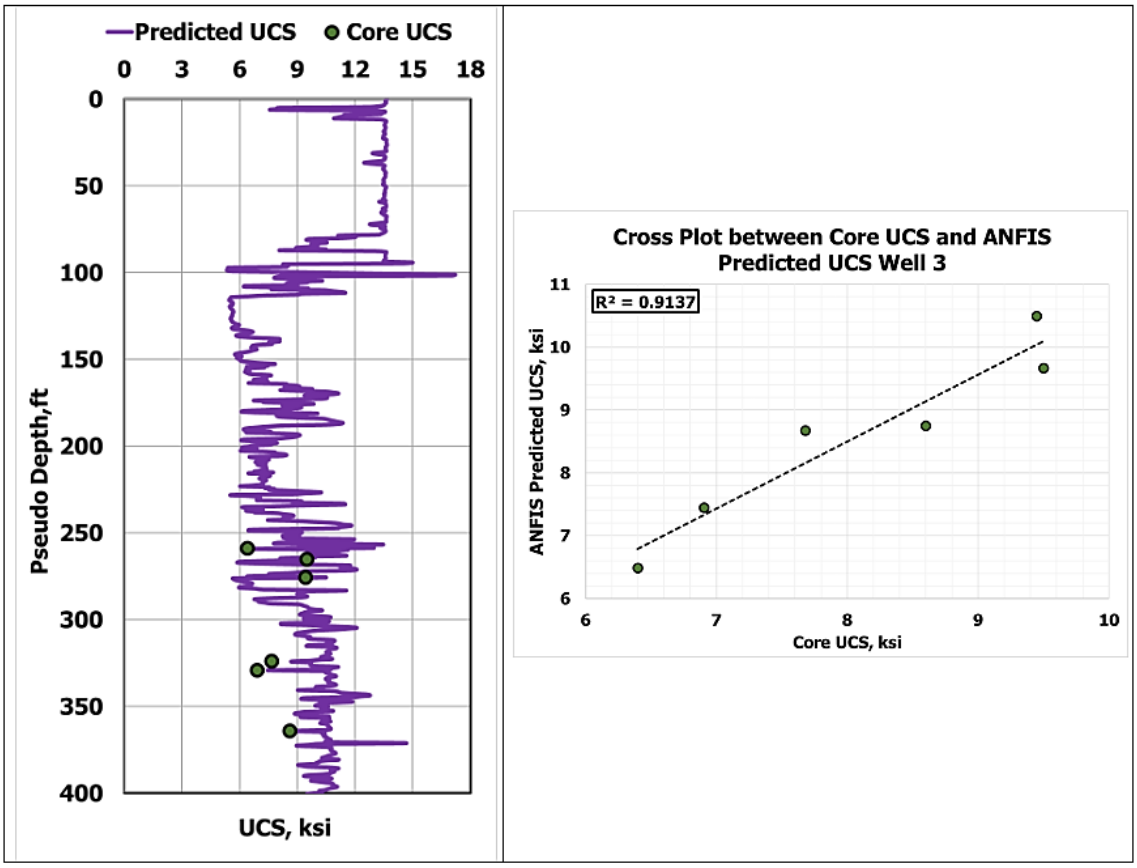

Figure 5.56 UCS prediction using proposed ANFIS model on Well No. 2.

5.8.7 Model Validation on field Data using Two Step Prediction of UCS

Fig 5.57 shows the validation of two step prediction model for failure parameters on Well No. 2. Input data of Well No. 2 is given in Fig 5.55. Right side of Fig. 5.57 is the cross plot which shows the R^2 value of 0.86 between laboratory measured UCS values and ANFIS predicted UCS. Cross plot clearly indicates that the developed model based on ANFIS is capable of predicting UCS using four inputs.

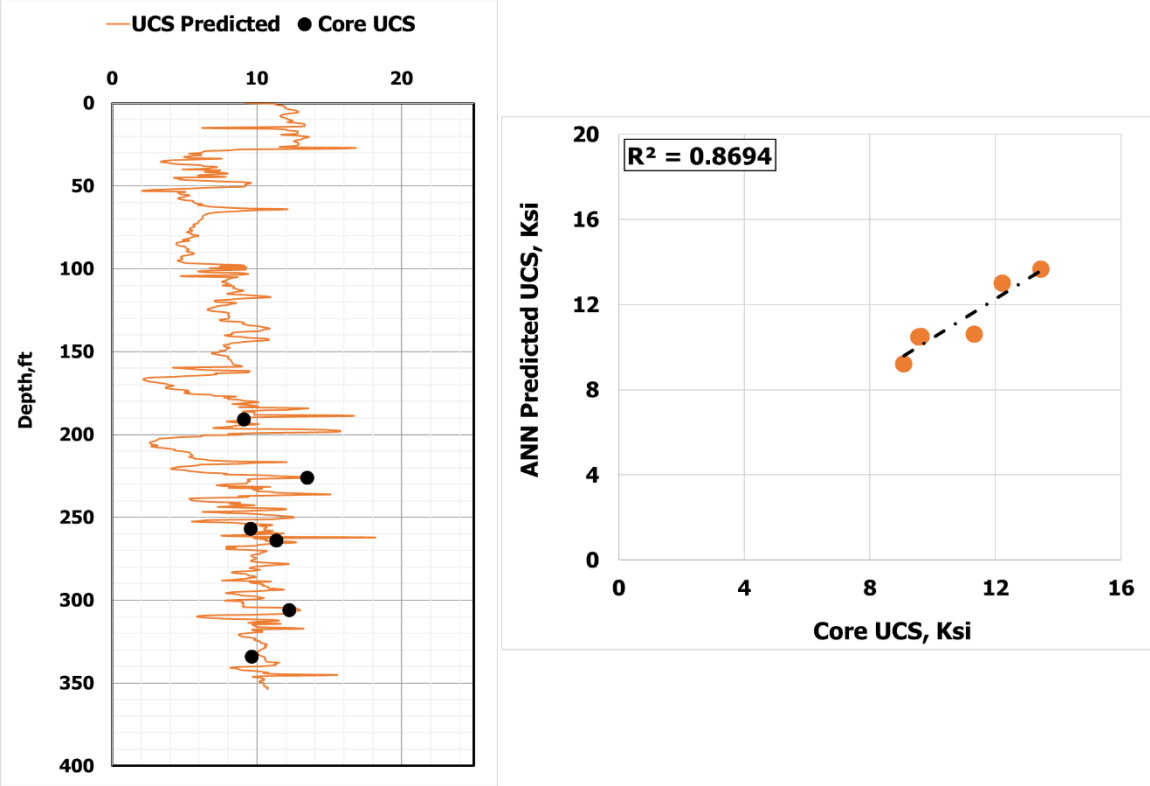

Figure 5. 57 UCS prediction using two step ANFIS model on Well No. 2.

5.8.8 Model Verification and Testing on Published Data

To further test the generalization capabilities of ANFIS based UCS model, it was tested on published data by Najeibi et al. 2013. The complete data set is given in Appendix A and complete logs profiles are given in Fig 5.58.

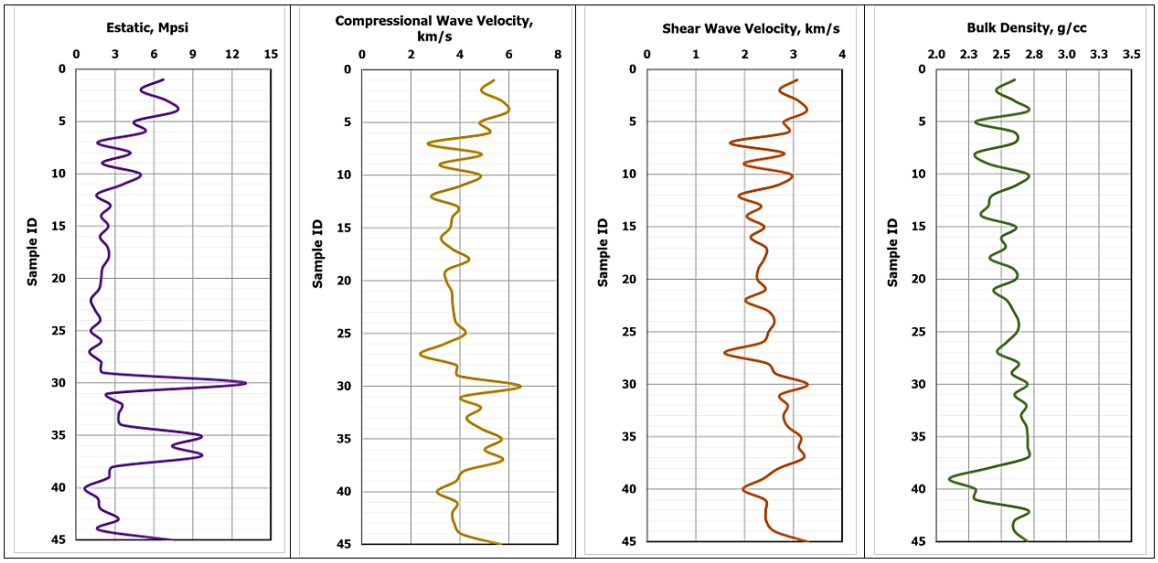

Figure 5.58 Published data as an input for UCS model.

Fig. 5.59 shows the UCS values predicted by ANFIS model. Right side of Fig. 5.59 is the cross plot which shows the shows the R^2 value of 0.86 between published laboratory measured UCS and ANFIS predicted UCS.

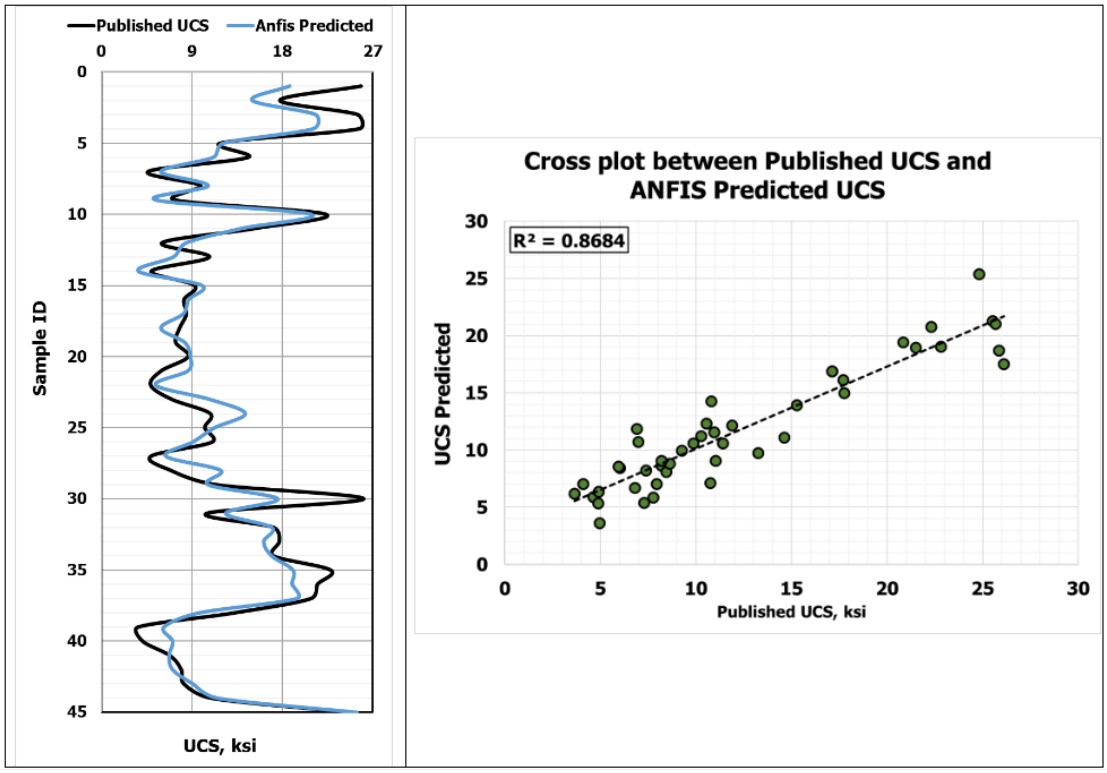

Figure 5.59 Verification of ANFIS predicted UCS with published data (Najeibi 2013).

5.8.9 Comparison of proposed model with the commonly used correlations in oil and gas industry

To further check the accuracy and performance of the proposed model, it was compared with the commonly used empirical correlations in the petroleum industry for the prediction of UCS (Chang et al. 2006, Militzer et al. 1973 and Golubev et al. 1976). Fig. 5.60 shows the comparison of ANFIS predicted with those predicted using correlations. The UCS predicted using proposed ANFIS model produced the best match with most of the data points. The complete statistical comparison is given in Table 5.36.

Table 5.36 Comparison of proposed UCS ANFIS model with commonly used empirical correlations for carbonate rocks.

CORRELATIONS	AAPE	R^2	Emin	Emax
Chang (2006)	37	0.79	4.18	77
Militzer (1973)	60	0.8	1.5	75
Golubev (1976)	35	0.73	.38	67
Proposed ANFIS Model	10.2	0.92	0.043	57

Fig 5.61 shows the cross plot comparison of results from the proposed ANFIS model with those from correlations.

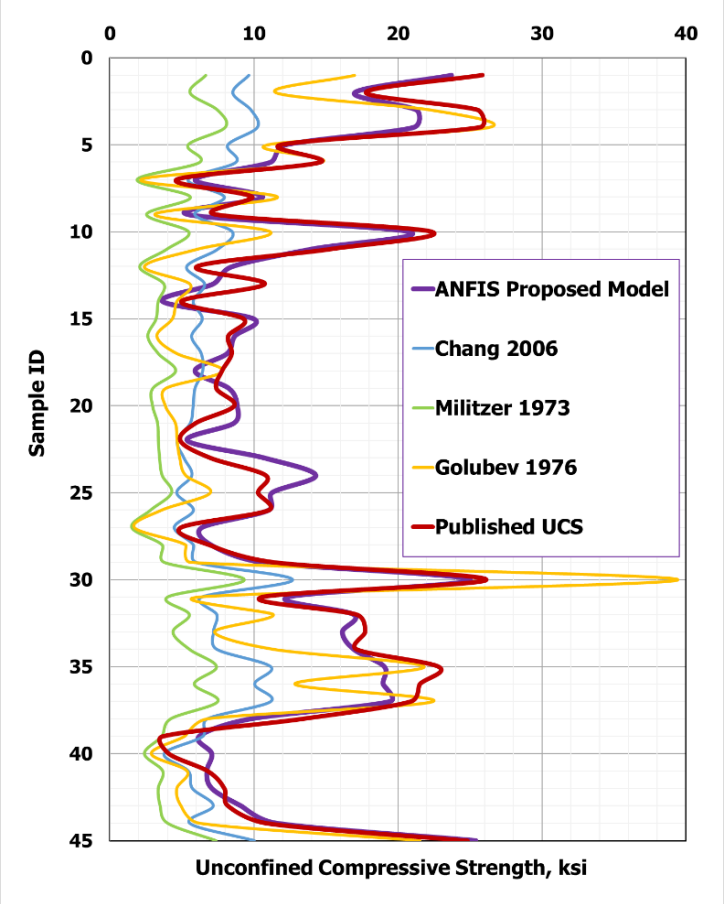

Figure 5.60 Comparison of ANFIS predicted UCS with other correlations.

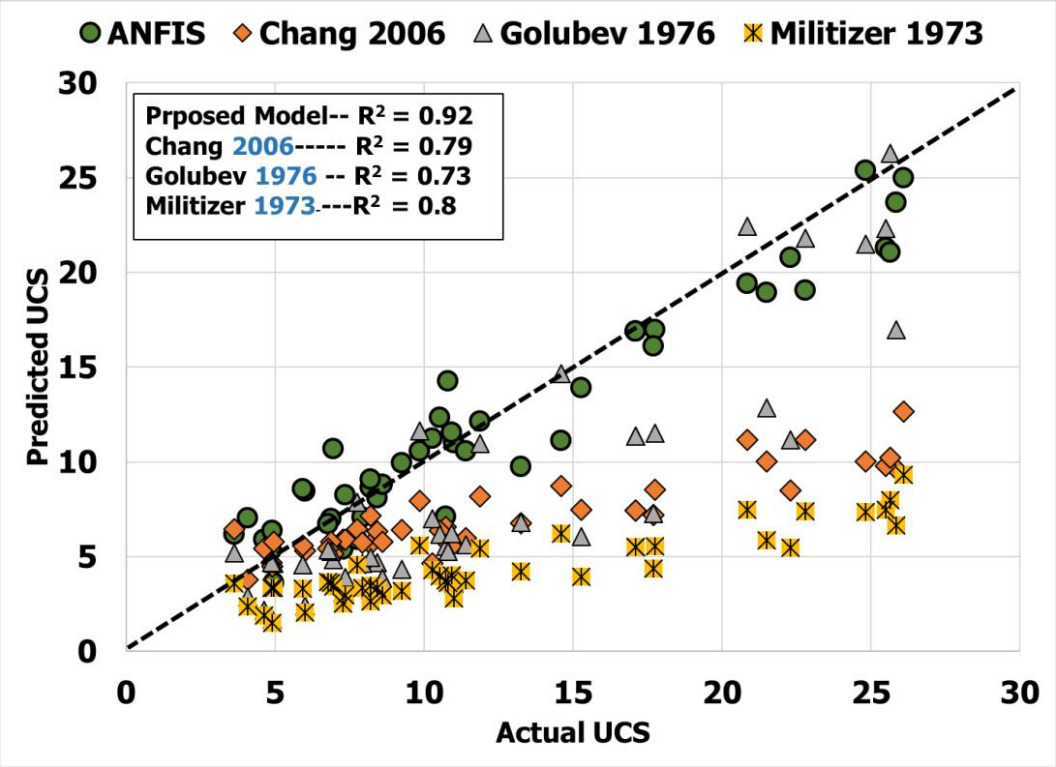

Figure 5.61 Cross plot comparison of proposed ANFIS UCS model with commercial correlations.

5.9 Modeling for Friction Angle Prediction

Table 5.37 shows the relative importance of various input parameters with friction angle in terms of correlation coefficient. Total data points used for friction angle prediction were 91.

Table 5.37 Relative importance of different logs with friction angle.

Parameters	Es MPsi	Δtc µs/ft.	Δts µs/ft.	Vp km/s	Vs km/s	NPHI v/v	RHOB g/cc	FANG Degrees
Es, MPsi	1.000							
Δtc, µs/ft	-0.51	1.000						
Δts, µs/ft	0.278	0.888	1.000					
Vp, km/s	-0.31	-0.988	-0.871	1.000				
Vs, km/s	-0.319	-0.879	-0.987	0.883	1.000			
NPHI, v/v	0.084	0.876	0.814	-0.866	-0.796	1.000		
RHOB, g/cc	-0.422	-0.933	-0.825	0.941	0.837	-0.791	1.000	
FANG	**0.45**	-0.326	-0.147	0.277	0.094	-0.318	0.202	1.000

In order to find the optimal input parameters for FANG prediction, five cases were designed which are as follows:

1. Case 1: Three inputs (Bulk Density, Compressional wave travel time and Shear wave travel time)
2. Case 2: Four inputs (Bulk Density, Compressional wave travel time, Shear wave travel time and Neutron porosity)
3. Case 3: Five inputs (Static Young's Modulus, Bulk Density, Neutron porosity, Compressional wave travel time and Shear wave travel time)
4. Case 4: Four inputs (Static Young's Modulus, Neutron porosity, Compressional wave travel time and Shear wave travel time)
5. Case 5: Four inputs (Static Young's Modulus, Bulk Density, Compressional wave travel time and Shear wave travel time)

In all of the above cases, static Young's modulus was used as an input. However, the end of this section shows a two-step approach to prediction of FANG, viz., prediction of static Young's modulus using AI techniques, and the use of the predicted value in addition to others to predict FANG.

5.9.1 Results from ANN to Predict FANG

Fig 5.62 shows the performance of ANN on different cases and Case 3 is found to be the best case. Final ANN model for predicting FANG was found to be the with 20 neurons and with tan-sigmoidal type activation function. Fig 5.63 shows the overall prediction performance of best ANN model for FANG prediction.

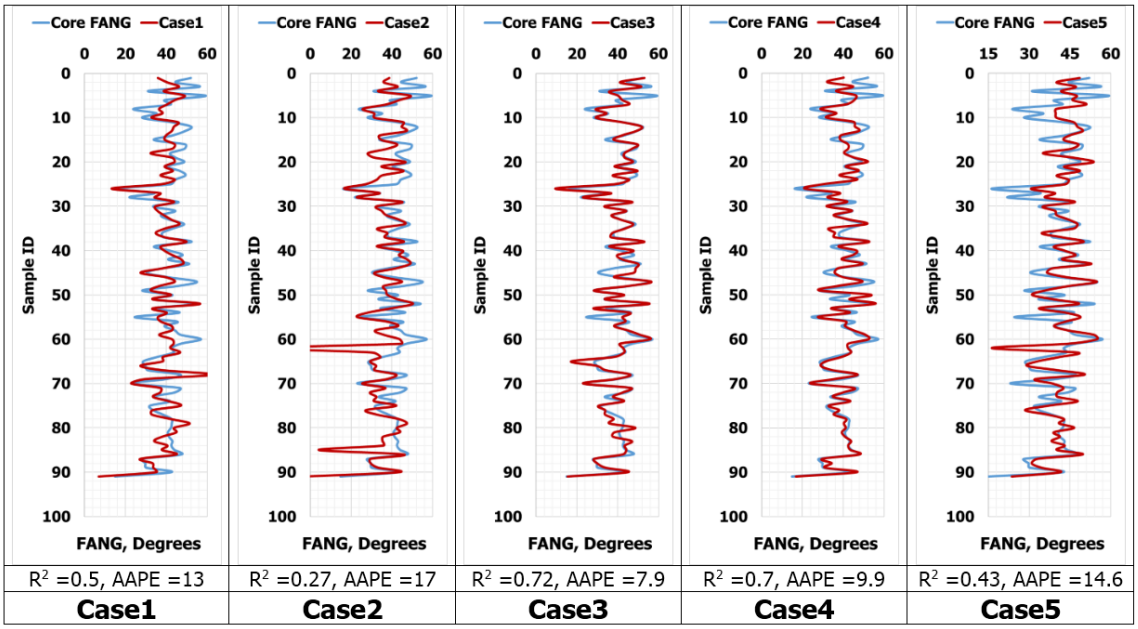

Figure 5.62 Comparison of different cases for prediction of FANG using ANN.

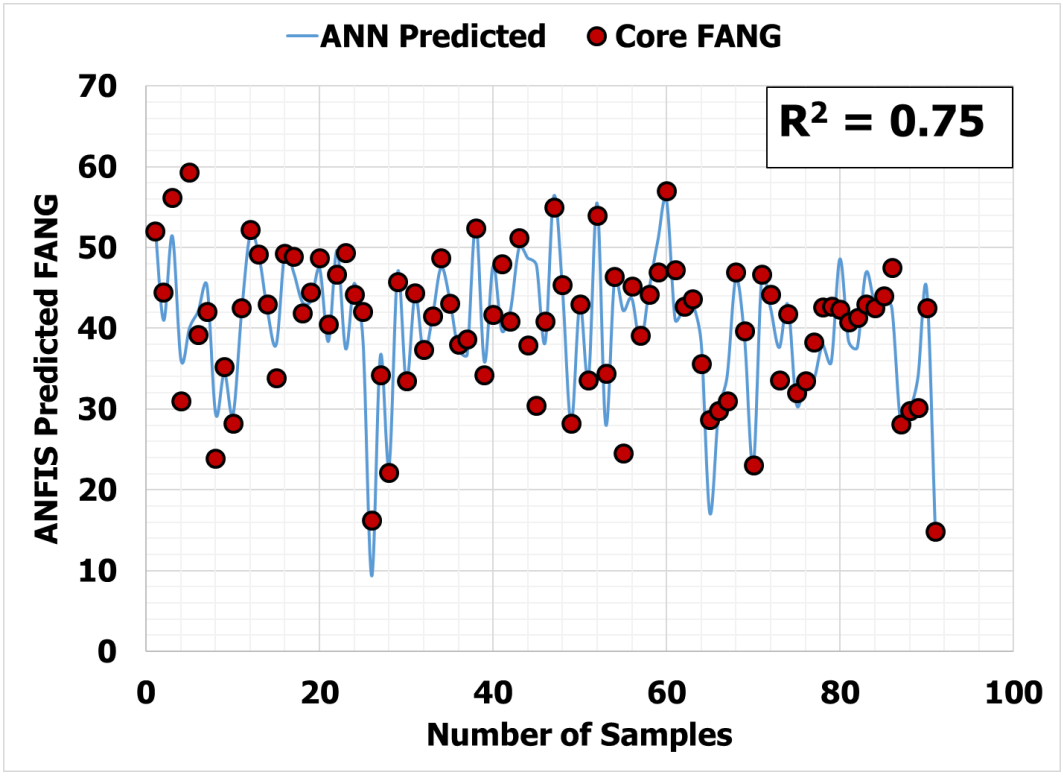

Figure 5.63 Overall performance of ANN based model for FANG prediction.

5.9.2 Results from ANFIS to Predict FANG.

ANFIS was applied on five cases as shown in Fig 5.64. Case 3 was selected as the best case on the basis of less AAPE and high correlation coefficient. Further improvement in the model was achieved by performing parametric study. Final ANFIS model to predict FANG model is based upon Genfis 2 with cluster radius size of 0.5. Optimum cluster radius was found out by performing the sensitivity of cluster radii between 0.1 – 1. Fig 5.65 shows the performance of optimum ANFIS model to predict FANG.

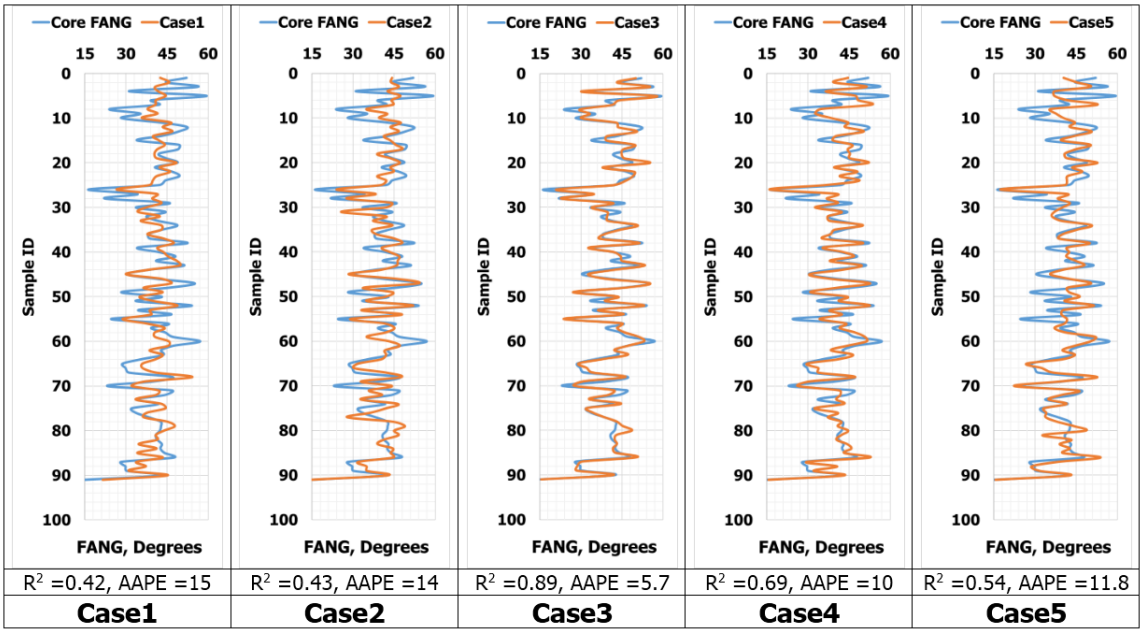

Figure 5.64 Comparison of different cases for prediction of FANG using ANFIS.

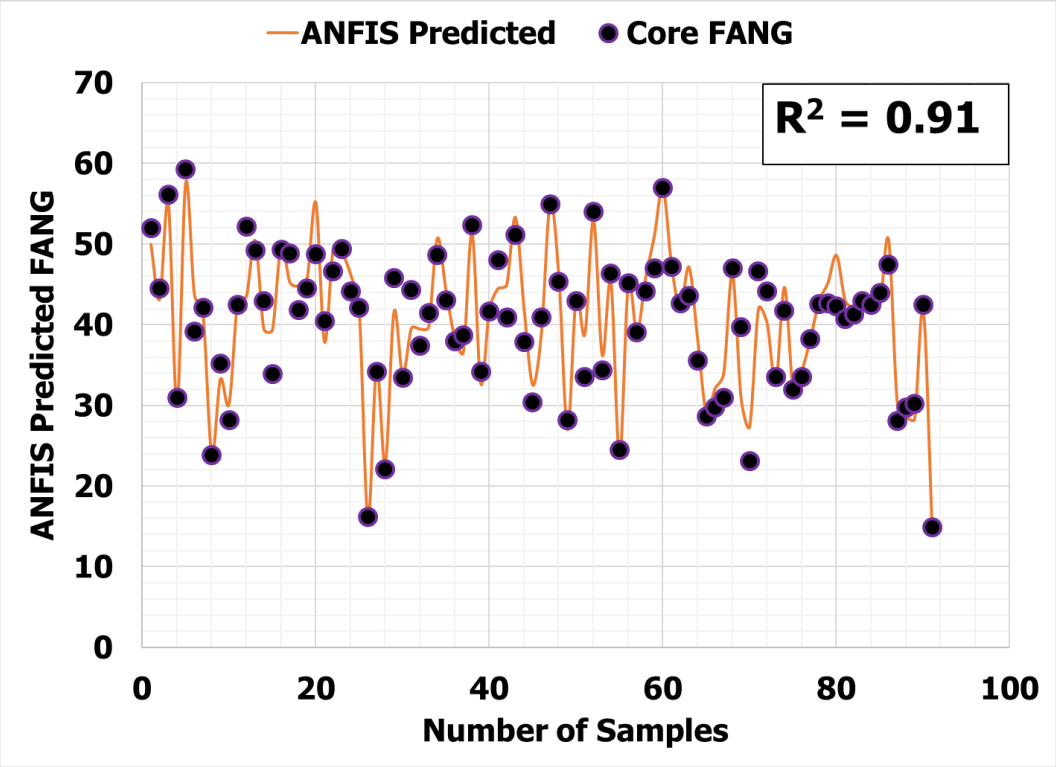

Figure 5.65 Overall prediction performance of ANFIS based model for FANG prediction.

5.9.3 Results from SVM to Predict FANG

SVM was applied on five cases as shown in Fig 5.66. Case 3 on the basis of less AAPE and high correlation coefficient was selected as the best case to predict FANG. Further improvement in the model was achieved by performing parametric study. Final SVM to predict FANG model was based on Gaussian type kernel function as shown in Fig 5.67.

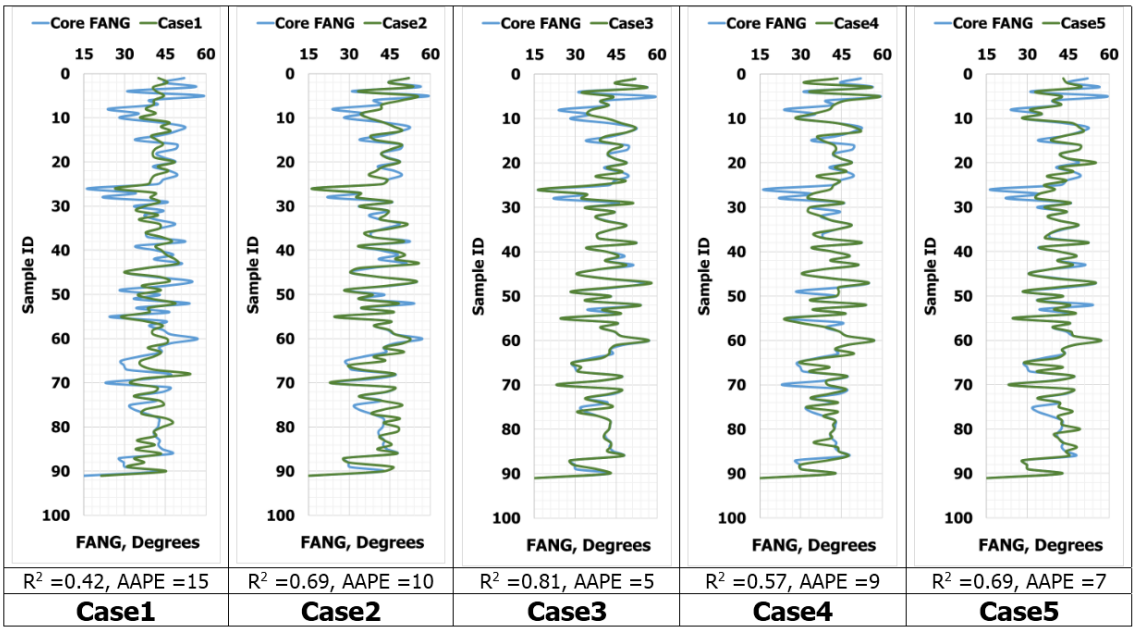

Figure 5.66 Comparison of different cases for prediction of FANG using SVM.

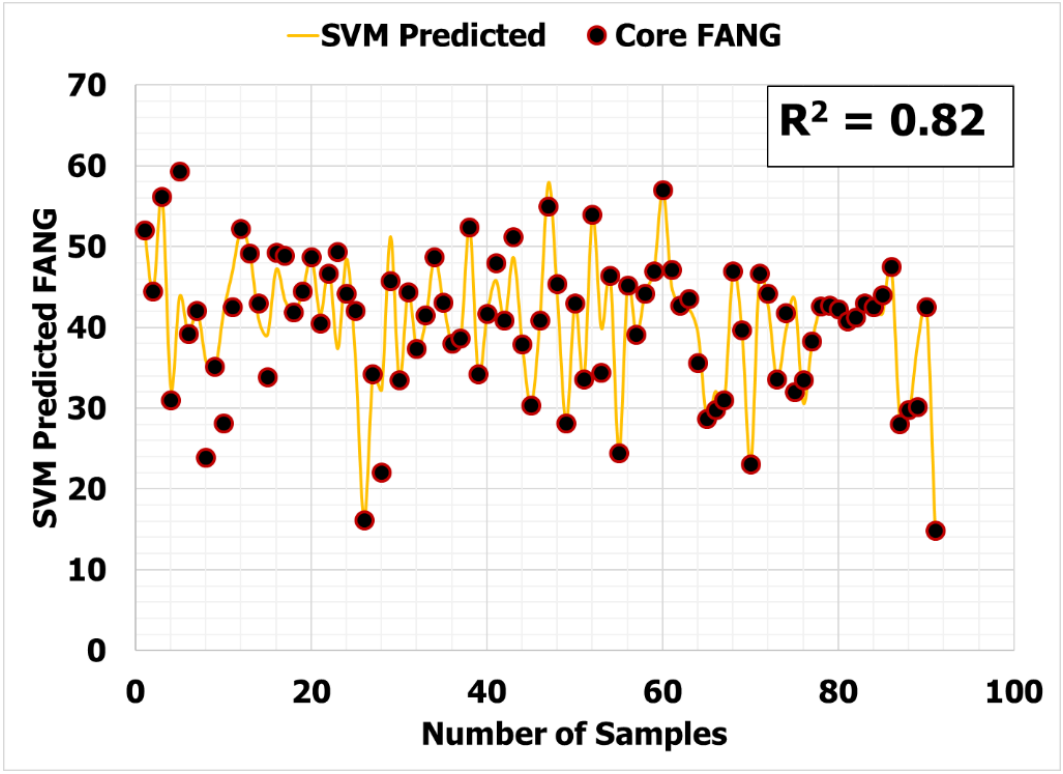

Figure 5.67 Overall prediction performance of ANN based model for FANG prediction.

5.9.4 Comparison of Three AI techniques on prediction of FANG

On comparing the performances of three best AI models on overall data, ANN on set of full data gave R^2 of 0.75 and an AAPE 15, ANFIS gave R^2 of 0.92 and an AAPE of 5.7 and SVM gave R^2 0.82 and an AAPE of 9 as shown in Figs 5.68 – Fig 5.71. From this comparison it is cleared that on the given set of data, ANFIS with five input parameters, namely, Static Young's modulus, bulk density, neutron porosity, compressional wave travel time and shear wave travel time is the optimum best model to predict friction angle.

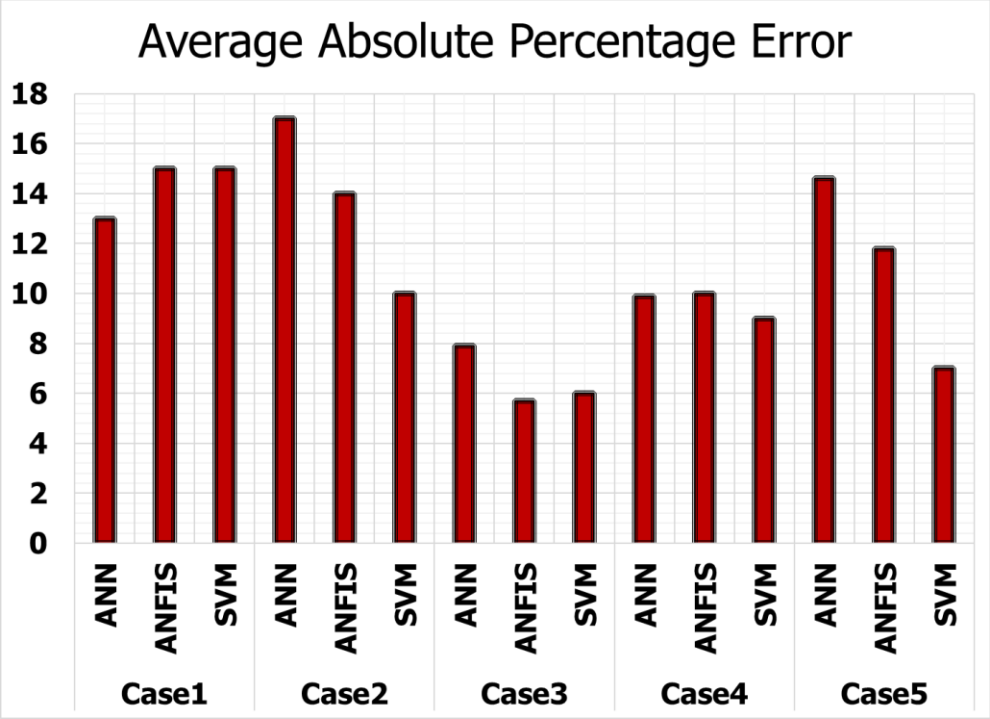

Figure 5.68 Average absolute percentage error comparison of five cases.

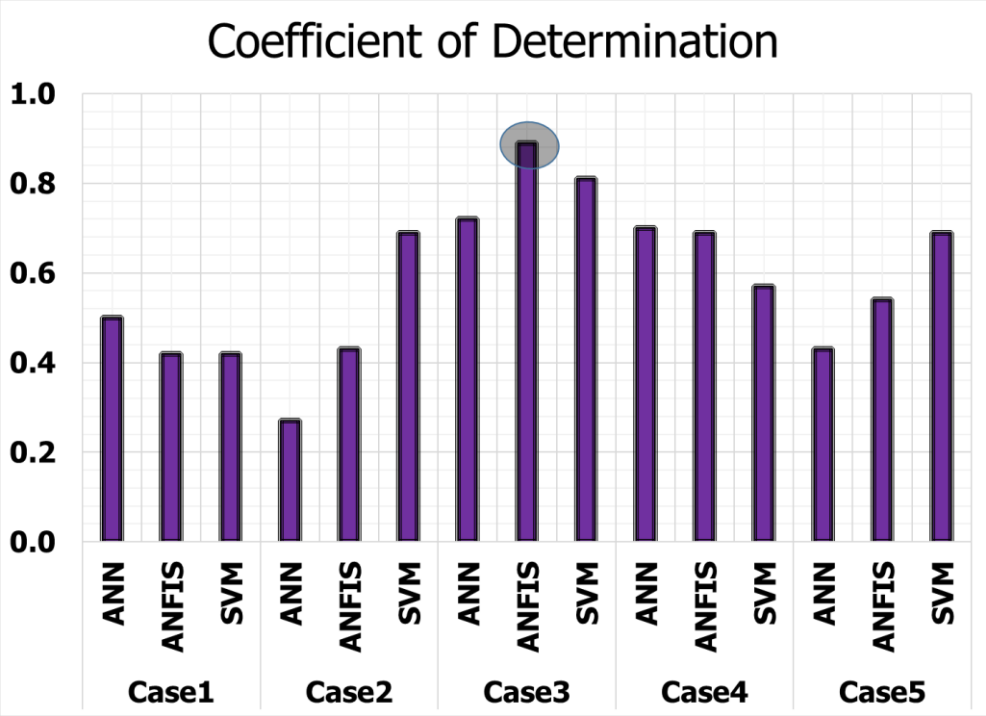

Figure 5. 69 Coefficient of determination comparison of five cases.

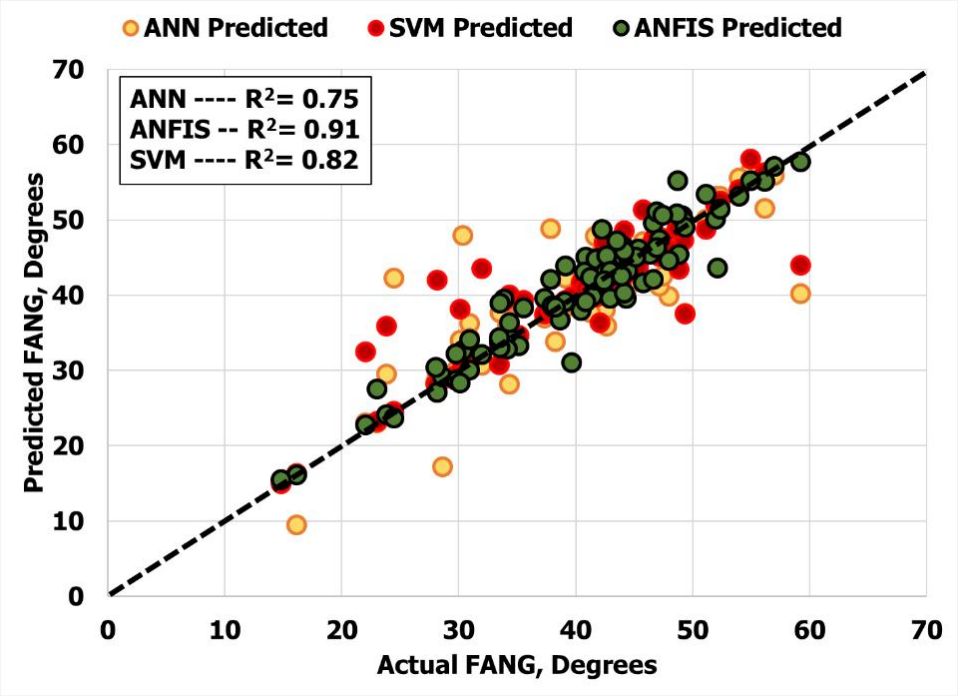

Figure 5. 70 Comparison of best AI models for the prediction of FANG.

5.9.5 Two Step Prediction for FANG using Optimized Model

Fig 5.71 shows the two step prediction of optimized ANFIS model on overall data. In two-step prediction approach, first, the static Young's modulus is predicted by using basic well logs, namely, bulk density, compressional time and shear time as given in section 5.5, and in second step the UCS is predicted using the predicted static Young's modulus along with other parameters, namely, bulk density, neutron porosity, compressional and shear wave travel times. From this approach it is clearly evident that model is capable of predicting FANG using aforementioned parameters.

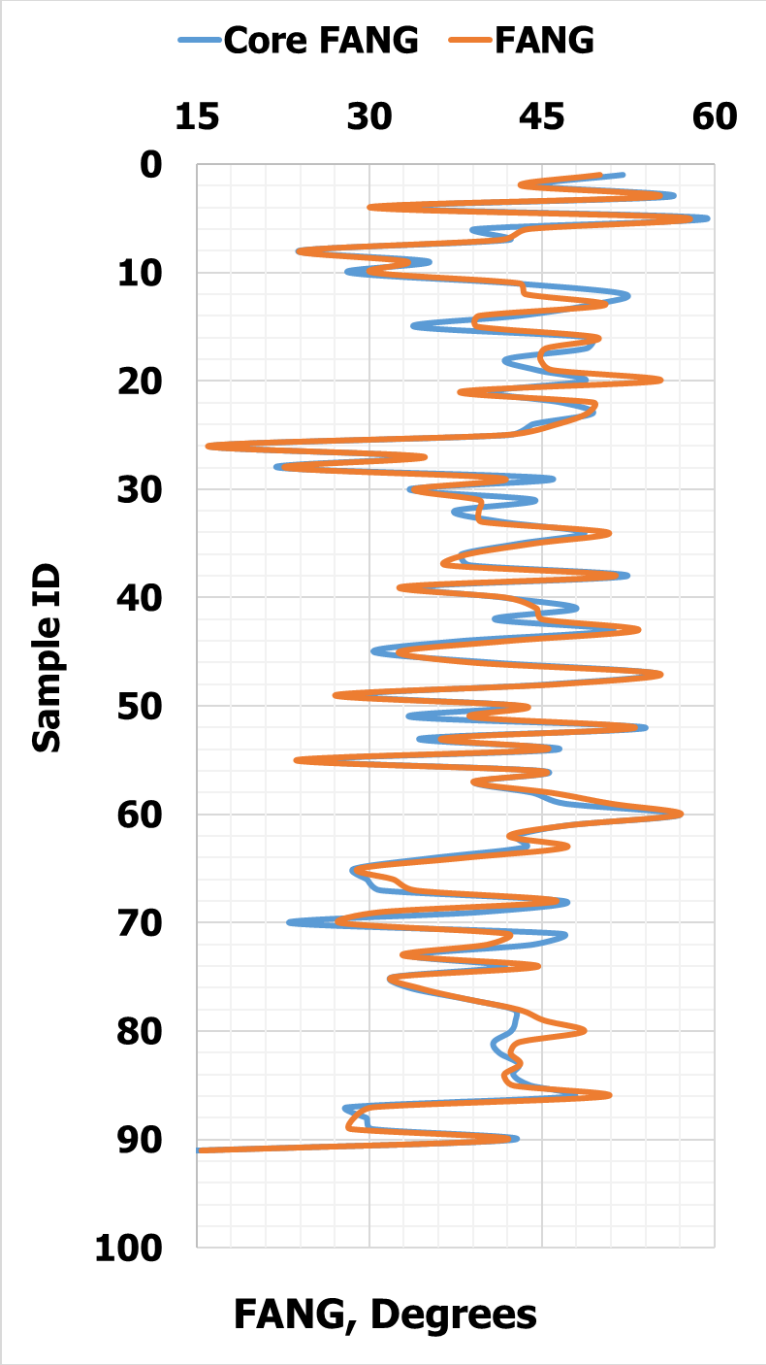

Figure 5. 71 Optimized two step ANFIS model prediction of FANG on overall data.

5.9.6 Validation of the Proposed Model for FANG on Real Field Data

5.9.6.1 Well No. 1

Input Data of Well No. 1 is given in Fig 5.64.

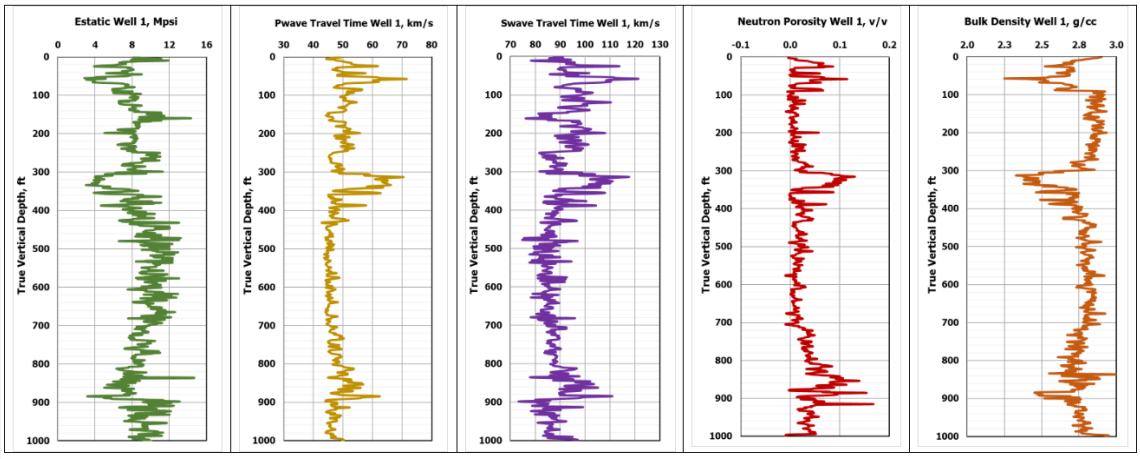

Figure 5.72 Input Data for Well No. 1 used for FANG model validation.

Fig. 5.65 shows the ANFIS predicted FANG for an interval of 1000 ft. This well contains 15 actual laboratory measured FANG values on core plugs retrieved from certain depth using triaxial compressional tests. Right side of Fig. 5.65 is the cross plot which shows R^2 value of 0.85 between laboratory measured FANG values and ANFIS predicted FANG values. The FANG profile in Fig. 5.65 and cross plot clearly indicates that the developed model based on ANFIS is fully capable of predicting FANG using five inputs.

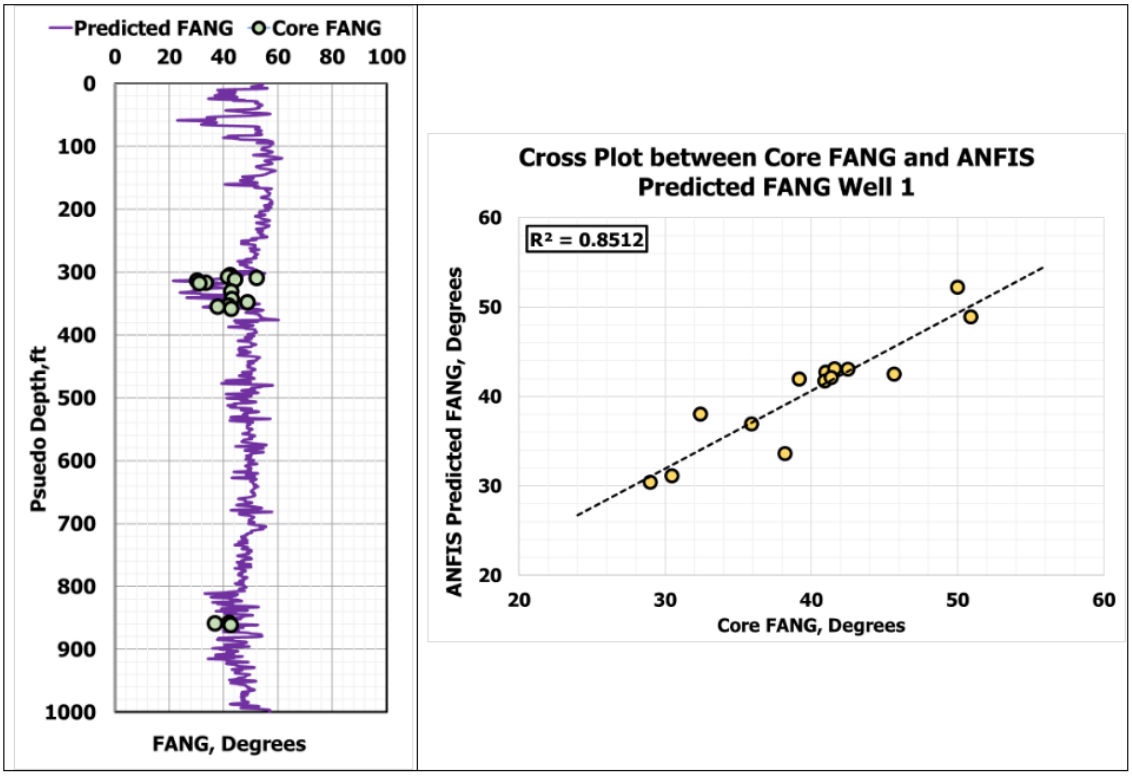

Figure 5.73 Field verification of ANFIS predicted FANG with real field data points on Well No. 1.

5.9.7 Model Validation on field Data using Two Step Prediction of FANG

Fig 5.74 shows the validation from two step prediction model on Well No. 1. Input data of Well No. 1 is given in Fig 5.72. Right side of Fig. 5.74 is the cross plot which shows the R^2 value of 0.83 between laboratory measured FANG values and ANFIS predicted FANG. Cross plot clearly indicates that the developed model based on ANFIS is capable of predicting FANG using five inputs, namely, predicted static Young's modulus, bulk density, neutron porosity, compressional and shear wave travel times.

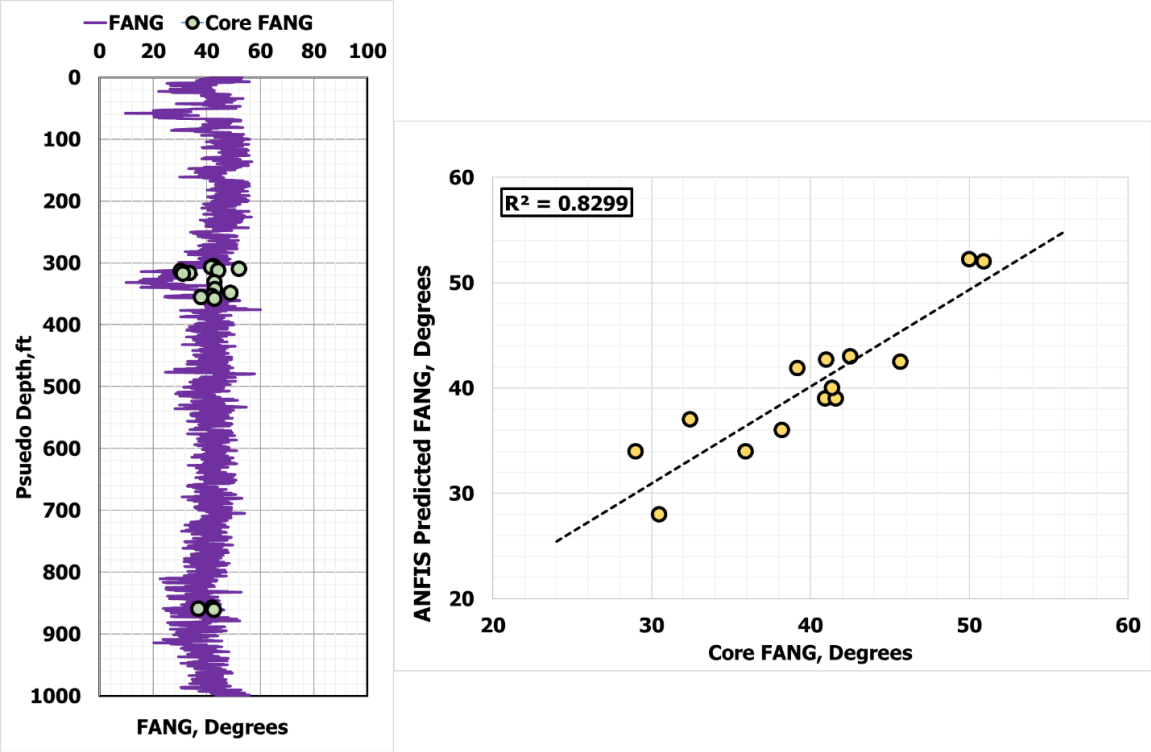

Figure 5. 74 FANG prediction using two step ANFIS model on Well No. 1.

5.10 Cohesion Prediction Modeling

Table 5. 38 shows the relative importance of various input parameters with friction angle in terms of correlation coefficient. Total number of data points used for cohesion prediction were 91.

Table 5.38 Relative importance of different logs with cohesion.

Parameters	Estatic MPsi	P-wave Time µs/ft.	S-wave Time µs/ft.	P-wave Velocity km/s	S-wave Velocity km/s	Neutron porosity v/v	Bulk Density g/cc	Cohesion ksi
Estatic, MPsi	1.00							
Compressional Time, µs/ft	-0.51	1.00						
Shear Time, µs/ft.	0.28	0.88	1.00					
Compressional Velocity, km/s	-0.31	-0.98	-0.87	1.00				
Shear Velocity, km/s	-0.32	-0.88	-0.987	0.88	1.00			
Neutron porosity, v/v	0.08	0.87	0.814	-0.86	-0.79	1.00		
Bulk Density, g/cc	-0.42	-0.93	-0.825	0.94	0.84	-0.79	1.00	
Cohesion, ksi	**0.45**	-0.32	-0.15	0.27	0.094	-0.32	0.20	1.00

In order to find the optimal input parameters for cohesion prediction, five cases were designed which are as follows:

1. Case 1: Three inputs (Bulk Density, Compressional wave travel time and Shear wave travel time)
2. Case 2: Four inputs (Bulk Density, Compressional wave travel time, Shear wave travel time and Neutron porosity)
3. Case 3: Five inputs (Static Young's Modulus, Bulk Density, Neutron porosity, Compressional wave travel time and Shear wave travel time)
4. Case 4: Four inputs (Static Young's Modulus, Neutron porosity, Compressional wave travel time and Shear wave travel time)
5. Case 5: Four inputs (Static Young's Modulus, Bulk Density, Compressional wave travel time and Shear wave travel time)

In all of the above cases, static Young's modulus was used as an input. However, the end of this section shows a two-step approach to prediction of cohesion, viz., prediction of static Young's modulus using AI techniques, and the use of the predicted value in addition to others to predict cohesion.

5.10.1 Results from ANN to Predict Cohesion

Fig 5.75 shows the comparison of ANN performance on five different cases defined above for the prediction of Cohesion. It is evident that case 3 is the best case which takes five inputs, namely, Static Young' s Modulus, Bulk Density, Neutron porosity, Compressional wave travel time, and Shear wave travel time. Further improvement in the model was achieved by performing parametric study. Final ANN model to predict

cohesion was based on 15 neurons with Tan-sigmoidal type activation function. Fig 5.76 shows the overall prediction performance of optimum ANN model.

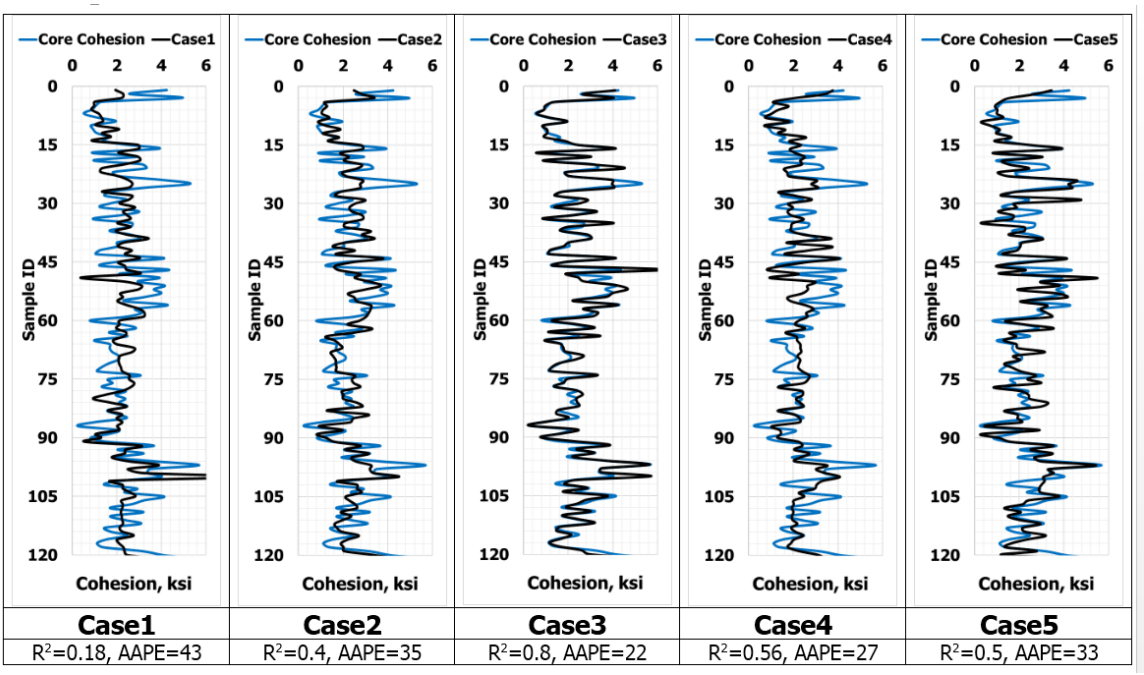

Figure 5.75 Comparison of different cases for the prediction of Cohesion using ANN.

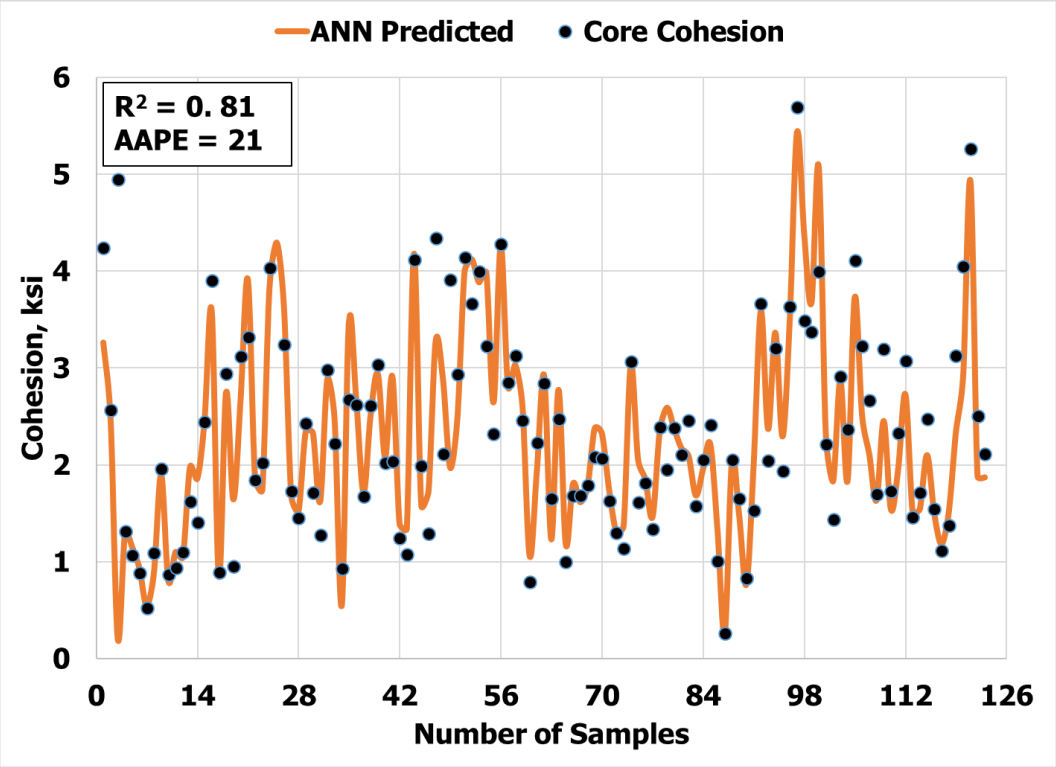

Figure 5.76 Overall prediction performance of ANN based model for Cohesion prediction.

5.10.2 Results from ANFIS to Predict Cohesion.

ANFIS was applied on five cases and case 3 was selected as the best case to predict cohesion on the basis of minimum error and high correlation coefficient. Further improvement in the model was achieved by performing parametric study. Final ANFIS model to predict cohesion was based on Genfis2 with cluster radius size of 0.25. Optimum cluster radius was found out by performing the sensitivity of cluster radii between 0.1 – 1. Fig 5.78 shows the performance of optimum ANFIS model to predict Cohesion.

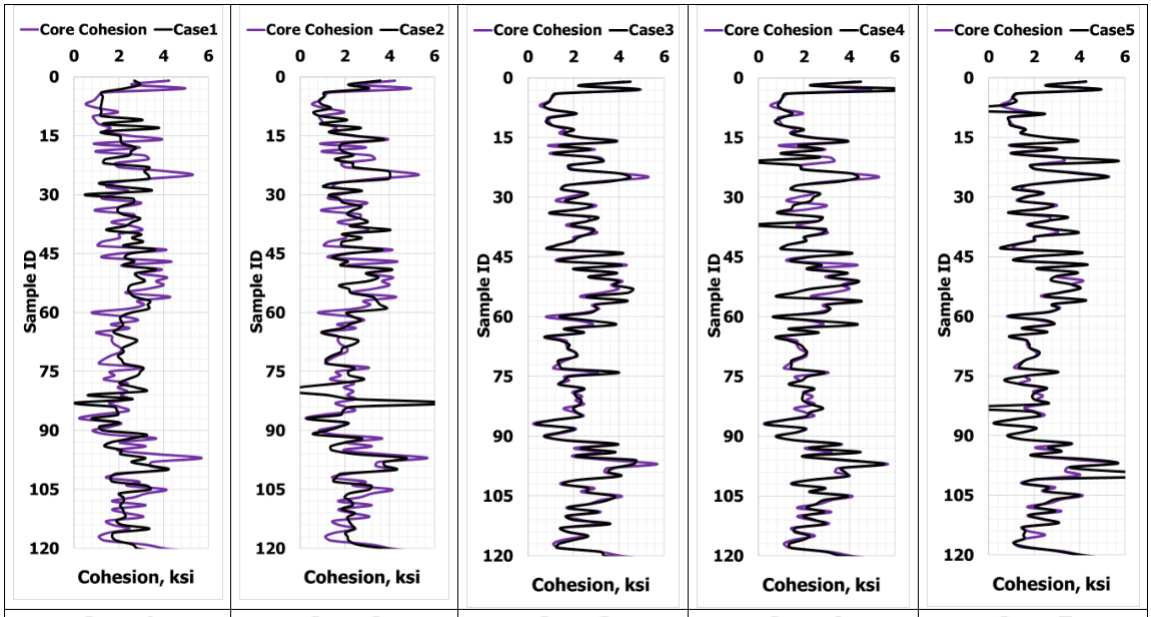

Case1	Case2	Case3	Case4	Case5
R^2=0.24, AAPE=38	R^2=0.36, AAPE=33	R^2=0.91, AAPE=11	R^2=0.72, AAPE=15	R^2=0.72, AAPE=15.5

Figure 5.77 Comparison of different cases for the prediction of Cohesion using ANFIS.

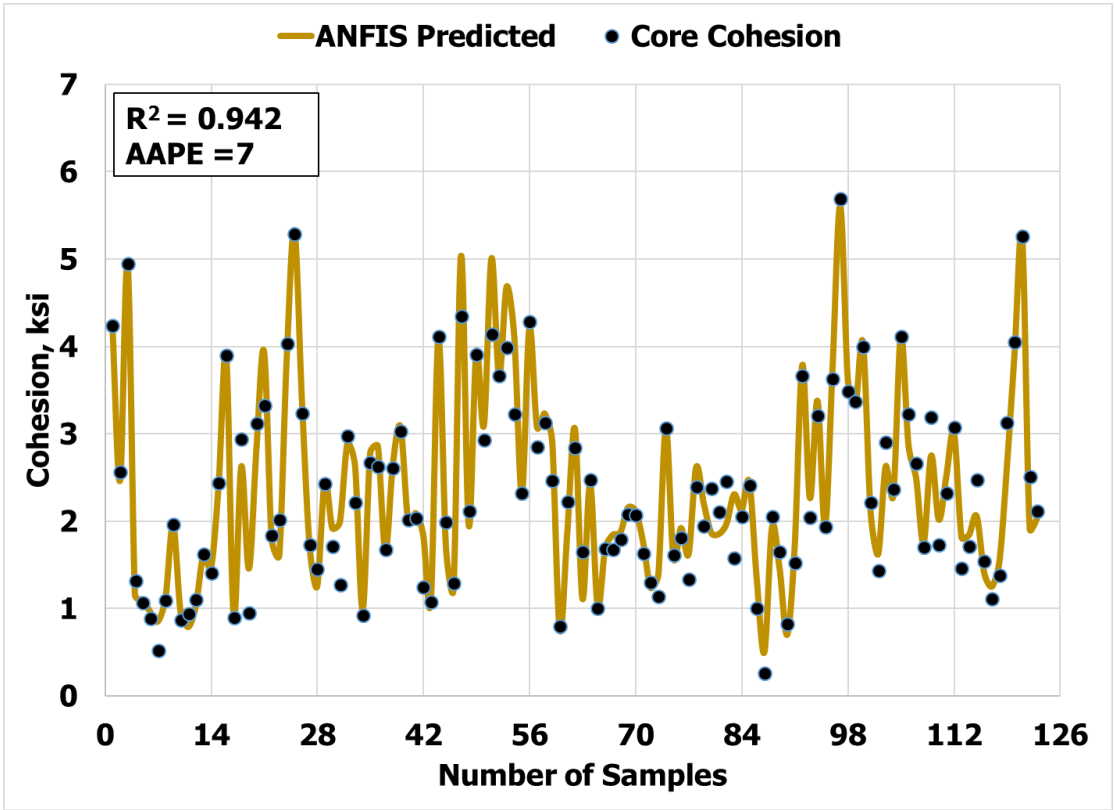

Figure 5.78 Overall prediction performance of ANFIS based model for Cohesion prediction.

5.10.3 Results from SVM to Predict Cohesion

SVM applied on five cases and case 3 which takes five inputs was selected as the best case on the basis of less AAPE and high correlation coefficient. Further improvement in the model was achieved by performing parametric study. Final SVM model to predict cohesion was based on 'Gaussian type' kernel function. Fig 5.80 shows the performance on overall data.

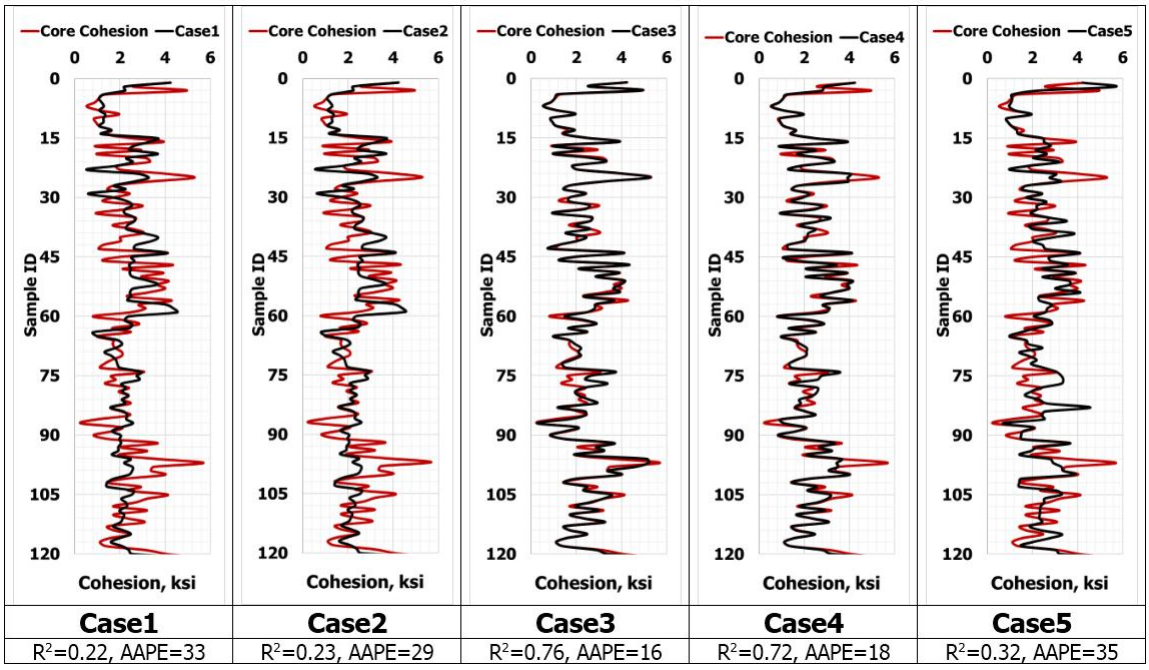

Figure 5.79 Comparison of different cases for the prediction of Cohesion using SVM.

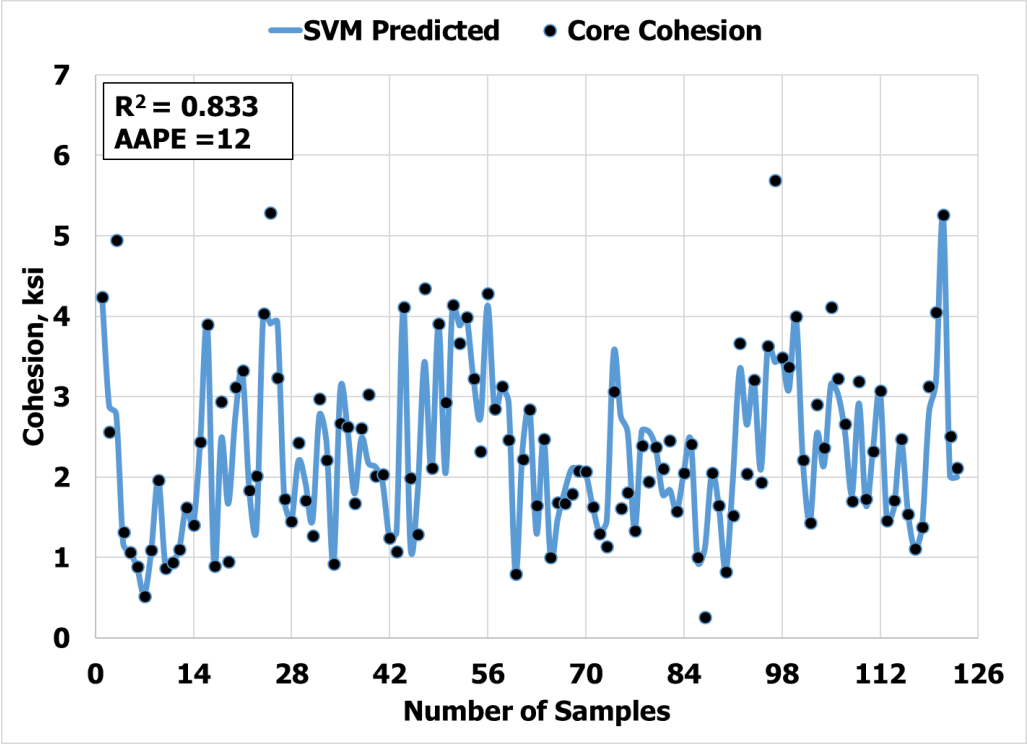

Figure 5.80 Overall prediction performance of SVM based model for Cohesion prediction.

5.10.4 Comparison of Three AI techniques on prediction of Cohesion

On comparing the performances of three best AI models on overall data, ANN gave R^2 of 0.81 and an AAPE 15, ANFIS gave R^2 of 0.94 and an AAPE of 9.2 and SVM gave R^2 0.74 and an AAPE of 16.3 as shown in Fig 5.81 - Fig 5.83. From this comparison it is cleared that on the given set of data, ANFIS is the optimum best model to predict cohesion.

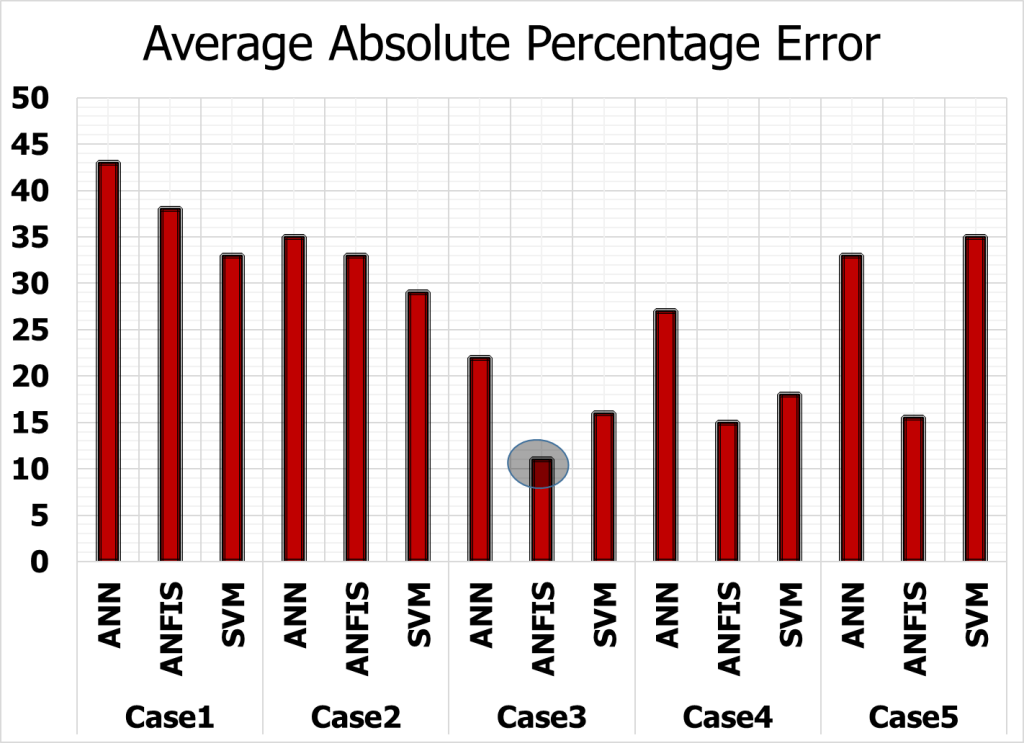

Figure 5.81 Average absolute percentage error comparison of five cases.

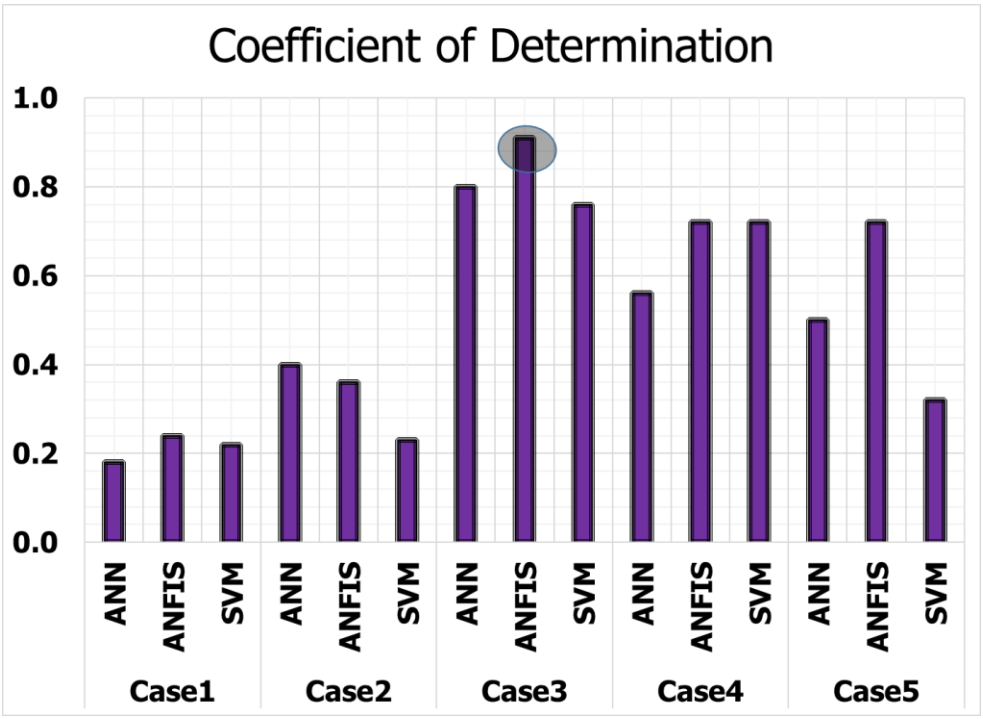

Figure 5. 82 Coefficient of determination comparison of five cases.

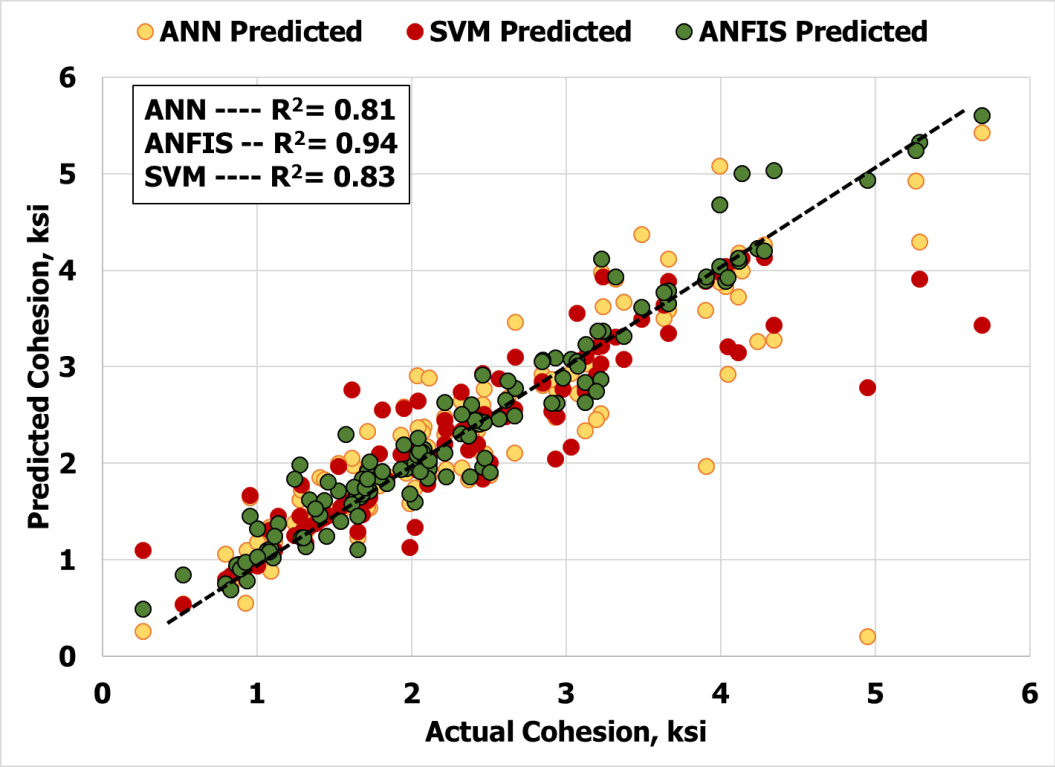

Figure 5. 83 Comparison of best AI models for the prediction of Cohesion.

5.10.5 Two steps prediction for Cohesion using Optimized Model

Fig 5.84 shows the two step prediction of optimized ANFIS model on overall data. In two-step prediction approach, first, the static Young's modulus is predicted by using basic well logs, namely, bulk density, compressional time and shear time as given in section 5.5, and in second step the UCS is predicted using the predicted static Young's modulus along with other parameters, namely, bulk density, neutron porosity, compressional and shear wave travel times. From this approach it is clearly evident that model is capable of predicting cohesion using aforementioned parameters.

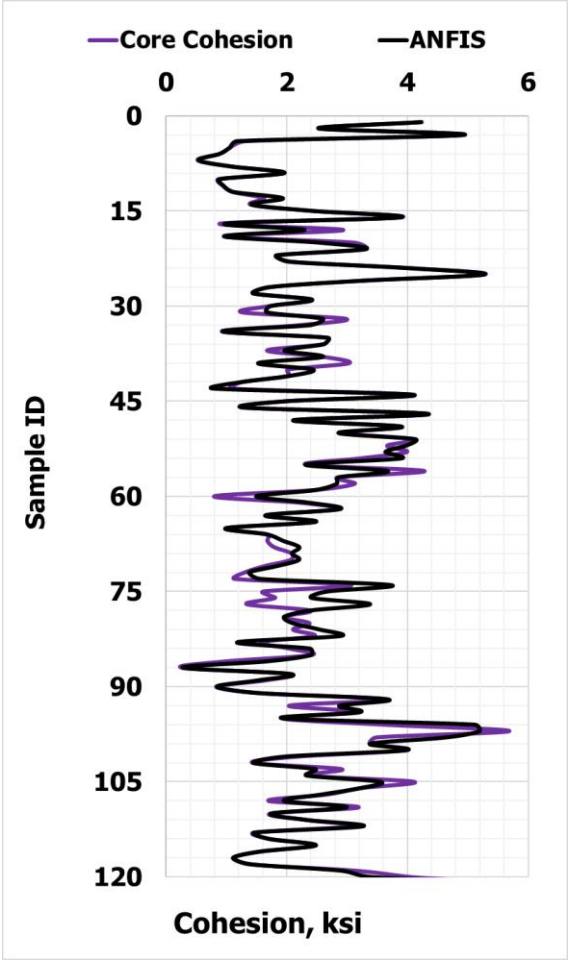

Figure 5. 84 Optimized two step ANFIS model prediction of Cohesion on overall data

5.10.6 Validation of the Proposed Model for Cohesion on Real Field Data

5.10.6.1 Well No. 1

Input Data of Well No. 1 is given in Fig 5.85

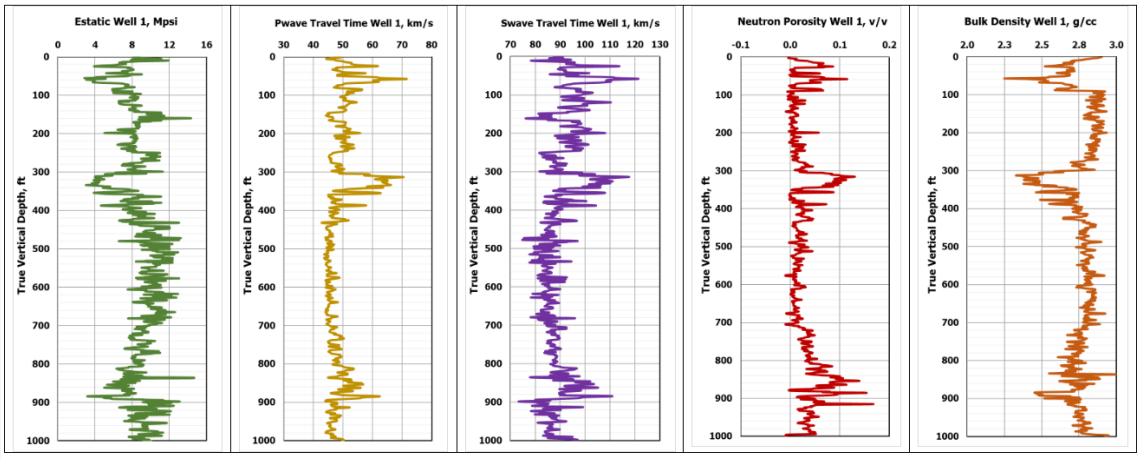

Figure 5.85 Real field wireline log input data for cohesion model Well No. 1.

Fig. 5.86 shows the ANFIS predicted cohesion for an interval of 1000 ft. This Well contains 15 actual laboratory measured cohesion values. Right side of Fig. 5.86 is the cross plot which shows the R^2 value of 0.87 between laboratory measured cohesion values and ANFIS predicted cohesion values at the same depth from where these core samples were retrieved. Cross plot clearly indicates that the developed model based on ANFIS is fully capable of predicting cohesion using five inputs.

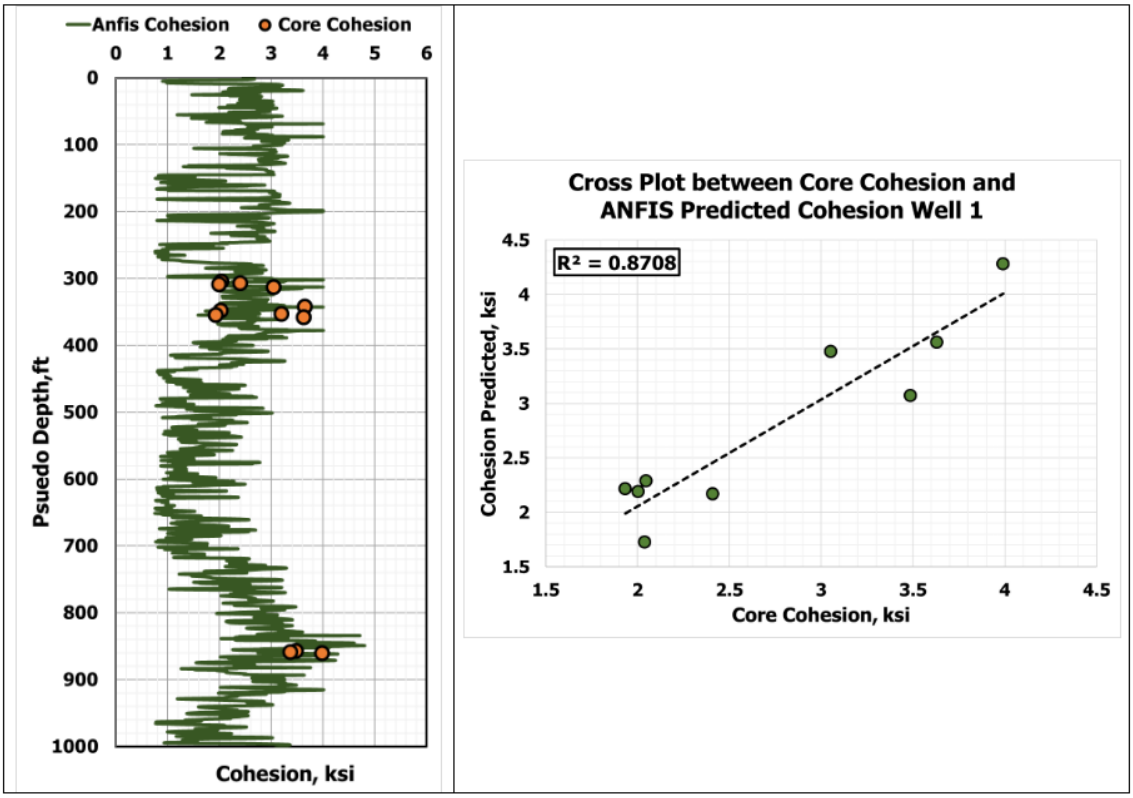

Figure 5.86 Field verification of proposed ANFIS model on Well No. 1.

5.10.6.2 Well No. 2

Input Data of Well No. 2 is given in Fig 5.87

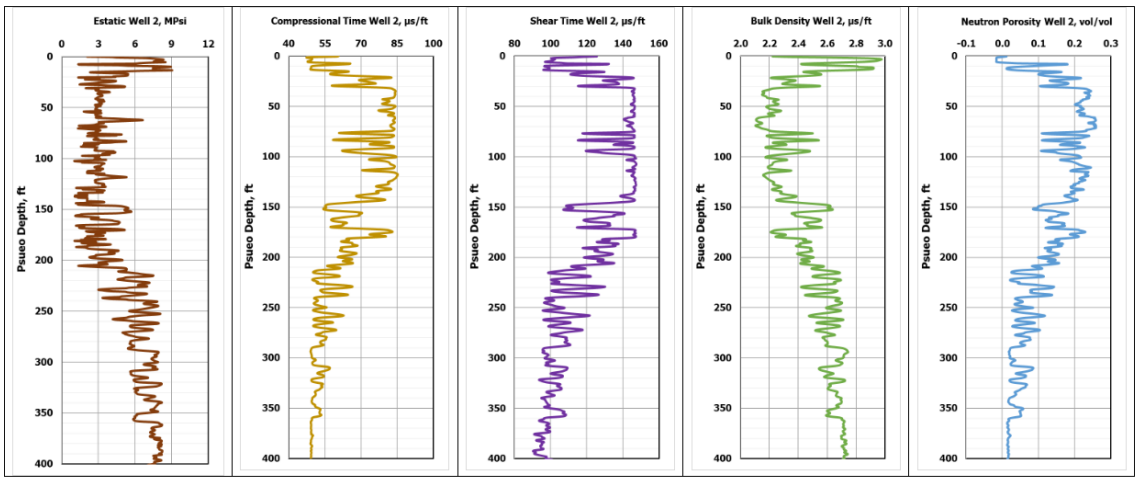

Figure 5.87 Real field wireline log as an input data for Well No. 2.

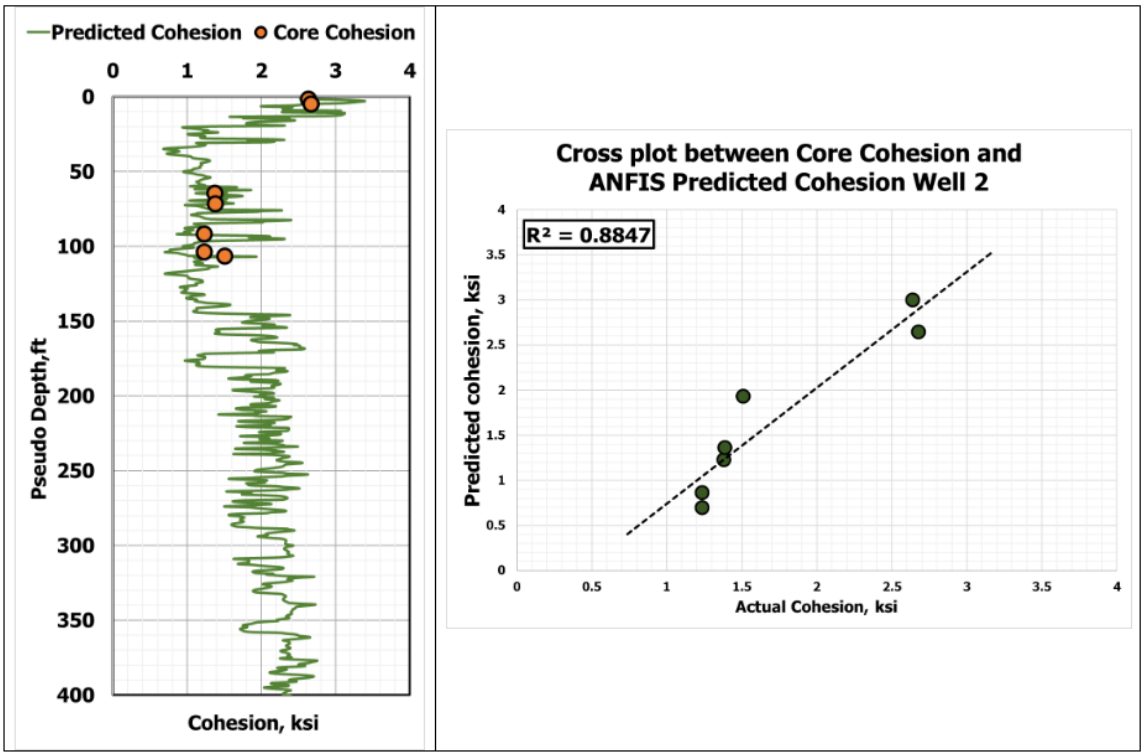

Figure 5.88 Field verification of proposed ANFIS model predicted Cohesion on Well No. 2.

On comparing with actual laboratory measurement values (Fig 5.88) it is clear that proposed ANFIS model gives very good results.

5.10.7 Model Validation on field Data using Two Step Prediction of Cohesion

Fig 5.89 shows the validation from two step prediction model on Well No. 2. Input data of Well No. 2 is given in Fig 5.87. Right side of Fig. 5.89 is the cross plot between laboratory measured cohesion values and ANFIS predicted cohesion. Cross plot clearly indicates that the developed model based on ANFIS is capable of predicting cohesion using five inputs, namely, predicted static Young's modulus, bulk density, neutron porosity, compressional and shear wave travel times.

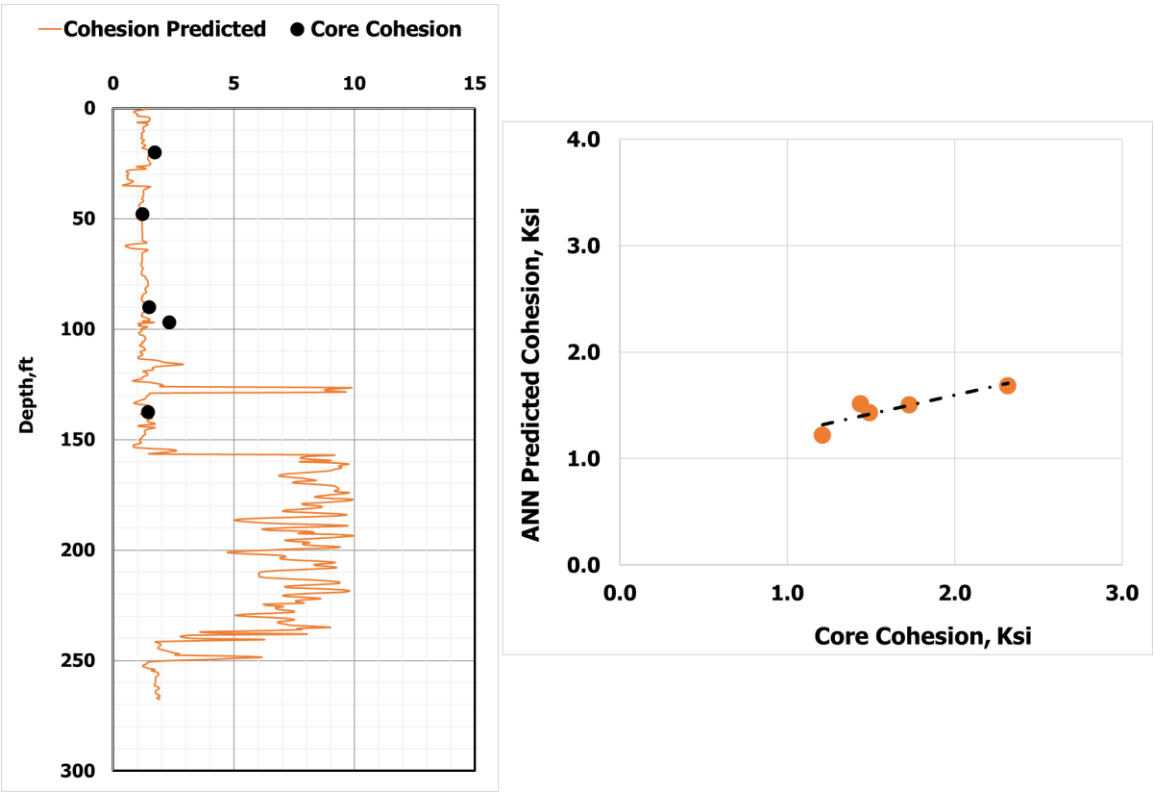

Figure 5. 89 Cohesion prediction using two step ANFIS model on Well No. 2.

CHAPTER 6

CONCLUSIONS AND RECOMMENDATIONS

6.1 Summary

This study was focused on the application of recent advanced artificial intelligence techniques to design robust and accurate models for predicting acoustic velocities, rock elastic and failure parameters (compressional and shear wave travel time, static Young's modulus, Poisson's ratio, unconfined compressive strength, cohesion, and friction angle).

The investigated artificial intelligence techniques include radial basis function neural network, feed forward neural network, adaptive neuro fuzzy inference system (Genfis1 and Genfis2) and support vector machine. In addition to that, the parameters of each technique were deeply investigated to arrive at the optimum best model.

At the end of each parameter prediction, a comprehensive comparative analysis was presented both in pictorial and in tabular form to highlight the accuracy and robustness of the best model during training and testing phases. Data from Middle Eastern carbonate reservoirs were used in this study.

6.2 Conclusions

Following conclusions can be drawn from this study:

1. For the case of acoustic waves travel time and elastic parameters, ANN outperformed all other AI techniques and proved that:
    - three parameters (Gamma Ray, bulk density and neutron porosity) are adequate for the prediction of acoustic velocities.
    - three parameters (Bulk density, compressional time and shear time) are adequate for prediction of elastic parameters
2. Four empirical models were derived from artificial neural network that depends on weights and biases, to predict compressional and shear wave travel times, static Young's modulus, and static Poisson's ratio.
3. The empirical models were compared with the existing commonly used correlations reported in the literature and on the real field data of carbonate rocks. The performance of the models was better than the reported correlations.
4. For the prediction of failure parameters, ANFIS performed better than other techniques. The data used to make failure parameters were smaller than those used for the elastic and acoustic models.
5. The new proposed ANFIS models for failure parameters were validated by comparing them with other commercial correlations on a set of real field and published data and it was observed that the results of proposed models were better than those from previous models reported in the literature.

6. From overall results it can be said that AI techniques can be used as a cost effective alternative in terms of saving the number of experiments to estimate aforementioned parameters in carbonate reservoirs.
7. The new empirical models derived from the Artificial Neural Network can be used for the prediction in new wells without the need of AI software.

6.3 Recommendation for Future work

Promising results were achieved by the use of the artificial intelligence techniques as reported in this study. However better generalization and more precision can be obtained by:

1. Exploring more data and additional input parameters for making better models.
2. Use resistivity log as an additional input because it gives the near well bore features.
3. Use hybrid optimization techniques to enhance the AI model prediction capabilities.
4. Use ANFIS and SVM to extract empirical equations.

References

Abdulraheem, A., Ahmed, M., Vantala, A., & Parvez, T. (2009, January 1). Prediction of Rock Mechanical Parameters for Hydrocarbon Reservoirs Using Different Artificial Intelligence Techniques. Society of Petroleum Engineers. doi:10.2118/126094-MS

Al-Anazi A. F., Gates ID (2010) A support vector machine algorithm to classify lithofacies and model permeability in heterogeneous reservoirs. Eng Geol 114(3–4):267–277

Al-Hmouz, A., Jun Shen, R., "Modeling and Simulation of an Adaptive Neuro-Fuzzy Inference System (ANFIS) for Mobile Learning", IEEE Transactions on Learning Technologies, vol. 5, no. , pp. 226-237, Third Quarter 2012, doi:10.1109/TLT.2011.36

Alarfaj, M. K., Abdulraheem, A., & Busaleh, Y. R. (2012, January 1). Estimating Dewpoint Pressure Using Artificial Intelligence. Society of Petroleum Engineers. doi:10.2118/160919-MS

Ameen, M. S., Smart Brian G. D., Mc J, Somerville S. H. and Naji N. A. 2009. Predicting rock mechanical properties of carbonates from wireline logs (a case study: Arab-D reservoir, Ghawar field, Saudi Arabia). Mar Petrol Geol 26(4):430–444

Asoodeh (2013) Prediction of Poisson's Ratio from Conventional Well Log Data: A Committee Machine with Intelligent Systems Approach, Energy Sources, Part A: Recovery, Utilization, and Environmental Effects, 35:10, 962-975, DOI: 10.1080/15567036.2011.557693

Bandar, A.D , Algarni, M. T., Tale, M., & Almushiqeh, I. (2011, January 1). Prediction of Poisson's Ratio and Young's Modulus for Hydrocarbon Reservoirs Using Alternating Conditional Expectation Algorithm. Society of Petroleum Engineers. doi:10.2118/138841-MS

Barree, R. D., Gilbert J. V., Conway M. W. (2009) Stress and rock property profiling for unconventional reservoir stimulation. Paper SPE 118703 presented at the SPE hydraulic fracturing technology conference, The Woodlands, Texas, 19–21 Jan 2009

Belikov, B.P., Alexandrov, T.W., and Rysova, T.W. 1970. Elastic Properties of Rock Minerals and Rocks. Moscow, Nauka.

Ben-Hur, A. H., David, S. H., and Vapnik, V.; "Support vector clustering" (2001) Journal of Machine Learning Research, 2: 125–137.

Bradford, I.D.R., Fuller, J., Thompson, P.J., Walsgrove, T.R., 1998. Benefits of assessing the solids production risk in a North Sea reservoir using elastoplastic modeling. SPE/ISRM Eurock '98 held in Trondheim, Norway, 8–10 July, 1998, pp. 261–269.

Brocher, T.M., 2005. Empirical relations between elastic wave speeds and density in the Earth's crust. Bulletin of Seismology of America. 95 (6): pp. 2081–2092

Burbidge, R., Trotter M, Buxton, B. (2001) Drug design by machine learning: support vector machines for pharmaceutical data analysis. Comput Chem 26(1):5–14

Castillo, A.Á.D., Santoyo, E., Garcia-Valladare, O., 2012. A new void fraction correlation inferred from artificial neural networks for modeling two-phase flows in geothermal Wells. Comput. Geosci. 41, 25–39.

Canady, W. J. (2011, January 1). A Method for Full-Range Young 's Modulus Correction. Society of Petroleum Engineers. doi:10.2118/143604-MS

Carroll, R.D., 1969. The determination of acoustic parameters of volcanic rocks from compressional velocity measurements. International Journal of Rock Mechanics and Mining Sciences & Geomechanics Abstracts, 6 (6): pp. 557–579.

Chang, C. M. D. Zoback, A. Khaksar. 2006. Empirical relations between rock strength and physical properties in sedimentary rocks. Journal of Petroleum Science and Engineering. 51: 223-237.

Cranganu, C., Luchian, H and Breaban, M. E., 2015. Artificial Intelligent Approaches in Petroleum Geosciences. ISBN 978-3-319-16531-8, pp 145-150

Castagna, J.P., Batzle, M.L., and Eastwood, R.L., 1985. Relationship between compressional and shear wave velocities in silicate rocks. Geophysics, 50 (4): pp. 571-581.

Castagna, J.P., Batzle, M.L., Kan, T.K., 1993. Rockphysics—the link between rock properties and AVO response. In: Castagna, J.P., Backus, M.M. (Eds.), Offset-Dependent Reflectivity—Theory and Practice of AVO Analysis. Society of Exploration Geophysicists, Tulsa, pp: 135-171.

Colin, C., Potter, S and Darren F., 1997. Formation elastic parameters by deriving S-wave velocity logs CREWES Research, 9: 1-10.

Cregger, D. M., & Lamb, T. J. (1984, January 1). Poisson's Ratio As A Parameter For Determining Dynamic Elastic Modulus. American Rock Mechanics Association.

Eissa, E. A. and Kazi, A. 1988. Relation between Static and Dynamic Young's Modulus of Rocks. International Journal of Rock Mechanics and Mining Sciences & Geomechanics, 25 (6): 479-482

Eskandari, H.,1 Rezaee, M.R., and Mohammadnia, M., 2004. Application of Multiple Regression and Artificial Neural Network Techniques to Predict Shear Wave Velocity

from Wireline Log Data for a Carbonate Reservoir, South-West Iran. CSEG Recorder. 29 (7): pp. 42-48.

Edlmann, K., Somerville, J. M., Smart, B. G., Hamilton, S.A., Crawford, B. R., 1999. Predicting rock mechanical properties of clastic reservoirs from wireline porosity. The 7th Annual EAGE Student Research Research Review, Geoengineering Forum, Aberdeen, UK 10 February.

Fjaer, E., Holt, R.M., Horsrud, P., Raaen, A.M., Risnes, R., 1992. Petroleum Related Rock Mechanics. Amsterdam, Elsevier.

Freyburg, E., 1972. Der Untere und mittlere Buntsandstein SWThuringen in seinen gesteinstechnicschen Eigenschaften. Ber. Dtsch. Ges. Geol. Wiss., A; Berlin 176, 911–919.

Frost, E. and Walter, F. H., 1982. Shear Wave Travel Time Determination Using an Unconventional Approach. Paper SPE 11032 Presented at the Annual Technical Conference and Exhibition held in New Orleans LA. 26-29 September

Gatens, J. M., Harrison, C. W., Lancaster, D. E. and Guldry, F. K. 1990 .In-situ stress tests and acoustic logs determine mechanical properties and stress profiles in the devonian shales. SPE Formation Eval 5(3):248–254

Gholami, R, Shahraki, AR, Jamali, P. M. (2012) Prediction of hydrocarbon reservoirs permeability using support vector machine. Math Probl Eng. doi:10.1155/2012/670723

Gorjainov, N.L. 1979. Seismic Methods in Engineering Geology. Moscow: Nedra.

Golubev, A.A., Rabinovich, G.Y., 1976. Resultaty primeneia appartury akusticeskogo karotasa dlja predeleina proconstych svoistv gornych porod na mestorosdeniaach tverdych isjopaemych. Prikl. Geofiz. Moskva 73, 109–116.

Graves, M., Liwicki, S., Fernandez, R., Bertolami, H., Bunke, J., Schmidhuber. A Novel Connectionist System for Improved Unconstrained Handwriting Recognition. IEEE Transactions on Pattern Analysis and Machine Intelligence, vol. 31, no. 5, 2009.

Howard, G. C., and Fast, C. R.: 1970 "Hydraulic Fracturing," Monograph Volume 2 of SPE.

Hinton, G. E., Osindero, S., Teh, Y., 2006. "A fast learning algorithm for deep belief nets" . Neural Computation 18 (7): 1527–1554

Huang Z, Shimeld J, Williamson, M. 1996 Permeability prediction with artificial neural network modeling in the Venture gas field, offshore eastern Canada. Geophysics 61(2):422–436

Inoue, M., and Ohomi, M. 1981. “Relation between uniaxial compressive strength and elastic wave velocity of soft rock.” Proc., Int. Symp. on Weak Rock, Tokyo, Japan, Balkema, Rotterdam, 9–13.

Jaeger, J.C., Cook, N.G.W., Zimmerman, R.W., 2007. Fundamentals of Rock Mechanics, fourth ed. BlackWell Publishing.

Jang, J.S.R. 1993. "ANFIS: adaptive-network-based fuzzy inference system". IEEE Transactions on Systems, Man and Cybernetics 23 (3). doi:10.1109/21.256541

Jeng, J. T., Chuang, C.C, Su,S.F. 2003 Support vector interval regression networks for interval regression analysis. Fuzzy Sets Syst 138(2):283–300

Kaydani, H, Mohebbi, A., Baghaie, A. 2012 Neural fuzzy system development for the prediction of permeability from wireline data based on fuzzy clustering. J Pet Sci Eng 30(19):2036–2045

Khaksar, A., Taylor, P.G., Fang, Z., Kayes, T., Salazar, A., Rahman, K. 2009 Rock strength from core and logs, where we stand and ways to go. Paper SPE 121972 presented at the EUROPEC/ EAGE conference and exhibition, Amsterdam, The Netherlands, 8–11 June 2009

Kahraman, S. 2002. "Estimating the direct P-wave velocity value of intact rock from indirect laboratory measurements." Int. J. Rock Mech. Min. Sci., 39(1), 101–104.

King, M.S. 1970. "Static and Dynamic elastic moduli of rocks under pressure" In: Proc 11th Us Symp. on Rock Mechanics, pp 329-351

King, M.S. 1983. Static and Dynamic Elastic Properties of Rocks from the Canadian Shield. International Journal of Rock Mechanics and Mining Science, 20 (5): 237-241.

Klir G. and Yuan B (1995) Fuzzy sets and fuzzy logic: theory and applications. Prentice-Hall, Englewood Cliffs

Kumoluyi, A.O., Daltaban, T.S. 1994 High-order neural-networks in petroleum engineering. In: Paper SPE 27905 presented at the 1994 SPE Western regional meeting, Longbeach, California, USA, 23–25 March

Lal, M., 1999. Shale stability: drilling fluid interaction and shale strength. SPE Latin American and Caribbean Petroleum Engineering Conference held in Caracas, Venezuela.

Ledbetter, H. 1993. "Dynamic vs static Young's Moduli a case study" Mater. Sci. Eng. A165, L9-L10

Larsen, I., Fjær, E., & Renlie, L. 2000. Static and Dynamic Poisson's Ratio of Weak Sandstones. American Rock Mechanics Association.

Lippmann, R.P., 1987. An introduction to computing with neural nets. ASSP Mag. IEEE 4, 4e22.

Liew S. S., (2015), An optimized second order stochastic learning algorithm for neural network training, Neurocomputing (2016), dx.doi.org/10.1016/j.neucom.2015.12.076i

Maleki, S., Moradzadeh, A., Riabi, R.G., Gholami, R., Sadeghzadeh, F. 2014. Prediction of shear wave velocity using empirical correlations and artificial intelligence methods. NRIAG Journal of Astronomy and Geophysics 3(1): pp. 70–81.

McCann, D.M., and Entwisle, D.C. 1992. Determination of Young's Modulus of the Rock Mass from Geophysical Well Logs, in Hurst A, Giffiths CM, and Worthington, PF (Eds.). Geological Applications of Wireline Logs II: Geological Society of Special Publications, 65: 317-325.

McNally, G.H., 1987. Estimation of coal measures rock strength using sonic and neutron logs. Geoexploration 24, 381–395.

Moos, D., Peska, P., Finkbeiner, T., Zoback, M.D., 2003. Comprehensive Wellbore stability analysis utilizing quantitative risk assessment. Journal of Petroleum Science and Engineering. 38 (1-4): pp. 97–110.

Mohaghegh, S., Ameri, S. 1995 Artificial neural network as a valuable tool for petroleum engineers. SPE paper 29220

Morals, R.H., and Marcinew, R.P. 1993. Fracturing of High-Permeability Formations: Mechanical Properties Correlations. SPE Paper 26561, Presented in SPE Annual Technical Conference and Exhibition, 3-6 October, Houston, Texas.

Militzer, H., Stoll, R., 1973. Einige Beitrageder geophysics zurprimadatenerfassung im Bergbau, Neue Bergbautechnik. Lipzig 3,21–25.

Najebi, A. R., Mohammad, G., Gholam, R. L. and Mohammad, R. A. 2015. Empirical relations between strength and static and dynamic elastic properties of Asmari and Sarvak limestones, two main oil reservoirs in Iran. Journal of Petroleum Science and Engineering,126 (2015) 78–82

Niculescu S. P. 2003 Artificial neural networks and genetic algorithms in QSAR. J Mol Struct Theochem 622:71–83

Nooruddin, H. A., Anifowose, F., & Abdulraheem, A. 2013. Applying Artificial Intelligence Techniques to Develop Permeability Predictive Models using Mercury Injection Capillary-Pressure Data. Society of Petroleum Engineers. doi:10.2118/168109-MS

Rammay, M. H., & Abdulraheem, A. 2014, September 15. "Automated History Matching Using Combination of Adaptive Neuro Fuzzy System (ANFIS) and Differential Evolution Algorithm." Society of Petroleum Engineers, doi:10.2118/172992-MS. SPE Large Scale Computing and Big Data Challenges in Reservoir Simulation Conference and Exhibition held in Istanbul, Turkey, 15–17 September 2014

Rammay, M. H. and Abdulraheem, A., "PVT Correlation for Pakistani Crude Oils using Artificial Neural Networks", Journal of Petroleum Exploration and Production Technology, pp 1-17, Feb 2016 DOI 10.1007/s13202-016-0232-z

Santarelli, F.J., Detienne, J.L., Zundel, J.P., 1989. Determination of the mechanical properties of deep reservoir sandstones to assess the likelihood of sand production. Paper ISRMI-IS-1989-100 was published at the International Symposium, Pau, France. 30 August-2 September

Soltanzadeh, H. (2013, November 5). Relations between Shear and Compressional Wave Velocities of Geological Formations in Alberta, Canada Based on a Log-derived Database. Society of Petroleum Engineers. doi:10.2118/167248-MS

Tabari, M., Tabari, O., and Tabari, M., 2011. A Fast Method for Estimating Shear Wave Velocity by Using Neural Network. Australian Journal of Basic and Applied Sciences, 5 (11): pp. 1429-1434.

Tahmasebi, P. (2012). "A hybrid neural networks-fuzzy logic-genetic algorithm for grade estimation" (PDF). Computers & Geosciences 42: 18–27.

Trontl, K, Smuc, T., Pevec, D. (2007) Support vector regression model for the estimation of γ-ray buildup factors for multi-layer shields. Ann Nucl Energy 34(12):939–952

Wadhwa, R.S., Ghosh N., and Rao, C. H. 2010. Empirical relation for estimating shear wave velocity from compressional wave velocity of rocks. Journal of Indian Geophysical Union. 14 (1): pp. 21-30.

Wang, Z. 2000. Dynamic versus Static Elastic Properties of Reservoir Rocks, in Seismic and Acoustic Velocities in Reservoir Rocks. SEG Geophysics Reprint Series, 19: 531-539.

William H.; Teukolsky, Saul A.; Vetterling, William T.; Flannery, B. P. (2007). "Section 16.5. Support Vector Machines". Numerical Recipes: The Art of Scientific Computing (3rd ed.). New York: Cambridge University Press. ISBN 978-0-521-88068-8.

Appendix: Published Data for UCS and Es Prediction

Table A. Published Data Najeibi 2013

Sample ID	Vp (km/s)	Vs (Km/s)	Density (g/cc)	UCS (ksi)	Es (MPsi)	Ed (MPsi)	Ed/Es
1	5.381	3.073	2.6	25.85	6.70	8.96	1.33
2	4.876	2.712	2.46	17.75	4.97	6.70	1.34
3	5.737	3.102	2.6	25.51	6.97	9.38	1.34
4	5.951	3.261	2.7	25.66	7.73	10.70	1.38
5	4.809	2.797	2.3	11.88	4.49	6.49	1.44
6	5.189	2.893	2.6	14.61	5.27	8.04	1.52
7	2.690	1.703	2.6	4.63	1.65	2.55	1.54
8	4.887	2.809	2.3	9.86	4.17	6.59	1.57
9	3.170	1.981	2.4	7.28	2.01	3.21	1.59
10	4.831	2.942	2.7	22.31	4.93	8.16	1.65
11	4.036	2.691	2.62	15.27	3.61	6.04	1.67
12	2.826	1.884	2.43	6.02	1.58	2.75	1.74
13	3.924	2.337	2.4	10.73	2.63	4.65	1.76
14	3.691	2.043	2.35	4.95	1.92	3.64	1.88
15	3.600	2.402	2.61	9.25	2.48	4.80	1.93
16	3.229	2.123	2.5	8.19	1.84	3.65	1.98
17	3.694	2.44	2.53	8.44	2.42	4.85	2.00
18	4.373	2.405	2.41	7.76	2.50	5.19	2.06
19	3.454	2.281	2.59	7.37	2.03	4.35	2.14
20	3.445	2.261	2.61	8.62	1.92	4.33	2.24
21	3.663	2.419	2.44	5.93	1.76	4.61	2.60
22	3.696	2.012	2.54	4.87	1.14	3.84	3.35
23	3.746	2.475	2.59	6.96	1.45	5.11	3.53
24	3.852	2.608	2.63	10.81	1.85	5.58	3.00
25	4.221	2.488	2.62	10.27	1.13	5.80	5.12
26	3.353	2.357	2.54	11.01	1.94	4.13	2.12
27	2.381	1.587	2.47	4.90	1.02	1.98	1.92
28	3.855	2.461	2.63	6.89	1.94	5.33	2.74
29	3.935	2.644	2.58	11.40	2.10	5.7	2.71
30	6.48	3.288	2.7	26.11	13.0	11.2	0.86
31	4.063	2.719	2.6	10.53	2.43	6.10	2.50
32	4.854	2.88	2.69	17.11	3.53	7.94	2.24
33	4.274	2.794	2.65	17.69	3.27	6.75	2.06
34	4.854	2.88	2.69	17.11	3.53	7.94	2.24
35	5.707	3.149	2.7	22.81	9.57	9.94	1.03
36	5.016	3.108	2.7	21.49	7.39	8.99	1.21
37	5.744	3.206	2.7	20.84	9.57	10.2	1.07
38	4.185	2.69	2.4	13.26	2.82	5.78	2.04
39	3.834	2.368	2.1	3.64	2.52	4.07	1.61
40	3.064	1.963	2.3	4.08	0.68	2.95	4.34
41	3.877	2.418	2.3	6.79	1.66	4.61	2.76
42	3.69	2.43	2.7	7.93	1.88	5.16	2.73
43	3.77	2.44	2.6	8.19	3.26	5.11	1.56
44	4.072	2.618	2.6	10.94	1.74	5.93	3.40
45	5.689	3.289	2.7	24.82	7.35	10.59	1.43

Vitae

Name	:ZEESHAN TARIQ
Nationality	:PAKISTAN
Date of Birth	:11/1/1990
Email	:zeeshan_tariq3@hotmail.com
Address	:Phase 7, Defence Karachi, Pakistan
Academic Background	**MS in Petroleum Engineering (November, 2016)** King Fahd University of Petroleum and Minerals, Dhahran, Saudi-Arabia. **B.E in Petroleum Engineering (December, 2012) from** NED University of Engineering & Technology, Karachi, Pakistan
Research Interests	My research interests are in geomechanics, reservoir simulation, optimization and artificial intelligence.

Publications

1. **Tariq, Z.**, Elkatatny, S., Mahmoud, M., & Abdulraheem, A. (2016, November 14). A New Artificial Intelligence Based Empirical Correlation to Predict Sonic Travel Time. International Petroleum Technology Conference. doi:10.2523/IPTC-19005-MS

2. **Tariq, Z**., Elkatatny, S., Mahmoud, M., & Abdulraheem, A. (2016, November 7). A Holistic Approach to Develop New Rigorous Empirical Correlation for Static

Young's Modulus. Society of Petroleum Engineers. http://dx.doi.org/10.2118/183545-MS.

3. Elkatatny, S. M., **Tariq, Z**., Mahmoud, M., Abdulazeez, A., & Mohamed, I. M. (2016, June 26). Application of Artificial Intelligent Techniques to Determine Sonic Time from Well Logs. American Rock Mechanics Association.